Final Report RSC-4854

CROP MOISTURE ESTIMATION OVER THE SOUTHERN GREAT PLAINS WITH DUAL POLARIZATION 1.66 CENTIMETER PASSIVE MICROWAVE DATA FROM NIMBUS 7

by

M. J. McFarland

P. H. Harder II

G. D. Wilke

G. L. Huebner, Jr.

May 1984

Supported by

National Aeronautics and Space Administration
Johnson Space Center
Houston, Texas 77058

Contract NAS-9-16822

TEXAS A&M UNIVERSITY
REMOTE SENSING CENTER
COLLEGE STATION, TEXAS

Final Report RSC-4854

CROP MOISTURE ESTIMATION OVER THE SOUTHERN GREAT PLAINS WITH DUAL POLARIZATION 1.66 CENTIMETER PASSIVE MICROWAVE DATA FROM NIMBUS 7

by

Marshall J. McFarland
Paul H. Harder, II
Gregory D. Wilke
George L. Huebner, Jr.

Remote Sensing Center
Texas A&M University
College Station, Texas 77843

May 1984

Supported by

National Aeronautics and Space Administration
Johnson Space Center
Houston, Texas 77058

Contract NAS-9-16822

ABSTRACT

Moisture content of snow-free, unfrozen soil is inferred using passive microwave brightness temperatures from the Scanning Multichannel Microwave Radiometer (SMMR) on Nimbus-7. Investigation is restricted to the two polarizations of the 1.66 cm wavelength sensor. Passive microwave estimates of soil moisture are of two basic categories; those based upon soil emissivity and those based upon the polarization of soil emission. The two methods are compared and contrasted through the investigation of 54 potential functions of polarized brightness temperatures and, in some cases, ground-based temperature measurements. Of these indices, three are selected for the estimated emissivity, the difference between polarized brightness temperatures, and the normalized polarization difference. Each of these indices is about equally effective for monitoring soil moisture. Using an antecedent precipitation index (API) as ground control data, temporal and spatial analyses show that emissivity data consistently give slightly better soil moisture estimates than depolarization data. The difference, however, is not statistically significant. It is concluded that polarization data alone can provide estimates of soil moisture in areas where the emissivity cannot be inferred due to nonavailability of surface temperature data.

TABLE OF CONTENTS

TABLE OF CONTENTS (Continued)

TABLE OF CONTENTS (Continued)

LIST OF FIGURES

Figure Page

Figure Page

LIST OF TABLES

INTRODUCTION

Objectives

The purpose of this research is to determine methods of estimating soil moisture content over large agricultural areas using dual polarization passive microwave brightness temperatures from the Scanning Multifrequency Microwave Radiometer (SMMR) aboard the Nimbus 7 satellite. This will be done by testing functions of brightness temperatures in the horizontally and vertically polarized channels of the 1.66 cm SMMR sensor that relate to soil moisture under varying conditions of vegetation, surface roughness, land use, and rainfall. Specific objectives are:

1. Compare the performance of both emissivity and polarization measures as indicators of soil moisture.
2. Determine whether multiple correlation and principal component analyses can be used to combine soil moisture information from several different indices.
3. Demonstrate the use of both day and night data in microwave indices of soil moisture.
4. Demonstrate the ability of passive microwave indices to give quantitative measurements of soil moisture on winter wheat areas during seasons when the soil is essentially bare.

5. Demonstrate the ability of passive microwave indices to give quantitatively correct maps of soil moisture for large areas with a wide diversity of crops and land use.
6. Compare maps of soil moisture indices using model parameters developed for individual seasons versus the entire year and for individual locations versus large areas.

Applications of Passive Microwave Data

A number of activities require large area soil moisture estimates that can be obtained from satellite-borne passive microwave sensors. Among these are numeric modeling of energy and moisture fluxes in the boundary layer of the atmosphere, tractionability determinations for agricultural and military applications, and estimation of flood hazards due to watershed runoff. In particular, the projection of crop yields requires recurring estimates of soil moisture over large areas. Passive microwave sensors can provide estimates representing weighted averages over their entire field of view with very little restriction due to atmospheric conditions.

Passive microwave sensors intended for civil-sector use will be economically feasible because they can measure a wide range of other environmental variables. Kondratyev et al. (1977) showed that microwave data could be used to measure soil temperature profiles to a depth of several centimeters, as well as areally averaged soil moisture content. Blanchard et al. (1975), Blanchard (1977), and Walker (1978) showed that watershed hydrologic response characteristics can be inferred from passive microwave data. Allison et al. (1979) showed that

a satellite-borne instrument with a wave length of 1.55 cm could be used reliably to map flood waters in Australia. Burke et al. (1981) have investigated the use of microwave sensors in probing snowpacks. Many other phenomena could be cited, including sea ice, atmospheric water vapor content, and instantaneous rainfall rates. The soil moisture methods developed in this study represent only one of a number of practical uses for spaceborne microwave radiometers.

In particular, the microwave sensors likely to be available in the next decade will be useful in agricultural applications. Since these sensors will have extremely low resolutions, their use will be most helpful in applications requiring no better than 20 or 30 km resolution. Since current government methods of monitoring crop moisture are based on data with poorer resolution than this, a primary application of microwave data will be in sensing of crop condition and prediction of crop yield. These systems will have virtually all-weather capability and will be appropriate to the essentially bare-soil and monocultural regions of winter wheat.

Use of Polarization Data

This paper adds to earlier research by investigating the use of polarization data. Previous researchers have shown that single-polarization spaceborne radiometers can indicate soil moisture, at least in a general, qualitative way. Some, such as McFarland (1976) McFarland and Blanchard (1977), Theis (1979), and Theis et al. (1982), have shown that these sensors can be used to infer soil moisture quantitatively under some circumstances. These earlier efforts were based upon the

relationship between microwave emissivity and soil moisture content.

Briefly stated, the dielectric constant of soil varies strongly in response to the amount of liquid water held in the soil. The dielectric constant determines the soil emissivity which, together with soil temperature, determines the amount of microwave radiation emitted by the soil. By measuring the brightness temperature with a satellite sensor, and by estimating the soil temperature from ground-based weather observations, it is possible to estimatethe soil's emissivity and, hence, its moisture content.

Data presented by Newton (1977), however, indicated that the microwave radiation of moist soil is partially polarized, and that the degree of polarization increases with soil moisture content. If this relationship is reliable enough, and if it is sufficiently insensitive to surface temperature, it should give a means of monitoring soil moisture from space without reference to ground- based temperature measurements. There are many potential applications for such a purely remote sensing capability. For instance, some locations such as mountain valleys are not well instrumented for surface temperature, and have no consistent relationship to temperature observations from surrounding lowland weather stations. Second, there should be military applications for areas from which conventional surface weather observations may become inaccessible. Finally, there are many important agricultural areas for which the density of conventional weather observations may be too low to allow effective use of techniques requiring surface temperature measurements. This paper examines the polarization approach, using data from the Nimbus 7 satellite.

Ground Control Data

Researchers in satellite remote sensing projects frequently have difficulty assembling a comprehensive and accurate ground truth data base. In fact, such data are more appropriately termed "ground control," since their actual truth is in some doubt. This study is no exception. In order to interpret the soil moisture signal of microwave data from half a million square kilometers of the U.S. Great Plains, soil moisture data from the study area are needed. Conventional measurements of soil moisture over this area are not possible. Even a single instantaneous field of view (IFOV) cannot be instrumented adequately on the ground when it has a diameter of nearly 40 km. Some other approach is required.

The ground control data chosen for this study were generated by a common index from hydrologic engineering, the antecedent precipitation index (API). This index represents soil moisture as a Markov chain whose single input is the series of daily observations of total effective precipitation. Blanchard et al. (1980) showed that API varies almost linearly with soil moisture content.

Analytical Approach

This study relies primarily on regression analysis to relate satellite data to API. A number of functions of vertically and horizontally polarized brightness temperatures are subjected to simple and multiple linear regression models to establish which functions give the best

estimates of API for individual training sites. These functions are used to generate images of satellite-derived soil moisture estimates, which are compared to computer-generated maps of API to verify visually the effectiveness of the methods.

LITERATURE REVIEW

Review Articles

Several authors have published survey articles of the field of microwave radiometry and its applications in soil moisture sensing. Reeves (1975) presented a comprehensive summary including the physics of emission and radiative transfer, and the design and performance characteristics of radiometers. NAS (1977) summarized the basic physics of microwave sensing and the potential applications in many fields. Kondratyev et al. (1977) reviewed passive microwave remote sensing of soil moisture and evaluated the potential of microwave for several data retrieval applications. Basharinov and Shutko (1978) also reviewed the field of microwave sensing of soil moisture. Paris (1971) gave a detailed development of the fundamental physics of microwave radiometry.

Schmugge et al. (1979) and Schmugge (1978, 1980a,b) reviewed soil moisture measurement by gravimetric, nuclear, reflected solar, thermal infrared, and both active and passive microwave methods.

Newton (1980) presented a summary of research in microwave measurement of soil moisture done by the Texas A&M University Remote Sensing Center (RSC) from 1974 to 1980. These investigations included ground-based measurements, modeling, and simulation studies.

Physics of Microwave Remote Sensing of Soil Moisture

The radiation detected by a spaceborne passive microwave sensor is

expressed as a brightness temperature, a radiative effective temperature equal to the thermodynamic temperature of a hypothetical blackbody radiating exactly the same power as detected by the instrument. This brightness temperature can be expressed as the sum of three components: sky radiation reflected toward the radiometer by the surface, radiation emitted at the surface, and atmospheric radiation received directly at the sensor. Schmugge (1980b) gives the equation in this form:

$$T_B = \tau(r\ T_{sky} + (1-r)\ T_{surf}) + T_{atm} \qquad (1)$$

τ = atmospheric transmittance

r = surface reflectivity

T_{surf} = temperature of emitting layer at surface

T_{atm} = brightness temperature of atmosphere

The significance of each of the three components is discussed below.

Sky Radiation

Sky radiation sensed by a satellite-borne radiometer consists of surface reflections of the celestial background emission plus downwelling atmospheric radiation. Weger (1960) computed downwelling sky brightness temperatures for wavelengths from 0.43 cm to 3.00 cm, and for a variety of sky conditions. He found the following values for a wavelength of 1.80 cm and viewing angle of 50 degrees: about 10K for clear skies, 15K for moderate cloud, and 30K for uniform moderate precipitation. The sky brightness component of brightness temperature is the product of this downwelling brightness temperature, surface reflectivity, and atmospheric transmission from surface to detector. Since most naturally occurring substances have emissivities near unity, the

highest surface reflectivities of interest to this study are those of moist soil. The largest possible value of atmospheric transmission, 1.00, cannot occur simultaneously with the highest sky temperatures, which are associated with rain events. Nevertheless, an upper bound of this component can be estimated, for moist bare soil, by multiplying a maximum value of 30K by an assumed reflectivity of 0.30 and atmospheric transmission of 1.00. Thus, this component of microwave brightness temperature is less than about 10K. McFarland and Blanchard (1977) ignored this component.

Direct Atmospheric Effects

Atmospheric effects are of two kinds: the direct radiation from the atmosphere impinging upon the sensor, and the attenuation of radiation from the surface. The previous discussion of sky temperature suggests that direct radiation should also be negligible under most circumstances. The exceptions are those circumstances under which atmospheric attenuation is also significant; specifically, those occasions on which precipitating clouds are present between the surface and the radiometer.

Paris (1971) computed the absorption and scattering properties of gases and hydrometeors in the atmosphere, as well as effects of sea-surface roughness and salinity, extraterrestrial radiation, and emission of microwaves by the atmosphere, clouds, and precipitation particles. His computations show that the effects of absorption and emission by the atmosphere are small except in the presence of precipitating cloud.

McFarland and Blanchard (1977) chose to ignore atmospheric effects since the only case in which they are important is that of a precipitating cloud, the principal effect of which was to produce a brightness temperature lower than that of dry soil. That is, the rain has the same appearance in a microwave image as does moist soil; so it is at least qualitatively correct to interpret reduced brightness temperature as being associated with moist soil--soil beneath a rain shower.

Surface Emission

The microwave emission of the surfaces of soil, plants and other objects present in the IFOV of the sensor have been modeled in many ways. A number of detailed radiative transfer models are available, as well as simpler techniques.

Detailed Emission Models. Several investigators have reported models that account for the transfer of radiation within the soil body. These models have been derived in various levels of complexity, but allrequire fairly detailed information about the properties of the emitting soil layers. Some account for a rough surface or a vegetative canopy.

Stogryn (1970) used an electromagnetic fluctuations approach to derive equations for the brightness temperature of a medium with a flat surface and with temperature and dielectric constant varying only with depth.

Tsang et al. (1975) and Tsang and Kong (1975, 1976a, b, c, 1980) developed a general theory for computing the microwave emission from soils, and presented illustrations of special cases. The general

theory allowed a three-layer system of soil, air, and vegetation, with soil properties allowed to vary in three dimensions.

Njoku and Kong (1977) extended the work of Tsang et al. (1975) and Stogryn (1970), to give equations for the brightness temperature of a smooth-surfaced, vertically structured medium in which moisture content and thermodynamic temperature are assumed to be functions of depth.

Wilheit (1978) developed a radiative transfer model for plane stratified media, using a formalism equivalent to but simpler than that of Tsang et al. (1975). He defined thermal and reflective sampling depths, and showed that the former is of the order of one wavelength while the latter is an order of magnitude smaller. The reflectivity sampling depth is determined primarily by the real part of the dielectric constant; the thermal sampling depth, by the imaginary part.Thermal sampling depth is the layer whose effective temperature determines the amount of energy available for emission. Reflectivity sampling depth is the layer whose moisture content determines the effective emissivity of the soil. The thickness of this layer decreases with increasing soil moisture content.

Tsang and Newton (1980) developed a microwave emission model which accounted for the incorherent reflectivity modeled by Stogryn (1970) and the coherent reflectivity modeled by Choudhury et al. (1979). They used two roughness parameters, RMS height and RMS slope.

Wang et al. (1980b) used the random-dielectric theory of Tsang and Kong (1976b,c, 1980) to derive equations for the polarized brightness temperature of a smooth soil with a vegetative cover. Using the empirical model of Wang and Schmugge (1980) to describe the emission from

the soil surface, they computed the expected normalized brightness temperatures (effective emissivities) for a number of vegetative covers. Their model predictions agreed with measurements except for discrepancies that they explained by roughness which the model did not account for.

Simpler Emission Models. While instructive, the radiative transfer models generally require too much detailed information about the soil structure, roughness, and vegetation for practical use with low-resolution, satellite-mounted microwave radiometers. Simpler models in use assume that the soil can be represented as a single emitting layer whose effective temperature and emissivity can be represented by simple algorithms. In general, these models rely on the strong dependence of soil dielectric constant upon the moisture content. This effect is so strong that other effects are ignored or simply parameterized.

Newton (1977) presented model calculations showing that brightness temperature was a nearly linear function of soil moisture content, except over a region in the dry end of the moisture range in which microwave emission is not very sensitive to moisture content. He explained this behavior as caused by the tight bond of water molecules held very close to the soil particles under dry conditions. The effect of increasing the viewing angle from nadir was to increase the vertically polarized component and decrease the horizontally polarized component. He showed also that the mean of the two polarizations was nearly independent of viewing angle. He verified these conclusions using data from truck-mounted radiometers operating at wavelengths of 21 cm and 2.8 cm.

Figure 1 is a schematic view, abstracted from Newton (1977), of the response of soil brightness temperatures to variations in soil moisture. The figure presents two cases represented, respectively, as "dry" and "moist". Under the assumption that all other scene parameters such as temperature profile and surface roughness are the same for both cases, an increase in soil moisture is seen to result in a decrease in vertically polarized brightness temperature, a greater decrease in horizontally polarized brightness temperature, and a consequent increase in polarization. This polarization increase is greatest near the Brewster angle, the view angle at which T_V peaks.

Wang and Schmugge (1978 and 1980) presented a simple empirical model of the dielectric behavior of soil-water mixtures and demonstrated its superiority over previous mixing formula approaches. They included, as an adjustable parameter modeled in terms of soil texture, the transition moisture value beneath which the dielectric constant of a soil is not very responsive to moisture content.

Perhaps the simplest model of soil emission is that used by McFarland (1976) and by McFarland and Blanchard (1977), in which (1) was simplified by neglecting the sky and atmospheric effects, giving:

$$T_B = \varepsilon T \qquad (2)$$

ε = emissivity

T = temperature of surface emitting layer

This relationship holds in the microwave band of the spectrum, because of the validity of the Rayleigh-Jeans approximation to Planck's radiation law. Written in the form appropriate to the wavelength

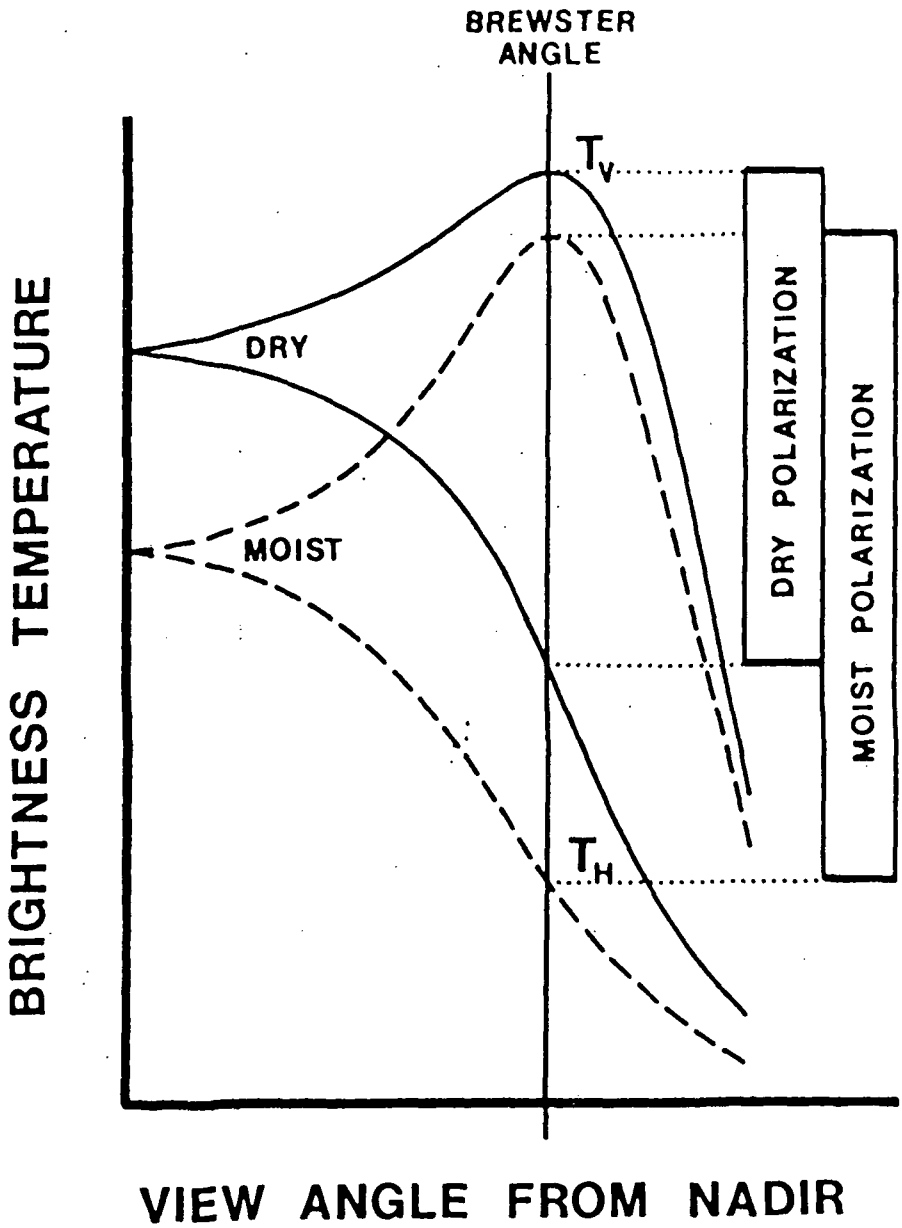

Figure 1. Schematic representation of the angular dependence of polarized brightness temperatures, illustrating the effect of soil moisture on brightness temperature and on polarization for a sensor viewing at the Brewster angle. Curves abstracted from Newton (1977).

domain, Planck's law is (Shortley and Williams, 1965)

$$M_\lambda = 2\pi hc^2\lambda^{-5}\left[\exp\left(\frac{hc}{\lambda kT}\right) - 1\right]^{-1} \quad (3)$$

where

M_λ = spectral exitance (Wm^{-3})

h = Planck's constant = $6.6256 \times 10^{-34} J.s$

c = speed of light in vacuum = $2.997925 \times 10^{8} ms^{-1}$

λ = wavelength (m)

k = Boltzmann's constant = $1.3805 \times 10^{-23} J/K$

T = temperature (K)

The exponential can be expanded as a Maclaurin series and, for wavelength in the microwave band, the higher order terms can be ignored, giving the Rayleigh-Jeans approximation:

$$M_\lambda = 2\pi ck\lambda^{-4}T \quad (4)$$

Defining $c_1 = 2\pi ck\lambda^{-4}$, this can be rewritten, for a blackbody, as:

$$M_\lambda = c_1 T_B \quad (5)$$

where T_B = brightness temperature

For a real radiating surface (4) takes the form:

$$M_\lambda = \varepsilon c_1 T \quad (6)$$

where ε = emissivity, defined as the ratio of exitance from a real body to the blackbody exitance for the same temperature. (2) is derived by taking the ratio of (5) and (6).

McFarland and Blanchard (1977) applied (2) by assuming that the effective temperature of the emitting material could be estimated from independent sources such as conventional weather observations. They computed a normalized brightness temperature, representing an estimated emissivity, by taking the ratio of brightness temperature to air temperature. They showed that this emissivity estimate was linearly related to API, which they used as an index of soil moisture. They suggested a methodology of determining empirical linear regression coefficients for each location and for each time of year, so that API could be estimated by applying these coefficients to computed values of emissivity.

Effects of Vegetation and Roughness. Vegetation and roughness are considered together here, since some of their effects are similar, in spite of the different physical processes by which they exert those effects. In general, both decrease the sensitivity of detected radiation to soil moisture. Newton (1977) presented model calculations that show these effects of roughness and vegetation.

These effects of vegetation and roughness are most important for shorter wavelengths. Blinn and Quade (1972) reported ground-based measurements at wavelengths of 0.95, 2.8, and 21 cm, showing that the longest wavelength's moisture sensitivity was least affected by vegetation and roughness. Measurements at wavelengths of 2.8, 6.0, 21, and 50 cm. showed that the wavelength with greatest sensitivity to soil moisture varied with vegetation cover, from 6.0 cm for bare soil to 50 cm for grasslands.

Choudhury et al. (1979) modified the Fresnel reflection coefficients by the inclusion of a single-parameter representation of the soil surface roughness. They found that this approach was not sufficient to characterize roughness, which must rather be described by two parameters: surface height variance and horizontal scale of roughness. Nevertheless, their model calculations were in general agreement with experimental results which indicate that roughness effects are greatest for wet soil.

Wang et al. (1980c) compared measurements at wavelengths of 6 and 21 cm with the theory of Wilheit (1978) and found that vegetation degraded soil moisture sensitivity by amounts in qualitative agreement with the results of Kirdyashev et al. (1979). The decrease of sensitivity was related to the amount of biomass moisture content of the vegetation present. This result pertained at both wavelengths. The soil type tested was a sandy loam, and the vegetation was grass, soybeans, and corn.

Wang and Choudhury (1981) described a modification of the microwave emission model of Wilheit (1978), to include a two parameter representation of soil surface roughness. They related these two parameters to combinations of the vertically and horizontally polarized normalized brightness temperatures, and they showed that moisture content may be inferred from knowledge of the relationship between the Fresnel reflection coefficients and moisture content if the values of the two parameters are known. They suggested that these parameters could be estimated empirically from a time series of data, if roughness could be assumed constant. The brightness temperature combinations they used

were $X = (T_V-T_h)/(1-[0.5(T_V+T_h)])$, which was related to the polarization mixing parameter; and $Y = 1-[0.5(T_V+T_h)]$, which was related to the roughness height parameter. T_V and T_h are, respectively, the vertical and horizontal polarized brightness temperatures measured by radiometer.

Schmugge et al. (1978) used airborne thermal infrared measurements to demonstrate that the diurnal temperature range could be used to infer soil moisture or crop stress. This lends weight to the suggestion of McFarland (1982) that, if the emissivity of a dense crop canopy is relatively insensitive to the moisture content of the plants, then microwave brightness temperature variations observed from space must indicate changes in the crop temperatures. If air temperature is known from an independent source, the crop's stress is indicated; revealing, in turn, qualitative information about the soil moisture content. That is, the brightness temperature of a crop canopy responds to plant stress in much the same way as to the moisture condition causing that stress; and moisture content can be inferred, at least qualitatively.

Ground Control Data

Since conventional soil moisture measurements cannot be made for a representative sample of points within even one IFOV of a spaceborne microwave radiometer, the ground control data for these studies must be obtained through modeling.

Available Models

A number of models are available for the purpose. Baier and Robert-

son (1966) proposed a Versatile Budget (VB) model, representing the moisture content of several soil layers by a modified Markov press.Van Bavel and Lascano (1980) devised a computer simulation model called CONSERVB which combined energy balance and water balance methods, using weather observations to drive the model. Jackson (1980) developed a model that linked deep-layer moisture content to surface-layer moisture content through hydraulic equilibrium assumptions. Most of these detailed soil moisture models are too complicated for use in conjunction with spaceborne microwave sensing methods. They require data not generally available in real time at the necessary resolution.

Antecedent Precipitation Index

An antecedent precipitation index (API) can be designed to avoid these difficulties. While this model is very simple, it is nevertheless useful. For instance, McFarland and Beach (1981) used the farmer survey data reported by Reinschmiedt (1973) to relate farm field work delays to API. They found linear correlations exceeding 0.98.

Linsley et al. (1975) stated that the soil moisture index most commonly used in storm runoff models is the API, a simplified moisture balance approach in which addition of water to a profile is only through precipitation, and depletion of water is through a black-box process of evapotranspiration, etc., represented by a simple logarithmic decrease. They gave the formula $I_t = I_0 K^t$ where I_0 is the initial value of the index, k is a recession factor (or depletion coefficient) less than unity, and t is time in days. Letting t = 1, the index for any day is seen to be the value for the previous day multip-

lied by k. They noted that the k-factor should be formulated as a function of potential evapotranspiration (PET) or of season, which determines PET to some extent. They further noted that errors in initialization of the model decay logarithmically and tend to vanish after a few weeks at most.

Saxton and Lenz (1967) estimated soil moisture with an antecedent retention index (ARI) very similar to API. The principal difference in their model is the use of an estimate of potential evapotranspiration to deplete moisture during the constant-rate stage of drying. During the falling-rate stage, depletion is modeled by a multiplicative depletion coefficient as in API. Use of the ARI formulation requires sufficient meteorological data to estimate PET by one of the familiar methods.

The form of the API equation used by McFarland and Harder (1982) is

$$API = ki \cdot API_{i-1} + P_i^{0.891} \qquad (7)$$

where

API_i = API on day i (mm)

k_i = recession factor for day i

P_i = precipation on day i (mm)

In form, (7) is a first-order Markov process. Its utility lies in its parameterization of water depletion processes in a single factor that can be modeled in terms of readily available information.

There are several ways to assign a value to the depletion coefficient, k. One formula is that of McFarland and Blanchard (1977), who

used a single value of k specified for each month of the year. A more sophisticated method is that of McFarland and Harder (1982), who used a sinusoid with a minimum in summer and a maximum in winter. Further refinement could incorporate an estimate of PET based upon temperature and sky cover data, possibly involving thermal or visual imagery from weather satellites.

Choudhury and Blanchard (1981) gave an equation in which PET estimates could be used to compute k. They derived the API equation from a water balance equation used in global climate models and showed that the recession factor is

$$k = \exp[-E/Z(FC-WP)] \tag{8}$$

where E is the potential evapotranspiration for the previous day, Z is the soil thickness, FC is soil field capacity, and WP is the permanent wilting point.

A very useful feature of the API formula is that it can be inverted to give estimates of effective rainfall. Blanchard et al. (1981) used this to construct a two-layer API model in which the API of a shallow surface layer was inverted to give an estimate of the amount of water infiltrating into a deeper layer, which was in turn depleted by a second API model with larger-valued recession factor. They suggested that the top layer API could be related to microwave radiometer data, providing a way to remotely monitor soil moisture for a deeper soil layer.

There are two principal difficulties in using API in the present investigation. First, the index models all water losses from the layer

of interest as a simple exponential decay. While this method may be appropriate for a deep layer, the lack of attention to specific processes such as insulation and head advection must introduce some errors when the model is used with a layer as shallow as the sensing depth of the 1.66 cm band of SMMR. Second, for these shallow layers, the best maximum and minimum values of the K-factor have not been well established at many locations. Nevertheless, McFarland and Blanchard (1977) did report successful use of the index in connection with data from the 1.55 cm radiometer on Nimbus 5.

Experiments in Microwave Sensing of Soil Moisture

Simulation Studies

Smith and Newton (1983) modified the CONSERVB model of van Bavel and Lascano (1980) to accept input data solely from a microwave radiometer instead of observed weather data. The resulting soil moisture predictions were almost identical to those produced by the full CONSERB model. They used a simluation approach, based upon experimental data, to examine the utility of two wavelenghts, 6 and 21 cm. They found little difference between the accuracy of model outputs from the two wavelengths, except that the shorter wavelength tended to saturate at lower rainfall amounts; that is, the longer wavelength was a better quantitative indicator of heavier rainfall events. An important conclusion from this experiment was that microwave data should have the capability to provide information about the moisture content of soil, without requiring the use of such data as solar radiation, wind speed, air humidity and temperature.

Blanchard and Bausch (1979) used a simulation to demonstrate the potential of dual wavelength (X-band and L-band) sensing of the moisture in the top 1.5 m of soil. They noted that the L-band sensor could monitor the moisture of the top 21 cm, and that the ratio of change in X-band and L-band emissivities could be used to predict the amount of water infiltrating to depths below the 21 cm level. They also noted that their method would require daily observations to estimate soil moisture with acceptable accuracy.

Ground-based and Airborne Sensors

Many experiments have investigated the ability of passive microwave sensors to indicate soil moisture conditions under realistic conditions. Several results of ground-based and airborne trials with wavelengths near SMMR's 1.66 cm sensor are summarized here.

Edgerton et al. (1971) found that brightness temperatures at a wavelength of 2.2 cm responded strongly to the moisture content of the top centimeter of soil.

Schmugge et al. (1974 and 1976) showed an approximately linear relationship between soil moisture and the 1.55 cm brightness temperature of an airborne radiometer. They noted a breakpoint value of soil moisture approximately equal to wilting point, below which the radiometer showed little response. They demonstrated a means of accounting for soil texture by expressing moisture content in terms of fraction of field capacity.

Barton (1978) computed emissivity as the ratio of microwave brightness temperature to thermal infrared brightness temperature, using a

2.56 cm microwave radiometer and a Barnes PRT-5 infrared radiometer. He found strong correlation between emissivity and gravimetric soil moisture content for base surfaces, but much worse relationships for vegetated fields.

Burke and Paris (1975) and Burke et al. (1979) examined the dual-polarized signature of soil moisture at a wavelength of 2.8 cm. They found that moisture and suface roughness effects could be separated by comparing values of the first two Stokes' Parameters, $P = (1/2)(T_v + T_h)$, and $Q = (T_v - T_h)$. They found that Q was nearly invariant with temperature, and that it was very sensitive to soil moisture at gravimetric moisture contents less than 15 percent, while P was more sensitive at values above 15 percent, and was nearly invariant with viewing angle. Q was better correlated with surface roughness than was P.

Burke (1980) analyzed aircraft data at L-, X-, and K-band wavelengths, modeled the effects of the vegetation canopy, and investigated the effects of the atmosphere at these wavelengths. She found that the first Stokes parameter, $P = 0.5(T_v+T_h)$, was more sensitive to soil moisture than were T_v and T_h by themselves; and that the second Stokes parameter, $Q = T_v-T_h$, showed considerable scatter related to surface roughness. She observed that L-band was relatively insensitive to vegetation cover, but that the shorter wavelengths showed no response to soil moisture in the presence of vegetation.

Satellite-based Sensors

Satellites Available. Several satellites have carried microwave

sensors useful for soil moisture experiments. Among these have been SKYLAB, Nimbus 5, and Nimbus 7. Such data will also be available in the future, with the addition of a microwave sensor, the Special Sensor Microwave/Imager (SSM/I) to the DMSP spacecraft, expected in 1985.

SKYLAB carried a scanning Ku-band radiometer, the S193 instrument, which had a resolution of 11 km at nadir. SKYLAB also carried the S194 instrument, a non-scanning L-band radiometer.

Nimbus-5 had the electrically scanning Microwave Radiometer (ESMR), which scanned directly across the track direction, and had a resolution of 25 km at nadir. The sensor operated at a wavelength of 1.55 cm, with circular polarization.

The SMMR sensor on the Nimbus-7 satellite is described by Gloersen and Barath (1977) and by Madrid (1978) with wavelengths of 0.81, 1.36, 1.66, 2.80, and 4.54 cm, each operating in both horizontal and vertical polarizations. The absolute accuracy in all ten channels is better than 2 k rms. The 3 db beamwidths are, respectively, 0.8, 1.4, 1.5, 2.6, and 4.2 degrees. The resulting IFOVs are, respectively, 27x18, 46x30, 55x41, 91x59, and 148x95 km. The sensor uses a conical scan pattern so that the beam makes a nearly constant angle of about 50 degrees with the earth's surface. The satellite is in a near-polar orbit with an altitude of 955 km and a swath width of 822 km. SEASAT also carried a SMMR sensor.

The SSM/I sensor on the DMSP satellite has been described by Hollinger and Lo (1983). It will have wavelengths of 0.36, 0.81, 1.35, and 1.55 cm. All four wavelengths will have vertical polarization, and all

but the 1.35 cm channel will have horizontal polarization. The sensor will use a conical scan like that of SMMR, with a constant earth-incidence angle of 53.1 degrees. Resolution will range from about 15 km for the shortest wavelength to about 55 km for the longest. The satellite will be sun-synchronous like its predecessors and will view each point on the earth's surface twice daily, one at night and once in daylight. The satellite will be in a near-polar orbit with an altitude of 833 km. The swath width will be 1390 km. Several other satellites have carried microwave sensors, but no others have had scanning radiometers. The DMSP satellite is the only planned operational satellite-borne passive microwave imager.

Satellite Experiments. Several investigators have reported useful relationships between data from satellite-borne microwave radiometers and indicators of soil moisture.

Stucky (1975) found correlation coefficients near -0.9 between the brightness temperature from SKYLAB'S S193 KU-Band sensor and a 10-day API computed with a constant depletion coefficient of 0.9. He found that the correlation coefficient diminished almost linearly to about -0.2 as viewing angle increased to 40 degrees. He also found that for viewing angles less than 25 degrees, the 10-day API was better correlated with brightness temperature than was a 6-day API.

McFarland (1975 and 1976) reported excellent linear correlation between an 11-day API and brightness temperatures from the SKYLAB SL94 L-Band sensor. This sensor had a wavelength of 21 cm and a circular IFOV 115 km in radius. His data were from June and August of 1973, and he reported correlation coefficients of 0.97 and -073, respectively.

He explained the lower correlation of the August data as resulting from the spacecraft's flight over more varigated terrain, including the Texas High Plains an an area of dissected caprock.

Eagleman and Lin (1976) also related SKYLAB S-194 data to soil moisture. They correlated brightness temperatures with actual soil moisture samples collected in the field at times near the sensor overpass. They reported quadratic correlation coefficients very similar to the linear correlations of McFarland (1976). Interestingly, while many others have presented scatter plots showing the moisture insensitive region in the dry end of the moisture range, several of the figures in this paper showed a similarly insensitive region in the moist end, suggesting that there may be a minimum attainable emissivity for any given soil.

McFarland and Blanchard (1977), Theis (1979), and Blanchard et al. (1981) reported linear correlation coefficients exceeding 0.90 between emissivity estimated from Nimbus-5 ESMR brightness temperatures and soil moisture as represented by an API. They computed a normalized brightness temperature, which they called "emissivity", by dividing the brightness temperature by the daily maximum air temperature determined from weather records. They found the best correlations betwen emissivity and API in areas of winter wheat for the periods of near-bare soil conditions in fall and early spring. They also noted that the ESMR's side-to-side scan pattern, with consequent nonuniform viewing angle, led to problems of data interpretation. Schmugge et al. (1977) also reported a linear relationship between ESMR brightness temperature and antecedent rainfall totals for two test areas in Illinois-Indiana

and Oklahoma-Texas for periods when the soil was essentially bare.

Meneely (1977) found good correaltions between ESMR 1.55 cm horizontally polarized brightness temperatures and soil moisture expressed as percent of saturation for agricultural areas during periods when the soil had less than 40% vegetative cover. He found that additional vegetation badly degraded the relationship, and that regional empirical adjustments must be made to account for such local effects as soil type. He concluded that an independent estimate of soil temperature would be necessary. His measure of soil moisture was the model output for the top soil zone in the Versatile Budget Model of Baier and Robertson (1966).

McFarland and Harder (1982) found linear correaltion between emissivity as defined above and soil moisture indicated by an antecedent precipitation index (API). They further demonstrated that the scatter in the relationship could be described probabilistically in terms of value to classical decision theory, and that the "noisy" data could be used successfully in a discriminant analysis method of determining the antecedent precipitation category to which a given scene belonged.

McFarland and Harder (1983) used Nimbus-5 ESMR data to monitor soil moisture for essentially bare agricultural soils. They noted that the emissivity for frozen or snow-covered soils was distinctly different from that of bare unfrozen soil, giving a potential to discriminate between snow covered and bare unfrozen soils. They noted further that the radiometer responded to the moisture stress of crops when the canopy had developed enough to obscure the soil moisture signal, and the vegetation response was in the same sense as the variation from

soil moisture; thus, soil moisture conditions would be inferred from microwave data even when the soil itself was not directly viewed by the sensor.

Resolution of Satellite Sensors. Several authors have published results indicating that spatial resolutions attainable from space will be useful. Spaceborne sensors can provide resolutions of the same order as that of the rainfall events that contribute to soil moisture variations. Furthermore, degraded resolution does not result in less accurate information - only less detailed information.

Hardy et al. (1981) studied the spatial variability of rainfall amounts in order to determine the utility of hypothetical microwave - derived estimates of soil moisture at resolutions of 10 km and 1 km. They concluded that a 10 km sensor could adequately describe the shape of most precipitation events, but would probably underestimate the peak rainfall near the storm center. They also concluded that most U. S. government agencies now using soil moisture estimates could benefit from estimates at 10 km resolution. Although they did not report on the ability of lower resolution microwave sensors to delineate rainfall patterns, they did indicate that the rainfall amount at a distance of 10 km from most storm centers is greater than 50 percent of the central value and that the gradients of rainfall amount are weak outside of 5 km radius. They also noted that currently operational soil moisture models in government agencies use temperature and precipitation data from reporting stations with spacing on the order of 100 km. Thus, sensors with a resolution of 10 to 30 km would be an improvement over current practice.

In fact, Schmugge et al. (1976) stated that 10 km resolution will be feasible. They calculated that even an L-band sensor could be orbited at space shuttle altitude (400 km) and attain a 10 km resolution if its antenna dimensions were 10 m by 10 mi.

The effect of degraded resolution has been studied. Newton et al., (1982) simulated an array of three orbiting passive microwave sensors operating in X-band, C-band, and L-band. They found that the three sensors should have soil moisture sensitivities of respectively, -0.50, -0.85, and -1.5 k per percent soil moisture, under the assumption that the entire area of each sensor footprint had uniform moisture, and under the restriction that less than 40 percent of the footprint was forest. They found, contrary to expectations, that the sensitivity to soil moisture increased as the simulated sensor's resolution was degraded, and that the variability of sensitivity was greatest at a resolution of 20 km. Resolutions of 5 and 60 km produced equal variabilities.

McFarland and Harder (1982) demonstrated the effect of resolution, using data from the ESMR sensor on Nimbus-5. They simulated a resolution of about 50 km, by averaging the values of emissivity and API from five neighboring pixels. The resulting correlations between emissivity and API were as good or better than the original correlations for data with a resolution of 25 km, which showed that microwave data at any resolution respond to the area-weighted average soil moisture throughout the IFOV.

Retrieval of Geophysical Information. The most common information-retrieval algorithm used to date has been simple linear regression,

since the ESMR sensor had only one data channel. With the introduction of dual-polarization, multi-frequency sensing on Nimbus-7 and DMSP, more refined techniques are being developed. In fact, the thrust of most future research in satellite borne passive microwave sensing of soil moisture will be the development of better information retrieval algorithms. Most of the newer retrieval methods that have been used or planned for these newer satellite systems consist of some variation on multiple linear regression analysis, by which empirical coefficients are determined for each location and for each time of year.

Pandey and Kakar (1983) presented an efficient alogorithm for selecting the best fixed-size subset of the ten SEASAT SMMR data channels, to be used in a multiple linear regression model for retrieval of geophysical parameters. Their method used a large number of model atmospheres to circumvent the need to actually calculate multiple linear regressions for all of the possible combinations of n data channels. They illustrated the technique with retrieval of sea surface temperatures.

Spencer et al. (1983) employed a stepwise multiple linear regression approach to infer rainfall rates over land in the American Great Plains using Numbus 7 SMMR data. They found that the most useful channels were the 0.81 and 1.36 cm bands in both polarizations. Longer wavelengths added little to the variance explained by these shorter wavelengths. Unfortunately, they did not report results of significance tests. Nor did they indicate any theoretical support for a linear model. They reported an ability to discriminate between falling precipitation and either wet soil or water bodies on the basis of the

difference between vertical and horizontal polarizations at the 0.81 cm wavelength.

Burke and Ho (1981) presented a demonstration of the Statistical Parameter Inversion Method of Gaut (1967) and Burke and Ho (1981). They showed that the method can retrieve soil moisture for the 0-2 and 2-5 cm layers with an accuracy of about 5-6 percent for bare fields and grass-covered fields, using both polarizations of 21 cm and 2.8 cm microwave brightness temperatures. Their results did not improve when they accounted for the temperature dependence of brightness temperature by dividing the latter by the surfacetemperature. They suggested that this unexpected result may have been caused by the longer wavelength's response to soil temperatures deeper than the surface. One of their appendices gave the FORTRAN source code for the SPIM program and its subroutines. This algorithm has been selected for use with the SSM/I sensors on the DMSP satellites. Hollinger and Lo (1983) reviewed work done to date on the software for handling data from the SSM/I. They indicated that soil moisture retrievals will use only the 1.55 cm wavelength in both polarizations, using the SPIM developed at Environmental Research and Technology, Inc., as described above. They showed a graph of expected soil emissivity as a function of moisture content. They gave a brief discussion of the retrieval algorithm, which they call the "'D' matrix" method, due to the procedure of inverting a correlation matrix.

MATERIALS AND METHODS

Data Source

Passive Microwave Data

Computer tapes with one year's data (25 Oct 78 - 10 Nov 79) from the Nimbus-7 Scanning Multichannel Microwave Radiometer (SMMR) were provided by NASA's Goddard Space Flight Center. Nimbus-7, as described by Gloersa and Barath (1977) and by Madrid (1978), is a polar orbiting satellite that provides repeat coverage of each point of interest every two or three days on average. The spacecraft views the earth on both night and day passes, with average local observation times of about 0100 and 1100, respectively, with actual times varying as much as an hour or two from those values. The SMMR instrument, unlike the previous ESMR, uses a conical scan method so that it views the earth from a constant angular height about 50 degrees from the local zenith. Brightness temperatures in both horizontal and vertical polarizations were obtained from each of five wavelengths, of which the central wavelength, 1.66 cm, was used in this study in both vertical and horizontal polarizations.

The data tapes also provided the nominal latitude and longitude of each IFOV. These coordinates were assumed accurate. Spencer et al. (1983) did find sufficient control points in their SMMR analysis area, but the largest registration error they found was no more than one 18x27 km IFOV of the 0.81 cm sensor. Since the IFOV for the 1.66 cm

data used in this study was 41x55 km, such positioning errors were assumed negligible.

Climatic Data

Tapes of weather data were purchased from the National Climatic Data Center. Climatic data extracted from the tapes were daily values of maximum and minimum temperature, total precipitation, snowfall, and snow depth, from stations in the cooperative observing network.

Ancillary Data

Copies of National Weather Service weather radar summary charts were obtained for all SMMR overpass times, for use as a screening file to infer possible contamination of the soil moisture signature by precipitating clouds. USGS topographic and land use maps were used, along with reported crop production statistics, to select locations for case studies of individual time series plots.

Data Base Preparation

Objective Analysis of SMMR and Climatic Data

Two study areas were defined, with data windows and analysis grids as shown in Fig. 2. The data windows were the areas within which any data present were used in the analysis. The analysis grids were defined with 20 km square grid cells arrayed in 35 rows of 40 columns. Each grid cell was identified by its row and column number. Rows were numbered from 1 to 35, from the top, and columns were numbered from 1 to 40 from the left. Each study grid was a polar stereographic map projection.

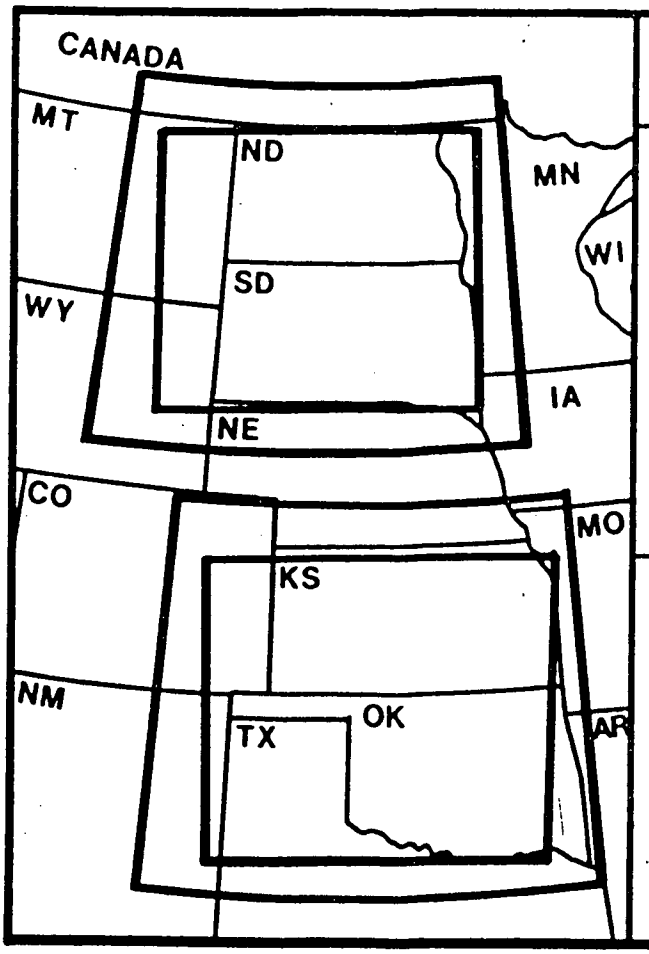

SPECIFICATIONS

20-KM GRID	NORTH	SOUTH
STANDARD		
LATITUDE	46.0	37.0
LONGITUDE	-100.0	-100.0
NW CORNER		
LATITUDE	48.8	39.8
LONGITUDE	-106.5	-104.0

DATA WINDOW	NORTH	SOUTH
MAX LAT	50.0	41.0
MIN LAT	42.0	33.0
MAX LON	-95.0	-94.0
MIN LON	-107.5	-105.0

Figure 2. Definition of study areas for database development. Standard latitude is that for which the scale is true. Standard longitude is a reference value near the center of the grid. "NW Corner" refers to the coordinates of the center of the grid cell at row 01, column 01. Data windows are the areas within which SMMR and climatic data were used to derive objectively analyzed fields for the grids.

This investigation was restricted to data from the southern area, which is shown in detail in Fig. 3.

SMMR and climatic data were analyzed objectively to these two grids, using an algorithm similar to that of McFarland and Blanchard (1977). This method used an exponential weighting function to interpolate nearby observations to the center of each grid cell. Separate shape parameters were selected, by trial and error, for brightness temperatures, air temperatures, and the precipitation variables, to minimize unnecessary smoothing of the data fields while avoiding holes in regions of sparse data. Further details of the analysis algorithm have been reported by Harder and McFarland (1984).

The output SMMR map files were structured in ten-channel band-interleaf format. That is, the first record had 40 bytes representing the 40 brightness temperatures of the northernmost row for the first channel (0.81 cm, horizontal polarization); the second record represented row one for the second channel, etc. The entire file comprised 350 records, representing 10 channels for each of 35 rows of pixels. Each byte held one brightness temperature, expressed in kelvins (minus 180) as an integer between -128 and +127 inclusive, with the value of -128 representing missing data.

The output climatic data map files were structured in five-channel band-interleaf format, with the following channels: maximum temperature, minimum temperature, precipitation, snowfall, and snowdepth. As for SMMR data, values were stored on-per-byte, with temperature expressed in degrees Celsius multiplied by 2.5, precipitation expressed as millimeters minus 126 and the snow variables as centimeters minus

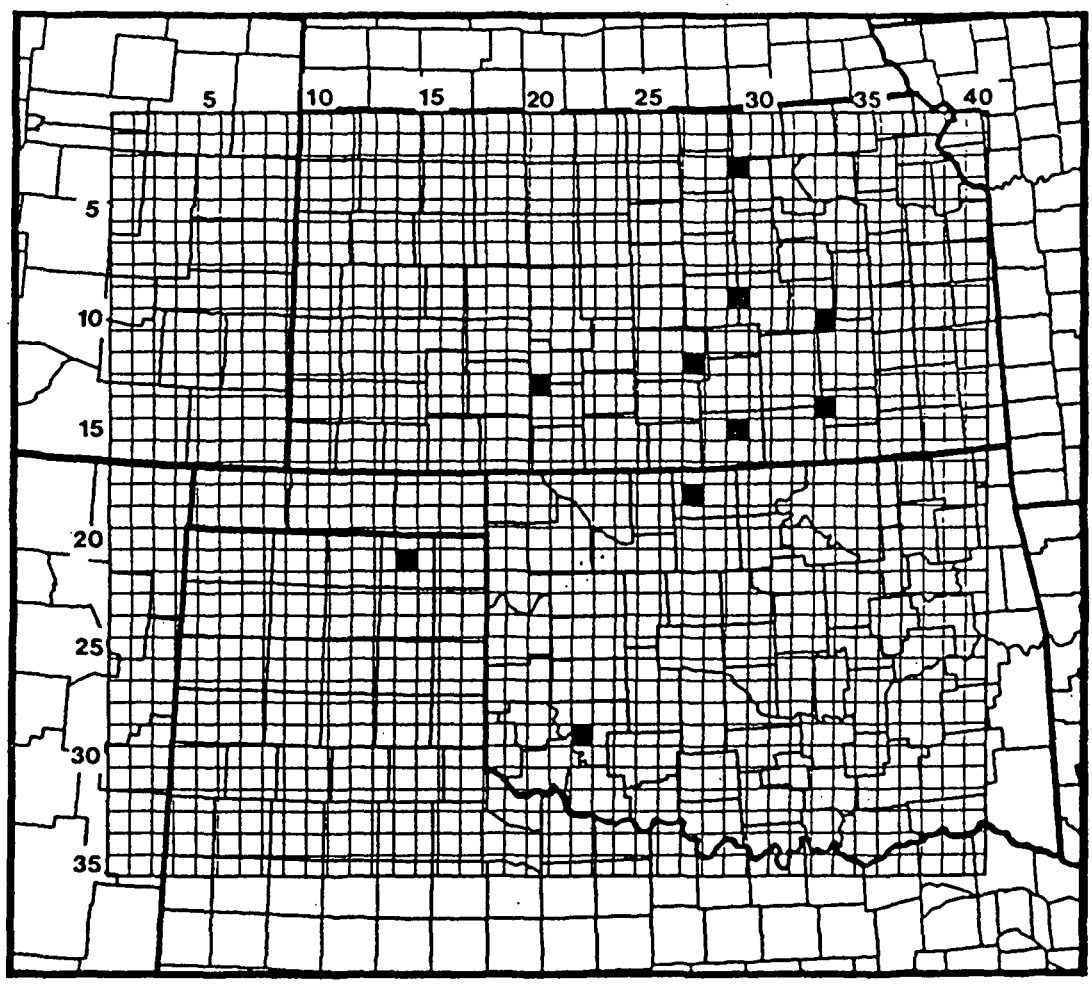

Figure 3. Detail of the southern study area. The locations of case study grid cells are darkened.

126. All values were rounded to the nearest integer, and the value of -128 reserved for a missing data indicator.

Antecedent Precipitation Index

An API was computed using an algorithm from McFarland and Blanchard (1977). The model was defined as :

$$API(i) = k^* API(i-1) + P(i)$$

Where k = depletion coefficient (9)

P = effective precipitation

The depletion coefficient was defined here as a sinusoid with a maximum value of 0.92 occurring on 1 February and a minimum of 0.70 occurring on 1 August. This range of K-values was arbitrarily selected for consistency with McFarland and Blanchard (1977). The effective precipitation was computed by raising the precipitation, in millimeters, to a power of 0.891, following Blanchard et al. (1980). This formulation of API thus represents the land-use, drainage, and meteorological conditions in Oklahoma where the work of McFarland and Blanchard (1977) and Blanchard et al. (1980) was done. For those days when snow depth was nonzero, API was held constant and all precipitation was assumed to accumulate as snow cover. On the first date with zero snow depth, the accumulated precipitation was added as effective precipitation, again using Blanchard's exponent. The API was initialized at a value of 50 mm for 1 July 1978, more than 100 days prior to the first SMMR data.

Map files of API were prepared for all dates from 1 July 1978 to 11

November 1979. The format of each file was similar to that of the SMMR and climatic map files, except that API map files had only one channel of data.

Prospective Microwave Indices of Soil Moisture

Fifty four functions of Microwave brightness temperatures, surface temperature, and/or day of the year were identified as possible indicators of soil moisture. These prospective indices are summarized in Table 1. Indices in the first group (ϕ_1 through ϕ_{18}) were suggested on

Table 1. Prospective Indices of Soil Moisture.

$\phi_{01} = [\sin(B*(DAY-DO)) + 1.0]$
$\phi_{02} = [T]$
$\phi_{03} = [T_h]$
$\phi_{04} = [T_v]$
$\phi_{05} = [T_h/T]$
$\phi_{06} = [T_v/T]$
$\phi_{07} = [T_v-T_h)]$
$\phi_{08} = [T_v-T_h)/T]$
$\phi_{09} = [T_v-T_h)/T_h)]$
$\phi_{10} = [T_v-T_h)/T_v]$
$\phi_{11} = [2.0*(T_v-T_h)/(T_v+T_h)]$
$\phi_{12} = [T_v+T_h)/2.0]$
$\phi_{13} = [T_v+T_h)/(2.0*T)]$
$\phi_{14} = [T_v+T_h)/(2.0*T_h]$
$\phi_{15} = [T_v+T_h)/(2.0*T_v]$
$\phi_{16} = [T_v-T_h)*2.0*T/(T_v+T_h)]$
$\phi_{17} = [T_v-T_h)*2.0*T_v/(T_v+T_h)]$
$\phi_{18} = [T_v-T_h)*2.0*T_v/(T_v+T_h)]$
ϕ_{18} to ϕ_{36} = sqrt[ϕ_{01} to ϕ_{18}]
ϕ_{37} to ϕ_{54} = square[ϕ_{01} to ϕ_{18}]

B = $2\pi/365$
DO = 32.0 + 365.0/4.0
DAY = Day of year (1-365)
T = Temperature
T_h = H-polarized Brightness Temp
T_v = V-polarized Brightness Temp

the basis of theory or previous experiment, and each incorporate one or more model coefficients to be derived empirically. The other indices listed are the square root or square of one of these basic indices.

These indices were numbered, for reference, and were called "phi" indices, represented either by the Greek letter ϕ and a subscript, or by the Roman letters "PHI" followed by a Number.

ϕ, a sinusoidal function of the day of the year, was included in case the soil moisture time series turned out to be partially composed of a simple cyclic function as a result of seasonal variations of precipitations and potential evapotranspiration.

ϕ_{02}, ϕ_{03}, and ϕ_{04} are simply the thermodynamic temperature of the air and the horizontally and vertically polarized brightness temperature. ϕ_{05} and ϕ_{06} are temperature normalized forms of the horizontally and vertically polarized brightness temperatures. These functions, as noted by McFarland and Blanchard (1977), represent approximations of the horizontally and vertically polarized emissivity of the emitting layer. They will be termed "emissivities" here.

ϕ_{07} is the simple difference between the polarization components and is termed here "polarization" or "polarization difference". ϕ_{08}, ϕ_{09}, ϕ_{10}, and ϕ_{11}, are various normalized versions of this index.

ϕ_{12}, is the mean of the the polarized components, and ϕ_{13}, ϕ_{14}, and ϕ_{15} are normalized forms of ϕ_{12}. ϕ_{16}, ϕ_{17}, and ϕ_{18} are the ratios of the polarization difference to various normalizations of the mean of the two polarized components. Conceptually, these indices are ratios of polarization to various indices of emissivity.

Analysis Methods

Temporal Analysis

Statistical analyses of data in the time domain were performed for the ten case study grid cells shown in Figure 3. These grid cells are also listed in Table 2.

TABLE 2

Case Study Grid Cells

ROW	COLUMN	LAND USE	STATE	COUNTY	1980 WHEAT AREA
09	29	Agriculture	KS KS	McPherson Marion	45% 27%
03	29	Agriculture	KS KS	Cloud Clay	36% 29%
10	33	Range	KS	Chase	6%
12	27	Mixed Ag, Range, Water	KS	Reno	42%
13	20	Mixed Ag, Range	KS KS	Edwards Kiowa	28% 22%
14	33	Range	KS	Elk	5%
15	29	Agriculture	KS	Sumner	66%
18	27	Agriculture	OK	Grant	65%
29	22	Agriculture	OK	Kiowa	41%
21	14	Agriculture	TX	Ochiltree	42%

Wheat areas listed are county land area percentage planted to non-irrigated winter wheat, computed from county land areas and crop acreages reported in the county agricultural statistics published annually by the state Crop and livestock Reporting Services.

These wheat acreage data are presented graphically in Figure 4. A single grid cell, located at Row 9, Column 29, was selected for initial screening. This grid cell was selected on the basis of its predominantly agricultural land use and the moderately high wheat area fractions of the two surrounding counties. Three of the fifty-four indices were chosen as a result of analysis of data from this single grid cell. These three indices were then tested on six additional grid cells in Kansas. These grid cells were chosen to represent a range of land use types and were separated by at least two grid cell widths, since the SMMR sensor IFO was approximately equal in area to four grid cells. Finally, observations from these analyses were verified using independent data from the last three grid cells, located in Oklahoma and Texas. These three grid cells were chosen on the basis of their high wheat area fractions.

Time domain analyses were performed for each of several seasons, as well as for the entire year. The year was divided into five seasons of 61 days each, followed by one season of 60 days. These seasons were referred to by number, from 1 to 6. They were also identified by month, season 1 corresponding roughly to January and February, season 2 to March and April, etc. When analyses were done for the entire year, the period was denoted "Season 0 (Full Year)". Analyses methods consisted of simple and multiple linear regression, including principal

SOUTHERN STUDY AREA

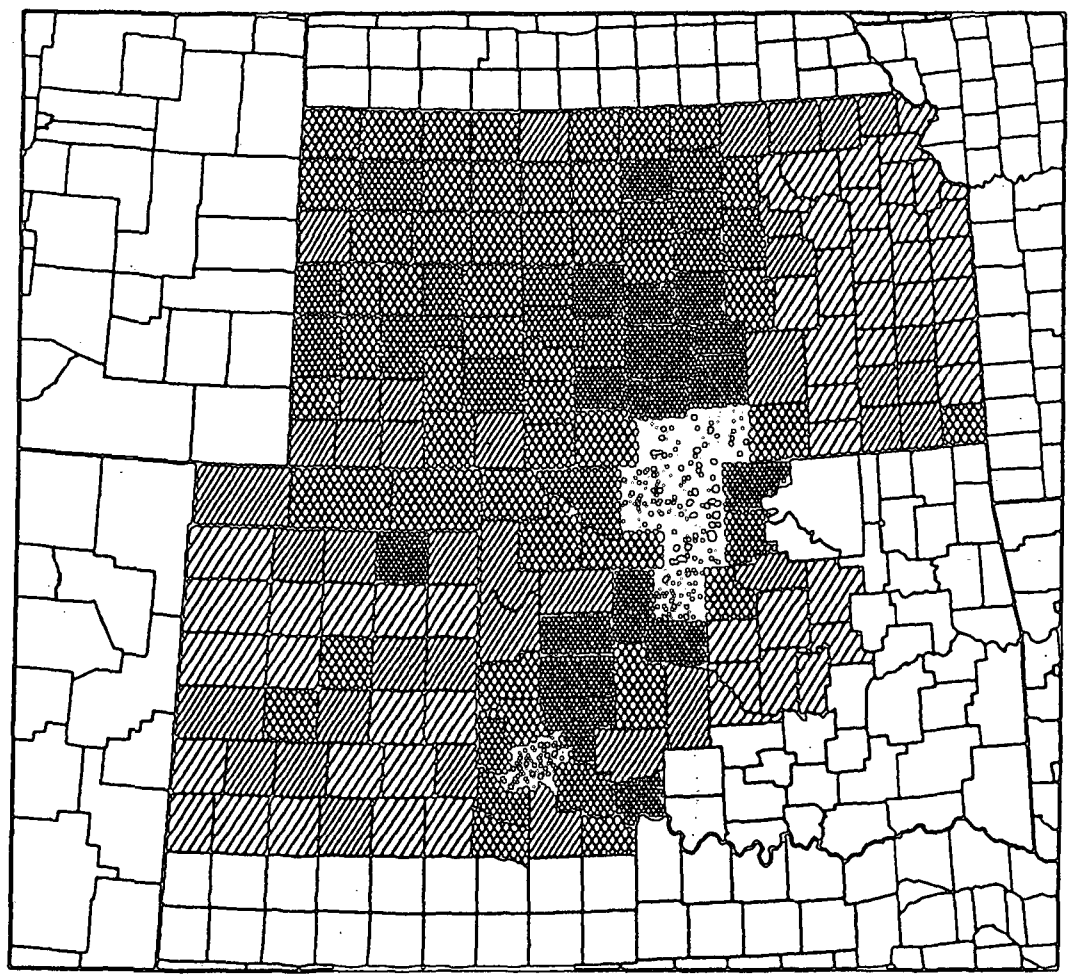

Figure 4. 1980 county land area fractions planted in dryland wheat for Kansas, Oklahoma, and Northwest Texas.

component analysis.

In all cases, the regression analyses were accompanied by calculation of two-way contingency tables. Three categories of API were defined, as follows:

CAT1: [API < 10 mm]

CAT2: [10 mm <= API < 20 mm]

CAT3: [20 mm <= API]

These categories were defined arbitrarily, to demonstrate the indices' skill in categorical estimation. Tables were constructed to show the frequency of occurrence of the nine different combinations of API categories and estimate of API from the regression models. For each such table, the fraction of correct model-estimated categories was computed and expressed as percent correct.

The results of the temporal analyses were presented graphically in two ways. Scatter plots were prepared, using a standard presentation with API on the vertical axis and model estimate of API on the horizontal. This method allowed a common graphical appearance for the different indices, which would not have been possible using the more common presentation with the independent variable on the horizontal axis. Additionally, time series plots were prepared, showing the temporal variation of both API and model estimate of API.

Correlation coefficients were compared using the Fisher Z' transform described by Brooks and Carruthers (1953). Specifically,

$$Z' = \frac{1}{2} \ln \left(\frac{1+r}{1-r}\right) \qquad (10)$$

where r is any correlation coefficient. This Z' statistic has an approximately normal distribution, with standard error given by

$$S.E._{Z'} = \frac{1}{\sqrt{n-3}} \tag{11}$$

where n is the number of observations from which the correlation coefficient was computed. These equations can be used in two ways. First, a value of Z' can be compared with zero to determine whether a regression has statistical significance. Second, given one correlations coefficient, a confidence interval on Z' can be constructed, and the limiting values can be transformed back to correlation coefficients using the inverse of (10):

$$r = \frac{\exp(2Z')-1}{\exp(2Z')+1} \tag{12}$$

Spatial Analysis

Spatial analysis consisted of visual comparison of maps of rainfall generated API and maps of API estimates from regression models. This imagery was prepared for illustrative purposes, and is not subjected to rigorous statistical tests. The regression model API images were generated with regression coefficients computed for each individual grid cell. For grid cells where the correlation coefficient was statistically insignificant, the resulting image data holes were filled by using the average of model coefficients for the entire area. The validity of this hole-filling strategy was verified subjectively by comparison of the resulting spatial patterns with the API

map. An additional set of images was produced using the area mean coefficients at all pixels. Both sets of imagery were produced for seasonal as well as annual regression models. The validity of this method, too, was checked subjectively by inspection of the patterns produced. Finally, the correlation coefficients were displayed as images. A sample case study for 10 May 1979 is reproduced here.

ANALYSIS AND DISCUSSION

Temporal analysis

Temporal analyses consisted of simple linear regressions, principal component analyses and multiple linear regression. The analysis proceeded in three phases. Initial screening used a single Kansas grid cell selected for its moderately high wheat acreage. The three indices selected in this first phase were then tested on six additional Kansas grid cells representing a variety of land use types. Finally, the conclusions from the second phase were verified using three independent grid cells in winter wheat regions of Oklahoma and Texas.

Phase I: Initial Screening

The first results are summarized in Table 3 from data presented in the appendix, tables D-1 through D-6. These tables were prepared for the entire year (Season 0) and for Seasons 2 through 6. Season 1 had insufficient data for analysis. Table 3 shows the correlation coefficients from the regressions of API upon each of the first 18 ϕ indices. Tables D-1 through D-6 additionally show the minimum significant absolute-value correlation coefficient and the interval [L,U] corresponding to the lower and upper bounds of the 95 percent confidence interval on Fisher's Z' transform.

The square-root and squared indices are not shown in Table 3, because they performed no differently than did their respective basic indices. In every case, the coefficients of the square-root and

TABLE 3

Correlation Coefficients Between API and Indices South, Row 09, Column 29.

SEASON

	0	2	3	4	5	6
ϕ_1	-0.37*	-0.93	-0.33*a	-0.20*a	-0.26*a	+0.04*a
ϕ_2	-0.25*	-0.10*a	-0.40*a	-0.10*a	-0.14*a	-0.69*
ϕ_3	-0.70*	-0.87*	-0.55	-0.58	-0.70	-0.90
ϕ_4	-0.59*	-0.72*	-0.39*a	-0.36*a	-0.62*	-0.80
ϕ_5	-0.81	-0.96	-0.35*a	-0.81	-0.82	-0.85
ϕ_6	-0.72*	-0.89	-0.05*a	-0.47*	-0.83	-0.57*
ϕ_7	0.75	0.93	0.76	0.72	0.70	0.80
ϕ_8	0.74	0.93	0.79	0.72	0.70	0.82
ϕ_9	0.76	0.93	0.78	0.74	0.73	0.82
ϕ_{10}	-.76	0.93	0.78	0.73	0.73	0.82
ϕ_{11}	0.76	0.93	0.78	0.73	0.73	0.82
ϕ_{12}	-0.66*	-0.82*	-0.48*	-0.49	-0.67	-0.87
ϕ_{13}	-0.80	-0.95	-0.17*a	-0.72	-0.84	-0.80
ϕ_{14}	0.76	0.93	0.78	0.74	0.73	0.82
ϕ_{15}	-0.76	-0.93	-0.78	-0.73	-0.73	-0.82
ϕ_{16}	0.77	0.93	9.76	9.73	9.73	0.81
ϕ_{17}	0.75	0.93	0.76	0.71	0.69	0.81
ϕ_{18}	0.75	0.93	0.76	0.72	0.70	0.80
Sample size	102	17	18	20	27	19

a - correlations were not significant at the 0.05 level.
* - correlations that differed significantly, at the 0.05 level, from the highest absolute value in the column.

squared indices were well within the interval [L,U] of the basic index. Subsequently, only the first 18 ϕ indices were considered.

These remaining 18 ϕ indices were grouped into three performance categories: weak, moderate, and strong.

The first category, that of weak performance, was assigned to ϕ_{01} and ϕ_{02} which had correlations with API that were insignificantly different from zero in the majority of Seasons 2 through 6. In Season 0, correlation coefficients were statistically significant, but they explained very little variance.

The second category, that of moderate performance, was assigned to the unnormalized brightness temperatures, ϕ_{03} and ϕ_{04}, to their mean, ϕ_{12}, and to the vertically polarized emissivity, ϕ_{06}. These results were consistent with theory presented previously. Since soil moisture content is related to emissivity through the Fresnel reflection coefficients, and since the Rayleigh-Jeans approximation allows emissivity to be expressed as the ratio of brightness temperature to thermodynamic temperature, the unnormalized brightness temperatures should not indicate moisture as well as would an appropriately normalized brightness temperature. Thus, air temperature is seen to be a useful approximation to the emitting layer temperature, as stated by McFarland and Blanchard (1977). The inferior performance of the vertically polarized emissivity can be explained by the fifty-degree viewing angle of the sensor, very near the Brewster angle at which the vertical component peaks regardless of dielectric constant. The vertical component is thus constrained to be less sensitive to soil moisture content than the horizontal component, which is unaffected by the Brewster angle.

The remaining 14 ϕ indices comprised the category of strong indices. Of these, the best was usually ϕ_{05}, the horizontally polarized emissivity used by McFarland and Blanchard (1977). None of the other indices' correlations with API were significantly different in annual analysis, but they exhibited more variability in the seasonal analyses. In fact, the "best" annual index, ϕ_{05}, was again the best in Season 2 and one of the worst in Season 3. In the other seasons, it was not very different from its annual value. In Seasons 5 and 6, when it was not "best", it was insignificantly different from the best. This erratic performance was duplicated by ϕ_{13}, the mean of ϕ_{05} and ϕ_{06}. The other indices, whether including or excluding the ground-sensed temperature, showed somewhat more stable performance annually and in seasonal analysis, and frequently had correlation coefficients numerically lower than that of ϕ_{05}, but never significantly so.

Another observation was that several of the correlation coefficients for individual seasons were higher than for the year as a whole. For instance, the correlation coefficient for ϕ_{05} was -0.81 in annual analysis, but -0.96 in Season 2. Figure 5 shows the annual and seasonal correlation coefficients for regressions of API upon each of three of the stronger indices. These values are plotted as heavy dots. The vertically oriented boxes depict, by their widths, the correlation values corresponding to the 95% confidence limits of the Fisher Z' transform. Similar confidence limits are shown by horizonal lines for each of Seasons 2 through 6. In most cases, annual and seasonal correlations are indistinguishable.

This point is further illustrated by the Z' transform values

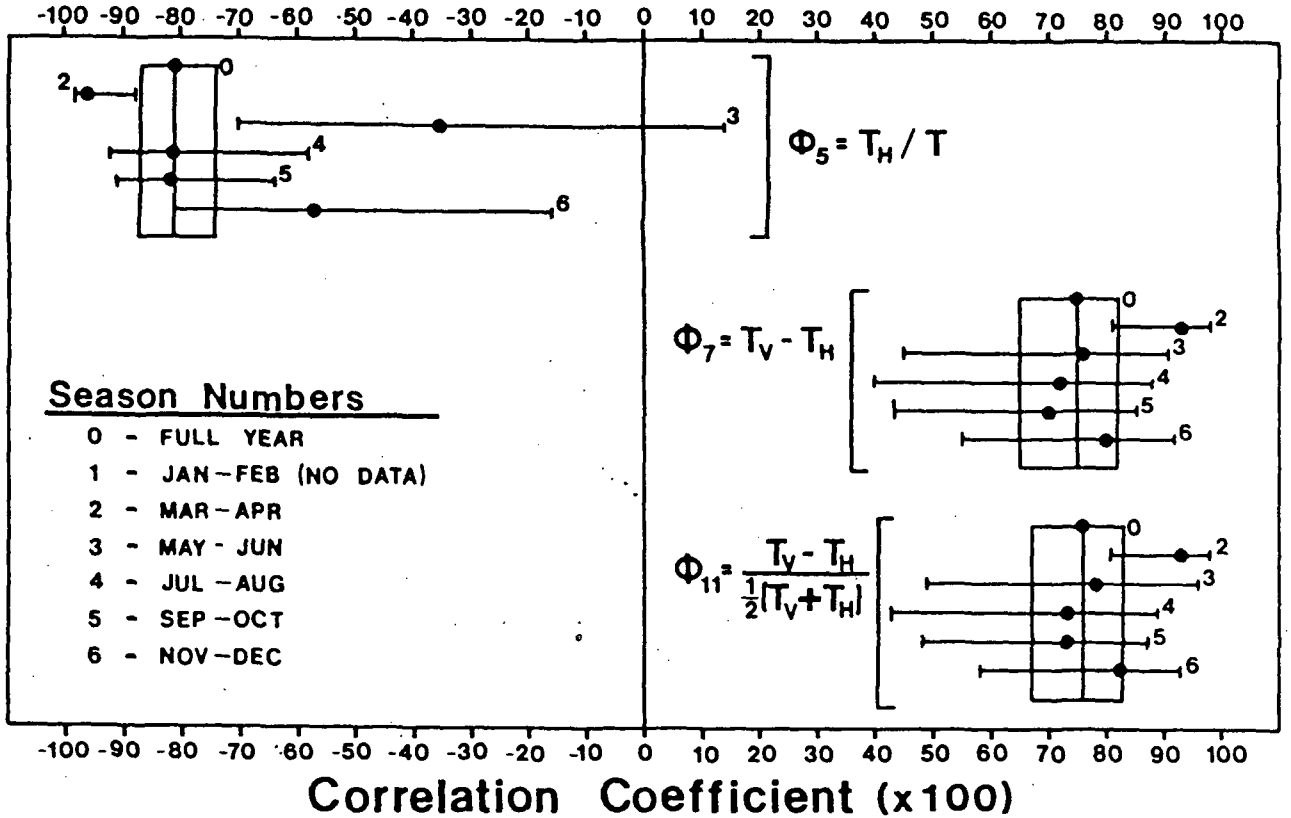

Figure 5. Comparison of annual and seasonal correlation coefficients and their 95% confidence limits based upon the Z' transform, for regressions of API upon each of three indices at row 9, column 29, southern study area.

themselves. For instance, the Z' value for ϕ_{05} was eleven standard errors different from zero in annual analysis. It was only seven standard errors from zero in Season 2. It would be consistent with theory if these indices performed better in early spring before the establishment of a dense vegetation canopy, Nevertheless, it would be difficult to conclude from these data alone that seasonal analysis is definitely more useful than annual analysis. This point will be illustrated later, with reference to the scatter plots of time-series data.

The next step added multiple linear regression and principle components analyses and was restricted to thirteen of the eighteen basic indices. Specifically included were indices ϕ_{01}, ϕ_{02}, and ϕ_{05} through ϕ_{15}. This list included strong, moderate, and weak indices, in case the weaker indices might be found to respond to soil moisture information absent in the stronger indices. The annual and seasonal multiple linear regressions of API on these indices failed due to ill-conditioned matrices. The decomposition into subsequent multiple regression on the first four components failed, again due to ill conditioned matrices. Table 4 shows the Season 0 variance-covariance matrix, which indicated that the strong indices were very well correlated with each other; hence they could not be expected to differ significantly in their information content. Subsequent analyses eliminated many of these indices for that reason.

The next run was restricted to only five indices: ϕ_{01}, ϕ_{05}, ϕ_{06}, ϕ_{07}, and ϕ_{11}. The results for Season 0 (full year) are summarized in Table 5. The multiple regression did not improve the correlation over

TABLE 4

Variance-Covariance Matrix for 13 Indices,

Season 0, Row 09, Column 29

PHI INDEX													
01	1.0												
02	0.6	1.0											
05	0.5	0.2	1.0										
06	0.3	0.0	0.9	1.0									
07	-0.6	-0.4	-0.9	-0.6	1.0								
08	-0.6	-0.5	-0.9	-0.6	1.0	1.0							
09	-0.6	-0.4	-0.9	-0.6	1.0	1.0	1.0						
10	-0.6	-0.4	-0.9	-0.6	1.0	1.0	1.0	1.0					
11	-0.6	-0.4	-0.9	-0.6	1.0	1.0	1.0	1.0	1.0				
12	0.7	0.8	0.8	0.5	-0.8	-0.8	-0.8	-0.8	-0.8	1.0			
13	0.4	0.1	1.0	1.0	-0.8	-0.8	-0.9	-0.8	-0.8	0.7	1.0		
14	-0.6	-0.4	-0.9	-0.7	1.0	1.0	1.0	1.0	1.0	-0.8	-0.9	1.0	
15	0.6	0.4	0.9	0.6	-1.0	-1.0	-1.0	-1.0	-1.0	0.8	0.8	-1.0	1.0

PHI INDEX	01	02	05	06	07	08	09	10	11	12	13	14	15

TABLE 5

Temporal Analysis of Five Indices
South Area, Row 09, Column 29
Season 0

MULTIPLE CORRELATION COEFFICIENT: 0.83

REGRESSION COEFFICIENTS:

PHI_01:	0.551
PHI_05:	41.8
PHI_06:	-25.2
PHI_07:	-6.15
PHI_11:	37.6
INTERCEPT:	8.76

VARIANCE-COVARIANCE MATRIX:

INDEX	ϕ_1	ϕ_{05}	ϕ_{06}	ϕ_{07}	ϕ_{11}
ϕ_{01}	1.0				
ϕ_{05}	0.5	1.0			
ϕ_{06}	0.3	0.9	1.0		
ϕ_{07}	-0.6	-0.9	-0.6	1.0	
ϕ_{11}	-0.6	-0.9	-0.6	1.0	1.0

PRINCIPAL COMPONENTS ANALYSIS:

PROMINENT EIGENVECTORS:

	ϕ_{01}	ϕ_{05}	ϕ_{06}	ϕ_{07}	ϕ_{11}
1:	0.33	0.50	0.41	-0.49	-0.49
2:	0.80	-0.23	-0.55	-0.08	-0.07
3:	0.51	0.05	0.59	0.46	0.42

FACTOR LOADINGS:

	ϕ_{01}	ϕ_{05}	ϕ_{06}	ϕ_{07}	ϕ_{11}
1:	0.64	0.98	0.80	-0.96	-0.96
2:	0.70	-0.20	-0.48	-0.07	-0.06
3:	0.31	0.04	0.36	0.28	0.26

MULTIPLE REGRESSION ON 3 PRINCIPAL COMPONENTS:

MULTIPLE CORRELATION COEFFICIENT: 0.82

SIGNIFICANT (AT ALPHA=0.05): EIGENVECTOR 1
EIGENVECTOR 2

MULTIPLE REGRESSION ON 2 SIGNIFICANT COMPONENTS:

MULTIPLE CORRELATION COEFFICIENT: 0.82

REGRESSION COEFFICIENTS:

EIGENVECTOR 1:	-4.66
EIGENVECTOR 2:	2.47
INTERCEPT:	8.76

any of the single linear regressions of the previous analysis. This suggested that any possible improvement to the coefficient of 0.82 was no worse than that of the previous analysis with five indices. Consequently, any soil moisture information present in weaker indices but not shared by the strong ones must be inaccessible to a simple linear combination algorithm. Again, the strong indices were well correlated, as indicated by both the variance-covariance matrix and the factor loadings. The two significant eigenvectors do not add to the explanation of the variance. The first merely restates the equivalence of the three strong indices. The second depends heavily on the two weak indices, neither of which is singly important in estimating API. Finally, the multiple correlation coefficient from the regression of API on the two significant eigenvectors did not differ from the simple correlation coefficient from ϕ_5. Subsequently, the multiple regression and principal component analyses were omitted.

The annual regression analyses for row 09, column 29, have been illustrated graphically in Figures 6, 7 and 8. These are scatter plots showing points plotted at coordinates given by the API and the regression model estimate of API. On these graphs, a diagonal line has been drawn for reference. Some care must be taken in interpreting these graphs. The diagonal line is the one-to-one ratio line, not the regression line. Furthermore, the abscissa is not the independent variable, ϕ_i; rather, it is the regression model estimate of API. This format was adopted to enable direct comparison of graphs for the three separate indices. Similar graphs for Seasons 2 through 6 are shown in Appendix A.

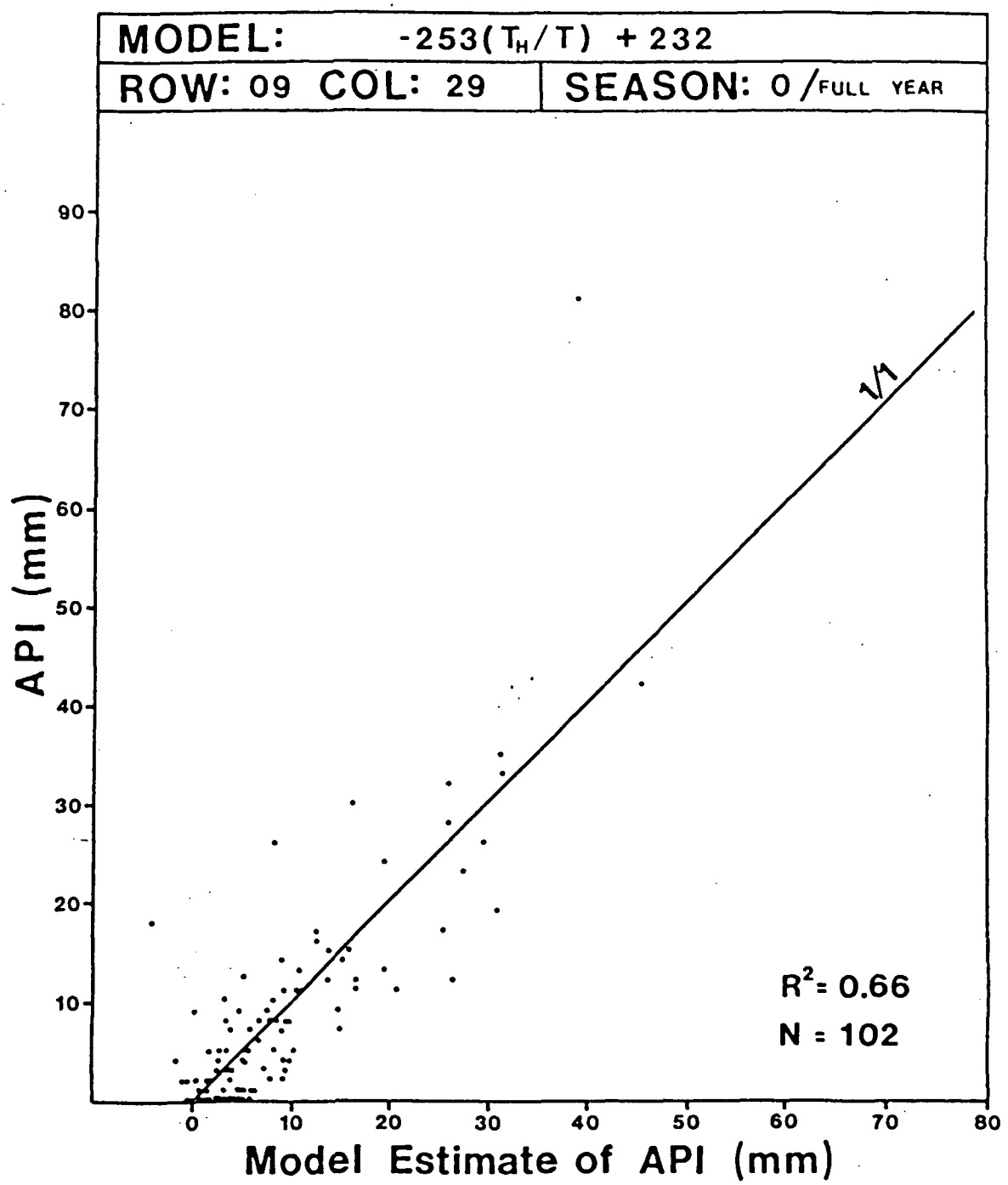

Figure 6. Regression of API of ϕ, season 0, row 09, column 29, south area.

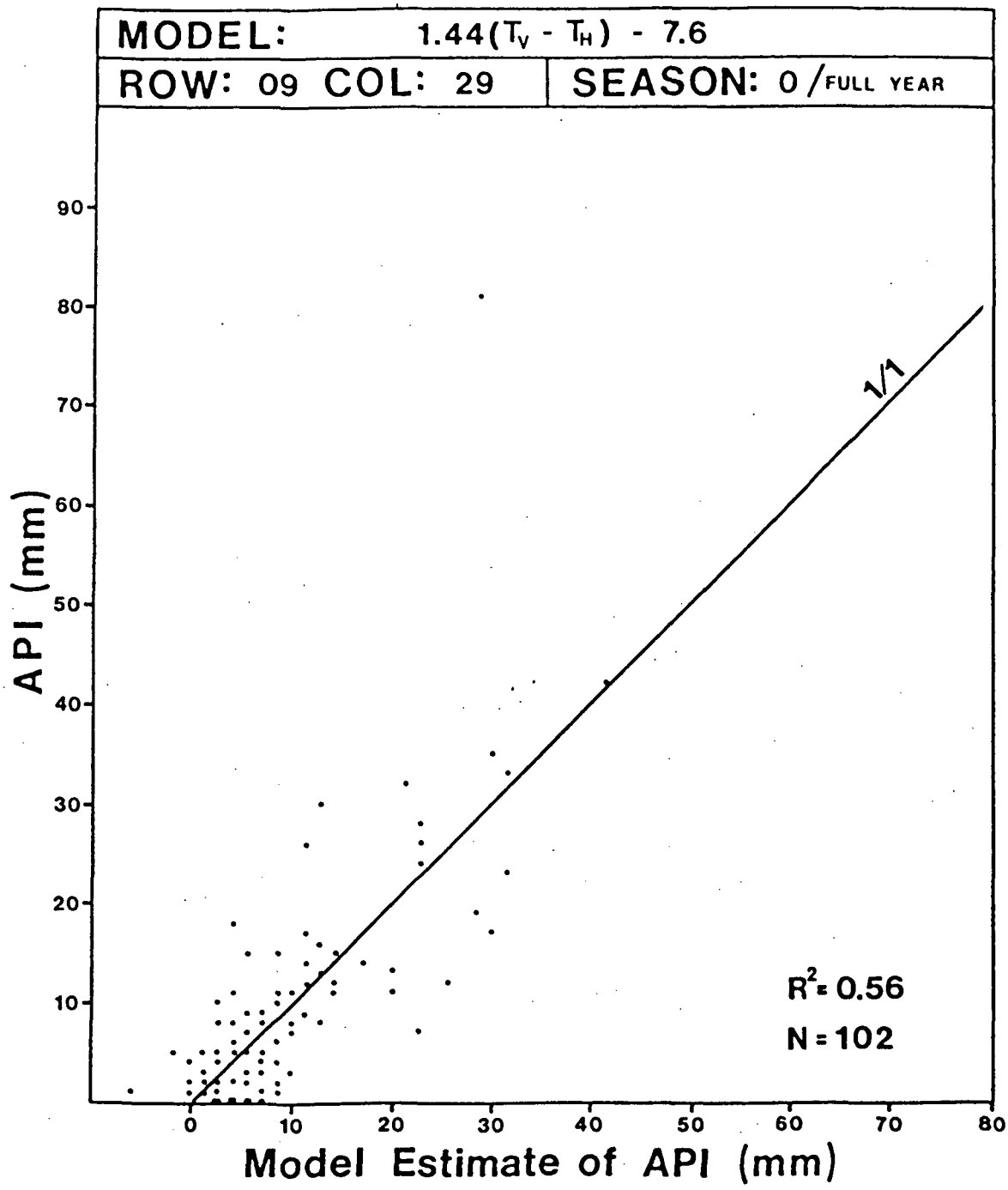

Figure 7. Regression of API of ϕ_i, season 0, row 09, column 29, south area.

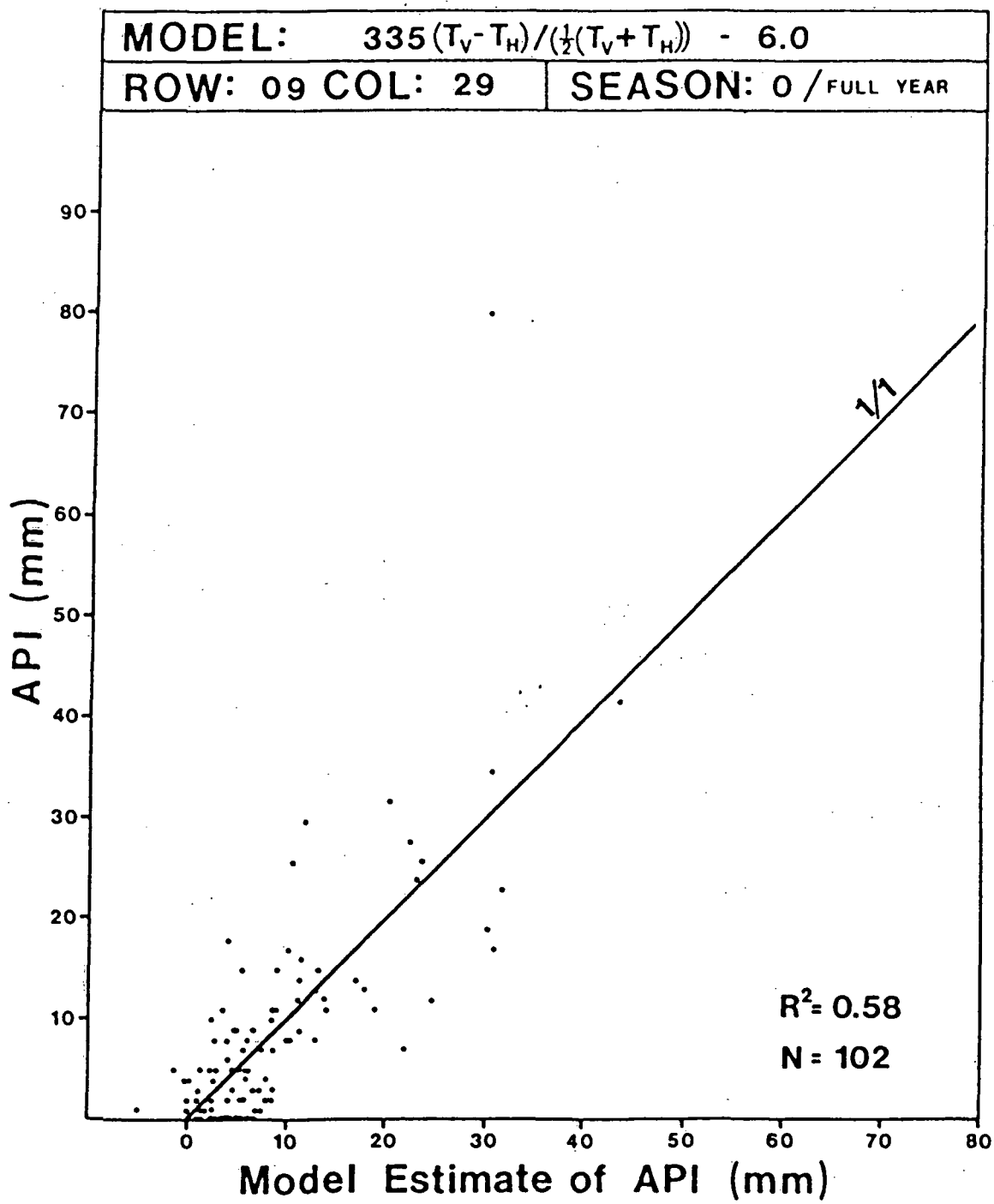

Figure 8. Regression of API of ϕ_{11}, season 0, row 09, column 29, south area.

Several points can be made from these graphs. First, as for the numerical evaluation, all of the three indices seem to perform equally well. Second, all of the indices have a tendency to underestimate the API in the aftermath of a heavy precipitation event. This behavior is seen in an anomalous point in the upper center of Figures 6-8. This point represents a heavy rain event that was recorded at many stations in the grid, some reporting more than 14 cm of precipitation over two days in October, 1979. The resulting underestimate of API is consistent with the very shallow sampling depth of the SMMR sensor. Its soil moisture signal saturates at low values of API. Finally, the sparsity of the scatter points on the seasonal graphs suggests that the seasonal analyses may not be quite reliable, even though they have significantly higher correlation coefficients in some cases. Figure A-4, for instance, shows only low values of API and a single heavy rainfall event. This season may be getting much of its apparent correlation from two well-separated clusters; a common source of faulty conclusions in regression analysis.

Time-series plots of the data are shown in Appendix B. Each series shows a solid line representing the API values computed from climatic data. These series can be compared to the regression model estimates, which are shown as dots. Both annual and seasonal models are shown, and the seasons are demarcated along the top of each graph for reference. Since this entire project has considered only data from days when snow cover was estimated as zero, and since the presence of snow on the ground produced a transient anomaly in the API model, the days of snow cover have been indicated along the bottom margins.

The time-series plots illustrate some of the same phenomena. Specially evident is the tendency to underestimate the magnitude of heavy precipitation events. For instance, in Figure 11, the values on days 140, 188, and 304 of 1979 show this effect, as do the same days in Figures B-2 and B-3. These plots also show the relative value of the annual and seasonal regression analyses. While the root-mean-square error of the seasonal regressions tended to be lower than that of the annual regressions, the difference was not particularly noticeable in time-series plots. In fact, there were times, such as days 120 to 130, 140 to 150, and 160 to 170 of 1979, when the annual model seems to follow the shape of the API line better than did the seasonal model; the seasonal model was closer to the line, but showed the wrong trend. For some applications, such as rainfall estimation, in which the daily change of API is more important than the actual value, this distinction could be crucial.

While the many contingency tables generated for this study cannot be reproduced here, a few are included for illustration. Table 6 shows the contingency tables from the screening grid cell, row 09, column 29, for the full year's analysis. These tables demonstrate the skill of the three microwave indices in making categorical estimates of soil moisture. Any differences between the contingency tables are not compelling.

Phase II: Tests of Three Indices

The three indices used in the final analysis of Phase I were selected for further examination using data from six other grid cells in

Kansas. These grid cells are shown in Figure 3, and listed with their land-use classification and wheat area percentages in Table 2. The indices tested in Phase II were ϕ_{05}, ϕ_{07}, and ϕ_{11}, one index of emissivity and two of polarization.

Linear regressions of API upon each of these indices were performed for all seasons and the full year. Results are presented in Appendix E and summarized in Table 7. The results of the Phase I grid cell (row 09, column 29) are included for comparison. Several observations can be made.

First, each of the three indices was significantly correlated to API in Season 0, the full year, for all of the grid cells. However, in the seasonal analyses, each of the indices failed to correlate significantly in at least some times and places. The statistics that do not differ significantly (alpha=0.05) from zero are underlined in the table.

Second, in most cases in which any two indices were significantly correlated with API for the same season and the same grid cell, the Fisher Z' transforms of the two correlation coefficients did not differ significantly from each other. The exceptions to this observation are surrounded with brackets wherever they occur in the tables. On the whole, however, each index is approximately as good an indicator of API as either of the other two.

Third, two grid cells that were classified as rangeland have the poorest correlations. It appears that rangeland vegetation interferes with the microwave signature of soil moisture more than does the vegetation of cultivated croplands. One reason for this phenomenon

TABLE 6

Sample Contingency Tables
South Area, Row 09, Column 29, Season 0

PHI_05:

APICAT OBSERVED	MODEL ESTIMATE CAT_1	CAT_2	CAT_3	% CORRECT = 84
CAT_1	66	3	0	[API < 10 mm]
CAT_2	6	12	4	[10 mm <= API < 20 mm]
CAT_3	1	2	8	[20 mm <= API]

PHI_07:

APICAT OBSERVED	MODEL ESTIMATE CAT_1	CAT_2	CAT_3	% CORRECT = 84
CAT_1	66	2	1	[API < 10 mm]
CAT_2	8	11	3	[10 mm <= API < 20 mm]
CAT_3	0	2	9	[20 mm <= API]

PHI_11:

APICAT OBSERVED	MODEL ESTIMATE CAT_1	CAT_2	CAT_3	% CORRECT = 82
CAT_1	64	4	1	[API < 10 mm]
CAT_2	8	11	3	[10 mm <= API < 20 mm]
CAT_3	0	2	9	[20 mm <= API]

MULTIPLE LINEAR REGRESSION:

APICAT OBSERVED	MODEL ESTIMATE CAT_1	CAT_2	CAT_3	% CORRECT = 84
CAT_1	66	3	0	[API < 10 mm]
CAT_2	8	11	3	[10 mm <= API < 20 mm]
CAT_3	1	1	9	[20 mm <= API]

TABLE 7

Correlation Coefficients Between API and Related ϕ Indices, by Season

			SEASON						
ROW	COLUMN	INDEX	0	2	3	4	5	6	Land Use
09	29	ϕ_5 ϕ_6 ϕ_7	-0.81 0.75 0.76	-0.96 0.93 0.93	-0.35a 0.76 0.78	-0.81 0.72 0.73	-0.821 0.70 0.73	-0.85 -.80 0.82	Agriculture (=35% Wheat)
03	29	ϕ_5 ϕ_7 ϕ_{11}	-0.81 0.71* 0.74*	-0.87 0.86 0.88	-0.80 0.85 0.86	-0.60 0.37a 0.38a	-0.84 0.56* 0.62*	-0.64 -.65 0.69	Agriculture (=30% Wheat)
10	33	ϕ_5 ϕ_7 ϕ_{11}	-0.52 0.34 0.36	-0.77 0.83 0.85	-0.46a 0.20a 0.21a	-0.43a 0.33a 0.35	-0.76 0.53 0.53	-0.22a 0.13a 0.22	Range (= 5% Wheat)
12	27	ϕ_5 ϕ_7 ϕ_{11}	-0.81 0.78 0.80	-0.96 0.93 0.94	-0.41a 0.47 0.54	-0.82 0.72 0.72	-0.94 0.91 0.92	-0.90 0.84 0.87	Mixed (=40% Wheat)
13	20	ϕ_5 ϕ_7 ϕ_{11}	-0.81 0.78 0.78	-0.90 0.89 0.89	-0.73 0.73 0.75	-0.90 0.89 0.89	-0.93 0.88 0.90	-0.57 0.74 0.76	Mixed (= 25% Wheat)
14	33	ϕ_5 ϕ_7 ϕ_{11}	-0.56 0.22* 0.24*	-0.51 0.39a 0.42a	-0.62 0.37a 0.39a	-0.65 0.07a 0.10a	-0.45 0.30a -0.29a	-0.27 0.27a 0.34a	Range (= 5% Wheat)
15	29	ϕ_5 ϕ_7 ϕ_{11}	-0.76 0.68 0.70	-0.91 0.85 0.87	-0.50 0.17a 0.22a	-0.53 0.38a 0.38a	-0.93 0.87 0.90	-0.66 0.58 0.61	Agriculture (= 65% Wheat)

*Correlation values differ significantly from the largest absolute value correlation for the grid cell and season. (alpha = 0.05). a=Values do not differ significantly from zero.

could be the area coverage of the vegetation. In range areas of Kansas, a nearly uniform vegetal cover extends unbroken for many miles. Agricultural regions, on the other hand, have many bare soil areas, such as roads, plowed fields, open spaces between crop rows, etc. Additionally, some crops, such as wheat, may have individual plant geometries which permit relatively unimpeded passage of microwave radiation during some seasons such as the few weeks after emergence.

Finally, the seasonal behavior of the correlation coefficients, while not conclusive, is nevertheless consistent with theory. Strictly monocultural areas, whether planted in wheat or in grassland range, should show a drop in correlation coefficient during those seasons when the vegetative canopy is most dense. This effect was seen in Seasons 3 and 4 for the rangeland grid cells and for the final agricultural grid cell, which was located in the heart of the most dense wheat cropping. The mixed agricultural and range grid cells and agricultural grid cells with only moderate wheat percentages did not show this late spring and summer drop in correlation, presumably because the presence of other crops with different development cycles insured the nearly continuous presence of enough bare ground to effect a sensor response to soil moisture variations.

Phase III: Verification with Independent Data.

The same three indices, ϕ_{05}, ϕ_{07}, and ϕ_{11}, were tested on data from three grid cells in the winter wheat producing regions of Oklahoma and Texas. The results are presented in Appendix E, Tables E-8 through E-10, and summarized in Table 8. These results are substantially the

TABLE 8

Correlation Coefficients Between API and Related ϕ Indices, By Season

ROW	COLUMN	INDEX	SEASON 0	2	3	4	5	6	Land Use
18	27	ϕ_5	-0.73	-0.92	-0.42	-0.75	-0.95	-0.69	Agriculture (=65% Wheat)
		ϕ_7	0.67	0.85	0.31a	0.73a	0.79*	0.68	
		ϕ_{11}	0.69	0.86	0.39a	0.73	0.83*	0.69	
29	22	ϕ_5	-0.70	-0.63	-0.70	-0.79	-0.70	-0.67	Agriculture (= 40% Wheat)
		ϕ_7	0.62	0.61	0.57	0.47*	0.65	0.71	
		ϕ_{11}	0.64	0.61	0.63	0.50*	0.66	0.74	
21	14	ϕ_5	-0.63	-0.71	-0.81	-0.65	-0.60	-0.83	Agriculture (= 40% Wheat)
		ϕ_7	0.58	0.63	0.65	0.68	0.50	0.88	
		ϕ_{11}	0.59	0.66	0.68	0.67	0.50	0.89	

*Correlation values differ significantly from the largest absolute value correlation for the grid cell and season. (alpha = 0.05). a=Values do not differ significantly from zero.

same as those of Phase II. Annual correlations were all significantly different from zero, with values ranging from about 0.60 to 0.70. Seasonal correlations were more varied, with the highest exceeding 0.90 while some values were insignificantly different from zero. In annual analysis, the performance of the three indices was statistically indistinguishable. The same behavior was typical in seasonal analysis. Again, the grid cell with high wheat percentage showed poorer correlations in Spring and Summer, while the other two grid cells with moderate wheat percentages were not so strongly affected.

The near equivalence of the emissivity and polarization indices is illustrated in Figure 9 which shows the annual and seasonal scatter plot of $\phi_{07}=T_V-T_h$ versus $\phi_{05}=T_h/T$ for the grid cell at Row 18, Column 27, in Grant County, Oklahoma, a nearly monocultural winter wheat region. Similar seasonal plots are presented in Appendix C. These graphs cluster tightly into a linear pattern with increased dispersion at the high values of T_h/T. This dispersion at the dry end of the soil moisture range can be explained by the increased relative importance, in the absence of water, of such other emission factors as soil roughness, vegetation cover, effect of wind on canopy geometry, etc., as well as by the effects of deeper layers of moisture not directly related to the API. The Season 3 plot also shows the reduced sensitivity of microwave indices to soil moisture under a well developed canopy.

Spatial Analysis

A case study from 10 May 1979 illustrates the spatial analysis

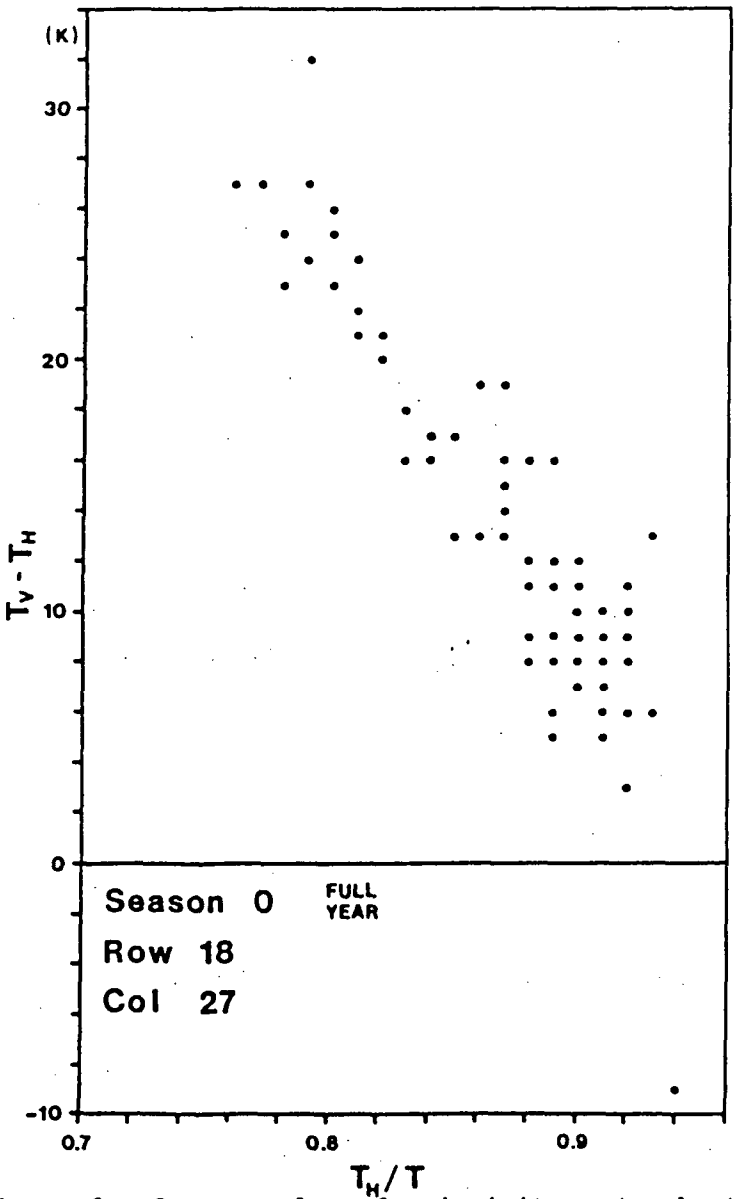

Figure 9. Scatter plot of emissivity and polarization indices, season 0, row 18, column 27 south area.

performed in this study.

Correlation Maps

Seasonal and annual correlation coefficient maps were generated showing results of simple linear regressions (in the time domain) of API on each of ϕ_{05}, ϕ_{07}, and ϕ_{11}, for each grid cell. The Season 3 correlations are shown in Figure 10, and the annual correlations in Figure 11. THe brightest pixels in both figures had correlation coefficients insignificantly different from zero (at alpha=0.05), while the darkest pixels showed high correlations, some exceeding 0.90 in seasonal analysis.

Both figures showed areas of weak correlation in the mountains of Southeastern Oklahoma, in the Flint Hills of east-central Kansas, and in the high plains of Colorado. These low correlations are consistent with the forests of Southeastern Oklahoma and the rangeland of the other two areas.

The other patterns were related to the development cycle of winter wheat. First, much of the winter wheat region shows very low correlation between API and any of these indices during Season 3. These low correlations can be explained by the dense canopy of wheat fields in May and June. On the other hand, the annual correlation maps show high values for the annual regression analyses. In fact, the annual correlation maps strongly resemble the 1980 map of wheat area percentage, in Figure 3. This result is attributable to the essentially bare soil surface of winter wheat lands during major portions of the year.

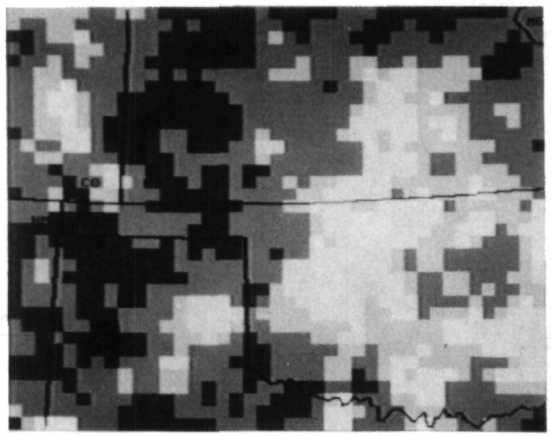

EMISSIVITY (ϕ_5).

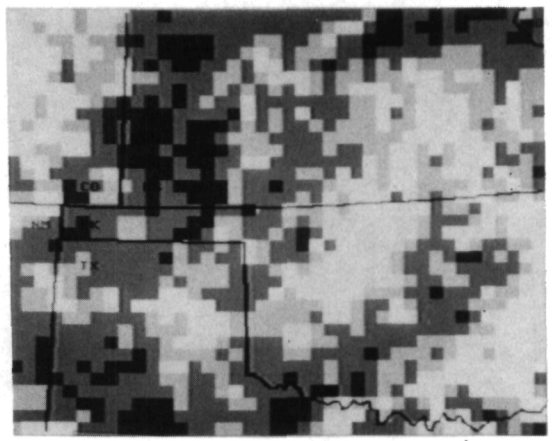

POLARIZATION DIFFERENCE (ϕ_7).

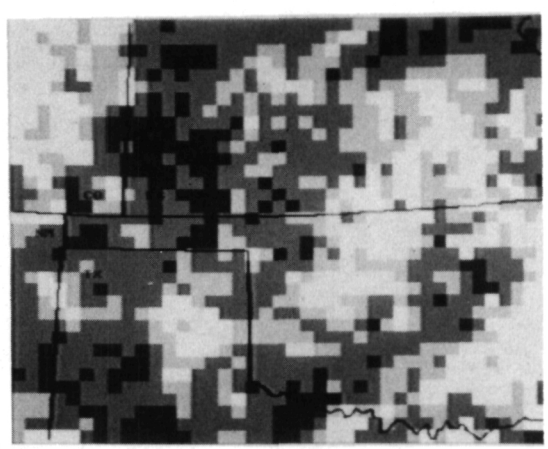

NORMALIZED POLARIZATION DIFFERENCE (ϕ_{11}).

Figure 10. Season 3 correlation coefficients from regressions of API on each of three indices at each grid cell. Darkest pixels represent values exceeding 0.90.

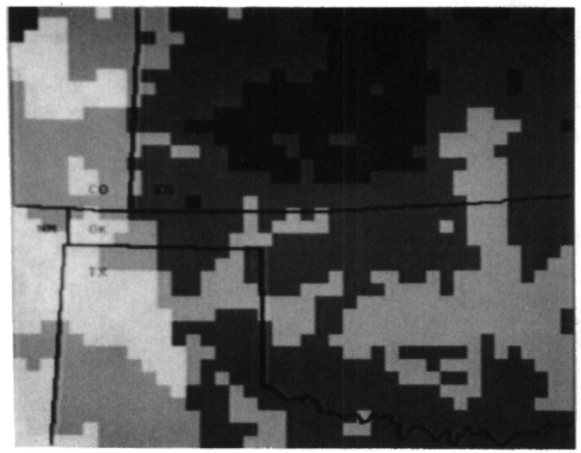

EMISSIVITY (ϕ_5).

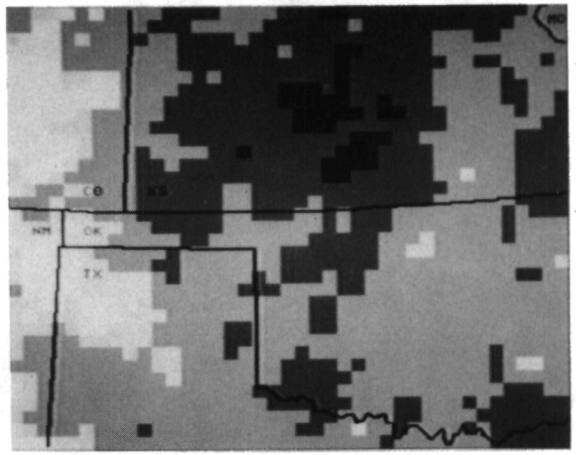

POLARIZATION DIFFERENCE (ϕ_7).

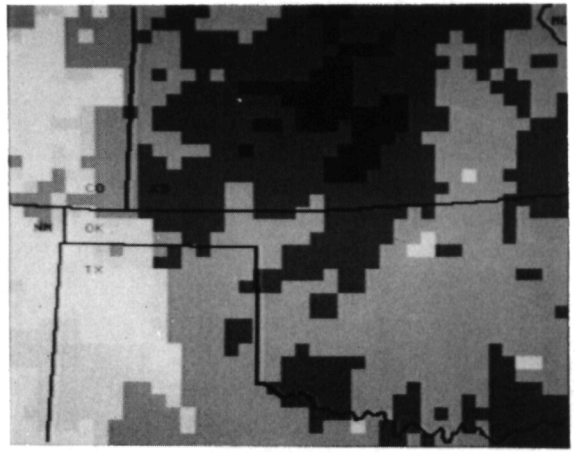

NORMALIZED POLARIZATION DIFFERENCE (ϕ_{11}).

Figure 11. Annual correlation coefficients from regressions of API on each of three indices at each grid cell. Darkest pixels represent values between 0.80 and 0.90.

Two further observations can be made from these images. While the seasonal correlation maps had higher maximum values than did the annual correlation maps, the latter had far fewer pixels with insignificant correlation. Finally, the areal patterns of correlation for all of the three indices were very similar.

Soil Moisture Maps

Images of model-estimated API were generated with model parameters from the same regression analyses that were used to produce the correlation maps. For comparison, maps of precipitation and resultant API are shown in Figure 12.

Figure 13 shows three maps of model-estimated API, produced from seasonal regressions of API on ϕ_{05}, ϕ_{07}, and ϕ_{11}. Model parameters for pixels with insignificant correlation were replaced by area average values. In Figure 14, all API estimates were generated using the area-mean values of regression parameters. The same sequence of maps produced from a per-pixel and area-mean parameters of annual regression models is shown in Figures 15 and 16.

Several observations can be made from these images. First, all of them succeeded in showing the major features of the API map in Figure 12. The process of remapping SMMR's conic-scan data to a rectangular grid did not destroy the spatial pattern. Second, seasonal model images of Figures 13 and 14 tended to depict the high values of API more accurately than did the annual models of Figures 15 and 16. Third, the emissivity tended to show high values of API more accurately than did either of the polarization indices. The low values, on the other hand,

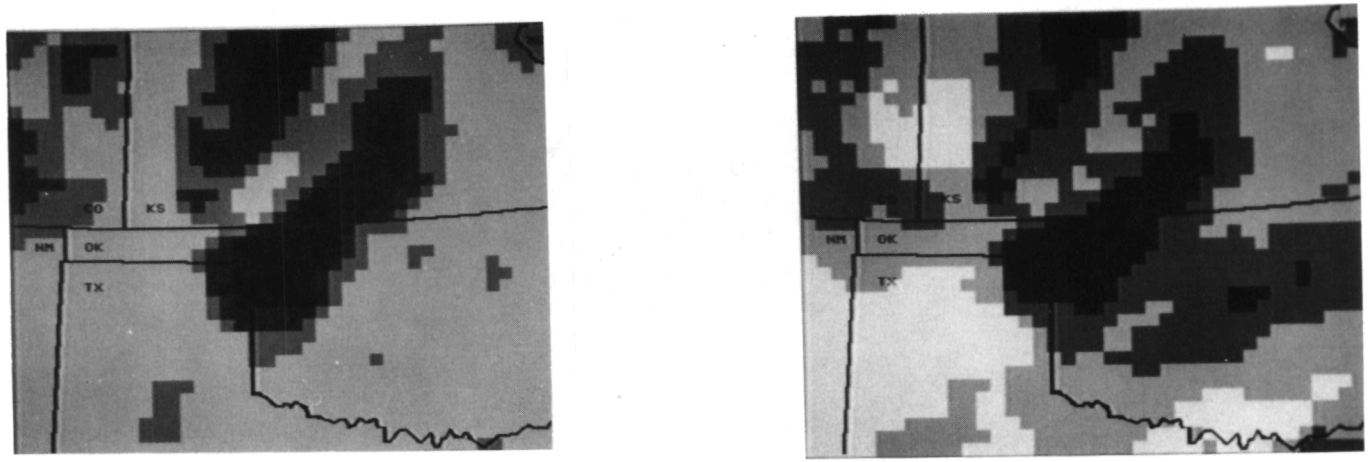

PRECIPITATION TOTALS

API

Figure 12. Maps of precipitation totals and API, 10 May 1979. Darkest pixels represent values exceeding 2 cm.

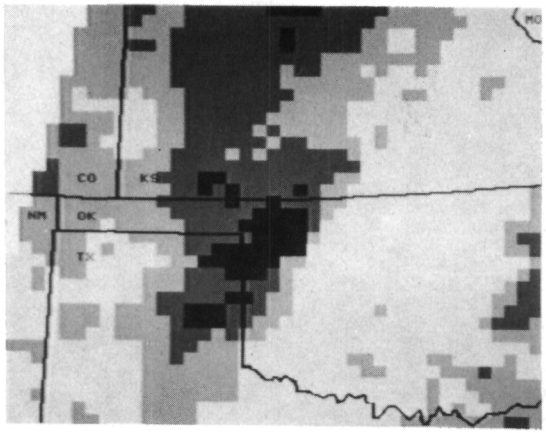

EMISSIVITY (ϕ_5).

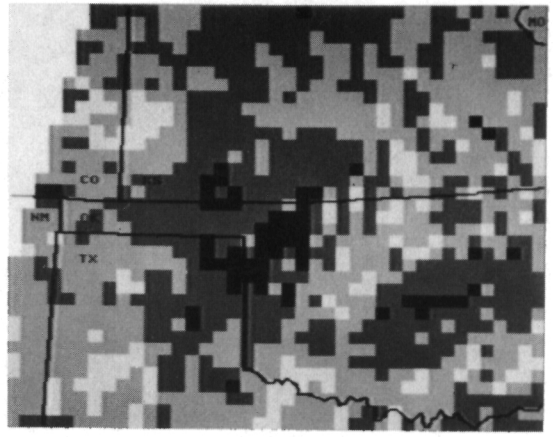

POLARIZATION DIFFERENCE (ϕ_7).

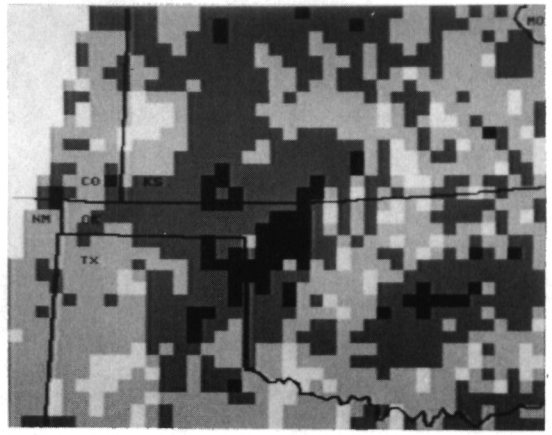

NORMALIZED POLARIZATION DIFFERENCE (ϕ_{11}).

Figure 13. 10 May 79 model estimates of API from season 3 regressions of API on three indices. Model parameters from pixels with insignificant correlation were replaced with area average parameter values. Darkest pixels represent values exceeding 2 cm.

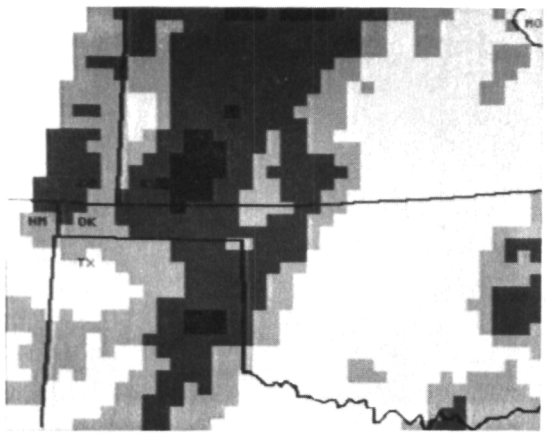

EMISSIVITY (ϕ_5).

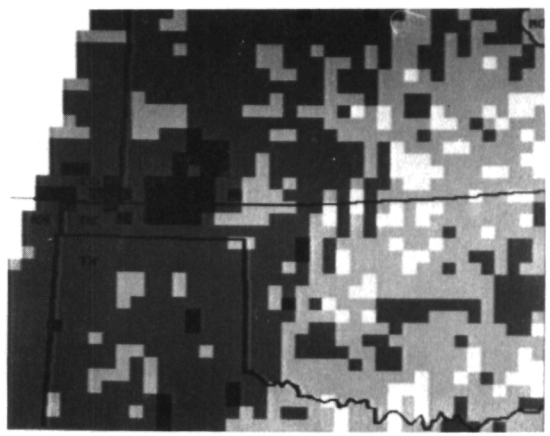

POLARIZATION DIFFERENCE (ϕ_7).

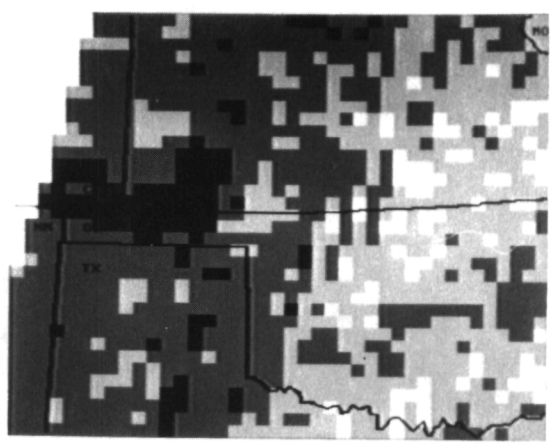

NORMALIZED POLARIZATION DIFFERENCE (ϕ_{11}).

Figure 14. 10 May 79 model estimates of API from season 3 regressions of API on three indices. Model parameters from all pixels were replaced with area average values of parameters. Darkest pixels represent values exceeding 2 cm.

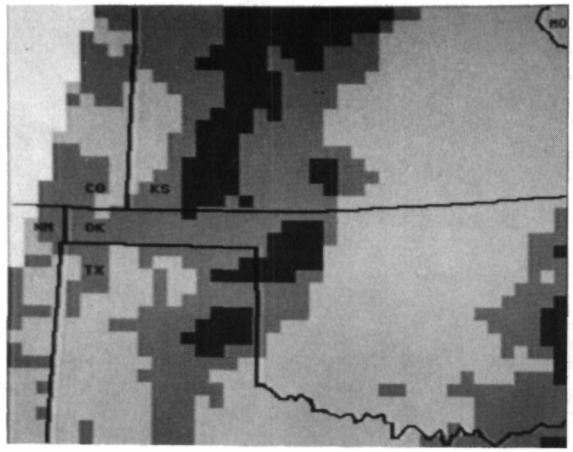

EMISSIVITY (ϕ_5).

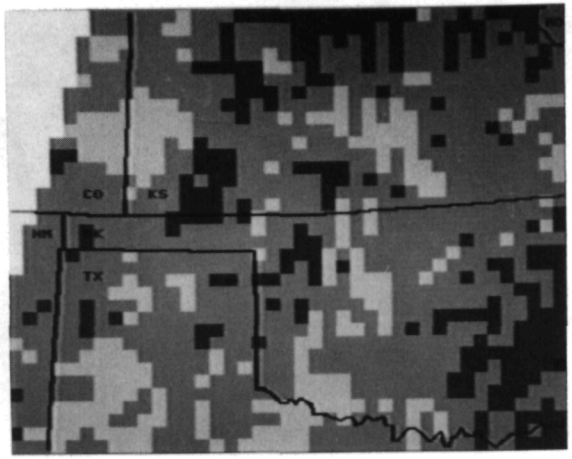

POLARIZATION DIFFERENCE (ϕ_7).

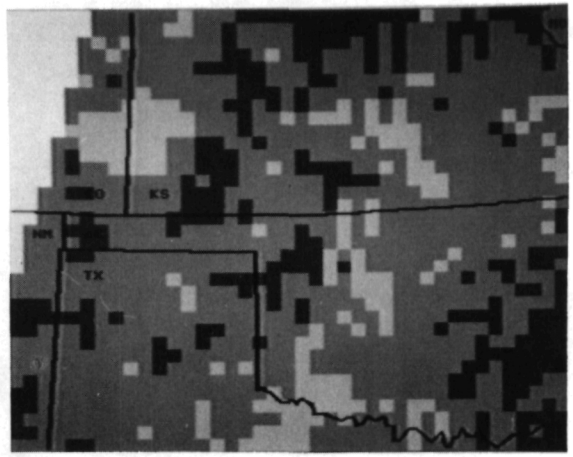

NORMALIZED POLARIZATION DIFFERENCE (ϕ_{11}).

Figure 15. 10 May 79 model estimates of API from annual regressions of API on three indices. Model parameters from pixels with insignificant correlation were replaced with area average parameter values. Darkest pixels represent values exceeding 2 cm.

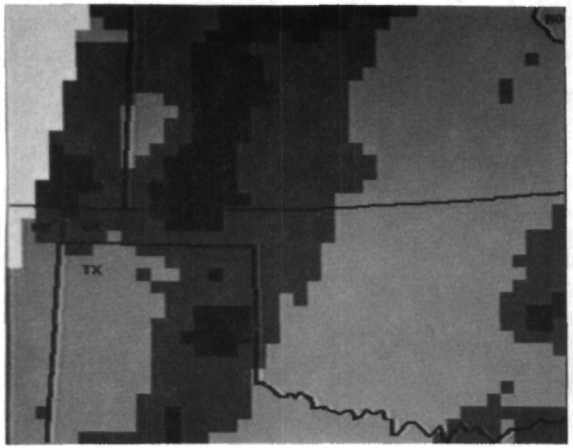

EMISSIVITY (ϕ_5).

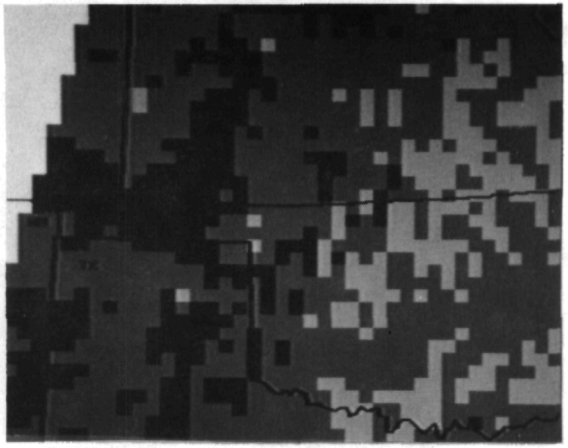

POLARIZATION DIFFERENCE (ϕ_7).

NORMALIZED POLARIZATION DIFFERENCE (ϕ_{11}).

Figure 16. 10 May 79 model estimates of API from annual regressions of API on three indices. Model parameters for all pixels were replaced by area average values of parameters. Darkest pixels represent values exceeding 2 cm.

were imaged better by the polarization indices. Compare, for example, two dry features of the API map with their counterparts in the model estimate images. The largest very dry area is shown in the Texas Panhandle on the API map, Figure 12, which also shows a weaker dry axis trending northeastward through central Oklahoma and eastern Kansas. The emissivity images reversed this pattern, depicting the Kansas-Oklahoma dry axis as broader and dryer than the Texas dry region. The polarization images derived from per-pixel regression parameters did not make this erroneous reversal. Finally, the images produced from area-mean parameter values preserved the general features of the API map in spite of their not accounting for site-specific properties, such as soil type, topography, land use and vegetation.

SUMMARY AND CONCLUSIONS

Summary

The major purpose of this research is to find ways to extract soil moisture information from the 1.66 cm polarized channels of the SMMR sensor. Using API as ground control data, this capability has been demonstrated for three microwave indices in winter wheat areas of Kansas, Oklahoma, and Texas. API estimates can be obtained from passive microwave data in areas with essentially bare soil for appreciable periods of the year. Consequently, these methods are useful in many monocultural areas, especially in winter wheat regions. They are less useful in forested areas and in dry climates where factors other than soil moisture can dominate the microwave signature of the soil and soil cover. Quantitative soil moisture estimates can be obtained from either emissivity or polarization data.

Conclusions

Soil moisture information can be derived from emissivity estimates. Specifically, an index computed by dividing the horizontally polarized brightness temperature by the air temperature is well correlated with API. Using data from the entire year, correlation coefficients typically exceed 0.80 in winter wheat areas. When analysis is restricted to the shorter periods of individual seasons, these correlation coefficients may exceed 0.90 in winter wheat areas during seasons when the soil is essentially bare. This emissivity index based

upon the horizontally polarized brightness temperature gives significantly better correlations with API than does a similar index based upon the vertically polarized component.

Alternatively, polarization data can be used to estimate soil moisture content. Two indices, the polarization difference and the normalized difference have been shown to have equal utility. These two polarization indices are also well correlated with API in winter wheat areas. The correlation coefficents are consistently lower than those of emissivity, but the difference typically is not statistically significant. Both of these polarization indices are effectively invariant with temperature over the nonfreezing range sampled in this study.

The emissivity and polarization indices convey nearly the same soil moisture information. Correlation coefficients of about -0.9 between horizontal emissivity and either polarization index are typical. Furthermore, multiple linear regression upon the three indices does not improve significantly upon the correlation of API with any single index.

Principal component analysis can be used to combine multiple indices into one which has the same correlation with API as does the best single index. However, since the emissivity and polarization indices carry substantially the same moisture information, this procedure does not result in significant improvement over the simpler approach of using any one of the single indices.

API estimates for specific sites can be obtained by objectively analyzing the conic-scan microwave data to a rectangular grid and performing regression analyses of precipitation-derived API values upon

microwave indices for each individual grid-cell. That is, moisture estimates need not be based directly upon microwave values from actual IFOVs, but may be remapped into convenient rectangular arrays, even at a resolution different from that of the sensor, while still preserving the spatial pattern of soil moisture.

Regression models from which API is estimated can be based upon year-round data or seasonal data. Seasonal models for bare-soil period typically give higher correlation coefficients than do annual models. However, the parameters of seasonal regression models can be unreliable due to sample size if the models are derived from a single season of data. Although the root-mean-square errors of seasonal models tend to be lower than those of annual models, the difference in correlation coefficient is usually not pronounced except in the early spring and late fall when vegetation cover is sparse. In fact, the correlation coefficients typically respond to the vegetation cover throughout the year with low or insignificant values in the Spring and Summer for winter wheat areas. This minimum is not so apparent in multicultural areas that have at least some bare ground throughout the year.

Individual grid-cell estimates of API can be assembled to form spatial maps of soil moisture. These maps generally have missing-data pixels due to lack of correlation at some of the grid-cells. These holes can be filled by using the average regression parameters for the surrounding area. Images have been presented showing that this procedure does preserve the general soil moisture pattern represented by the API map.

In fact, the general features of the API map are preserved even if all of the pixels of the microwave-derived image are computed with area-mean regression parameters. Thus, soil moisture can be mapped from space even in regions where no ground control data is available, if the regression parameters can be estimated from those of analogous regions where ground control data is available.

The satellite imagery presented here preserves the prominent features of the ground control API map even in areas which are not monocultural wheat lands. Consequently, passive microwave methods can be used in at least a qualitative sense for many regions in which their quantitative application would be an error.

Even in monocultural wheat regions, the quantitative value of passive microwave methods has some restrictions. The short wavelength of the SMMR sensor used in this report limits the sampling depth to a few millimeters. Consequently, the sensor saturates when rainfall exceeds some limit; that is, there is some value of API above which further increases of API are not attended by an increase of microwave-estimated API. This effect is demonstrated in the scatter plots of temporal analysis and by the 10 May 1979 imagery. In both cases, the microwave system underestimated the larger values of API.

The contingency tables presented here demonstrate, however, that passive microwave data do have quantitative value, since the majority of entries in the tables fall on the diagonal. Even if these methods are too rough to yield precise soil moisture measurements, they can be used to classify the moisture content of the soil into a few quantitatively defined categories.

Finally, microwave sensors have essentially all-weather, day/night capability. The time series for which the regressions were done in this study did not differentiate between day and night, yet the correlation coefficients were comparable to those of McFarland and Blanchard (1977), which were based upon midday observations. Neither did the presence of an active line of thunderstorms strongly contaminate the case study imagery of 10 May 1979, since the sensor IFOV is larger than the actively precipitating area of many thunderstorms.

Recommendations for Further Study

This paper reports the construction of a large database and the initial analyses of some of the data. Future efforts should be able to refine the work presented here. The possible avenues of improvement include better representation of the ground control data, i.e., a better API model; explicit consideration of atmospheric effects that were ignored in this study; and use of a simulation model of microwave emission.

The API formula used for ground control data was applied uniformly over the entire study area, without regard to land cover classification, spatial variations of climate or temporal variations of weather. Future analysis of this data should attempt to parameterize the API model coefficients in terms of these classes of information. For instance, the annual temperature pattern for specific locations could be used to modify the mean and amplitude of of the sinusoidal moisture depletion coefficient used in the API model. Alternatively, actual daily values of maximum and minimum temperature could be used to

compute a daily value of the depletion coefficient, eliminating reference to a sinusoidally varying function.

With a better representation of API, it should also be possible to better define API categories for contingency table analysis. The categories used in this study were purely arbitrary. It would be better to define catagories in terms of some phenomena with agronomic or hydrologic significance.

Atmospheric effects can be considered in connection with soil moisture studies. In particular, the other frequencies of the SMMR sensor could be exploited to monitor the moisture content and perhaps the mean temperature of the volume of air through which the microwave radiation passes. The same methods could allow explicit computation of the sky brightness temperature. It was assumed here that the effect of the atmosphere upon the brightness temperature would be less than 10K, and that this effect would be fairly uniform. These effects can be tested explicitly, though. Other sensor systems in everyday use can be employed to do this.

Finally, it is recommended that a simulation model of microwave emission be evaluated. Simulation methods can be used iteratively in inversion problems. If a model of soil and land-cover emission can be implemented, it could be used in an iterative inversion algorithm to extract soil moisture information. Personnel at Texas A&M University Remote Sensing Center have done some related emission modeling, such as Tsang and Kong (1980), Tsang and Newton (1980) and Newton et al. (1982). It should be productive to apply their theoretical work to the database and analytic insights developed in this investigation.

REFERENCES

Allison, L.J., T.J. Schmugge, and G. Byrne, 1979: A hydrological analysis of east Australian floods using Nimbus-5 electrically scanning radiometer data. Bull. Amer. Meteor. Soc., 60,1414-1427.

Baier, W., and G.W. Robertson, 1966: A new versatile soil moisture budget. Can. J. Plant Sci., 46,299-315.

Barton, I.J., 1978: A case study comparison of microwave radiometer measurements over bare and vegetated surfaces. J. Geophy. Res., 83,3513-3517.

Basharinov, A.Ya., and A.M. Shutko, 1978: Determination of the moisture content of soils by microwave radiometry (review). Radiotechnika I Elektronika, English trans. in Radio Eng. & Electronic Physics, 23,1-12.

Blanchard, B.J., 1977: Demonstration to characterize watershed runoff potential by microwave techniques. Final rep. RSC-3345, under NASA contr. NAS9-14898, Remote Sensing Center, Texas A&M Univ., 34 pp.

Blanchard, B.J., and W. Bausch, 1979: Algorithms to estimate soil moisture storage from microwave measurements. Final Rep. 3843 under NOAA contr. 04-8-M01-145, Remote Sensing Center, Texas A&M Univ., 95 pp.

Blanchard, B.J., M.J. McFarland, T.J. Schmugge, and E. Rhoades, 1980: Estimation of surface soil moisture with API algorithms and microwave emission. Water Resour. Bull., 17,767-773.

Blanchard, B.J., M.J. McFarland, S.W. Theis, and J.G. Richter, 1981: Correlation of spacecraft passive microwave system data with soil moisture indices (API). Final Rep. RSC-3622-4 under NASA contr. NSG-5193, Remote Sensing Center, Texas A&M Univ., 92 pp.

Blanchard, B.J., J.W. Rouse, Jr., and T.J. Schmugge, 1975: Classifying storm runoff potential with passive microwave measurements. Water Resour. Bull., 11,892-907.

Blinn, J.C., III, and J.G. Quade, 1972: Microwave properties of geological materials: Studies of penetration depth and moisture effects. Fourth Annual Earth Resources Program Review, NASA MSC-05937, Manned Spacecraft Center, Houston, TX, Jan 17-21, Vol II, pp 53-1 to 53.12.

Brooks, C.E.P., and N. Carruthers, 1953: Handbook of Statistical Methods in Meteorology. H.M.S.O., London, 412pp.

Burke, H.K., 1980: Evaluation of the effects of varying moisture contents on microwave emissions from agricultural fields. NASA CR-166679, Goddard Space Flight Center, Greenbelt, MD, 53 pp.

Burke, H.K., C.J. Bowley, and J.C. Barnes, 1981: Comparison of theoretical and actual satellite microwave brightness temperatures to determine snowpack properties. Final rep. ERT-A653-F, Environmental Research and Technology, Inc., Concord, MA, 78 pp.

Burke, H.K., and J.H. Ho, 1981: Analysis of soil moisture extraction algorithm using data from aircraft experiments. NASA CR-166719, Goddard Space Flight Center, Greenbelt, MD, 37 pp.

Burke, W.J., and J.F. Paris, 1975: A radiative transfer model for microwave emissions from bare agricultural soils. NASA TMX-58166, Johnson Space Center, Houston, TX, 29 pp.

Burke, W.J., T.J. Schmugge, and J.F. Paris, 1979: Comparison of 2.8- and 21-cm microwave radiometer observations over soils with emission model calculations. J. Geophy. Res., 84,287-294.

Choudhury, B.J., and B.J. Blanchard, 1981: A simulation study of the recession coefficient for antecedent precipitation index. NASA TM 83860, Goddard Space Flight Center, Greenbelt, MD, 25 pp.

Choudhury, B.J., T.J. Schmugge, A. Chang, and R.W. Newton, 1979: Effect of surface roughness on the microwave emission from soils. J. Geophy. Res., 84,5699-5706.

Eagleman, J.R., and W.C. Lin, 1976: Remote sensing of soil moisture by a 21-cm passive radiometer. J. Geophy. Res., 81,3660-3666.

Edgerton, A.T., F. Ruskey, D. Williams, A. Stogryn, G.Poe, D. Meeks, and O. Russell, 1971: Microwave emission characteristics of natural materials and the environment (a summary of six years research). Final Tech. Rep. 9016R-8, Aerojet-General Corp., El Monte, CA, 288 pp.

Gloersen, P., and F.T. Barath, 1977: A scanning multichannel microwave radiometer for Nimbus-G and SeaSat-A. IEEE J. Oceanic Eng., OE-2, 172-178.

Harder, P.H., and M.J. McFarland, 1984: Objective Analysis Software for the VAX 11/750. Tech. Memo in preparation, Remote Sensing Center, Texas A&M University, College Station, TX.

Hardy, K.R., S.H. Cohen, L.K. Rogers, H.K. Burke, R.C. Leupold, and M.D. Smallwood, 1981: An evaluation of the spatial resolution of soil moisture information. NASA CR-166724, Goddard Space Flight Center, Greenbelt, MD, 83 pp.

Hollinger, J.P., and R.C. Lo, 1983: SSM/I project summary report. NRL Memo Rep. 5055, Naval Research Laboratory, Washington, DC, 106 pp.

Jackson, T.J., 1980: Profile soil moisture from surface measurements. J. Irrigation and Drainage Div., Proc. ASCE, 106, 81-92.

Kirdyashev, K.P., A.A. Chukhlantsev, and A.M. Shutko, 1979: Microwave radiation of the earth's surface in the presence of a vegetative cover. Radiotechnika I Elektronika, English trans. in Radio Eng. & Electronic Physics, 24,37-44.

Kondratyev, K.Ya., V.V. Melentyev, Yu.I. Rabinovich, and E.M. Shulgina, 1977: Passive microwave remote sensing of soil moisture. Proc. 11th International Symposium on Remote Sensing of Environment, Vol II, 1641-1661.

Linsley, R.K., Jr., M.A. Kohler, and J.L.H. Paulhus, 1975: Hydrology for Engineers, 2nd ed., McGraw-Hill, New York, 482 pp.

Madrid, C.R., ed., 1978: The Nimbus 7 User's Guide, NASA Goddard Space Flight Center, Greenbelt, MD, 287 pp.

McFarland, M.J., 1975. The correlation of SKYLAB L-band brightness temperatures with antecedent precipitation. Proc. NASA Earth Resource Symposium, NASA TMS-58168. Houston, TX. 2243-2252.

McFarland, M.J., 1976: The correlation of SKYLAB L-band brightness temperatures with antecedent precipitation. Preprints Conf. Hydrometeor., Fort Worth, TX, Amer. Meteor. Soc., pp 60-65.

McFarland, M.J., 1982: Personal communication.

McFarland, M.J., and D.B. Beach, 1981. An API model to estimate field work delays. ASAE Paper 81-1023. ASAE Summer Meeting, Orlando, FL, 20 pp.

McFarland, M.J., and B.J. Blanchard, 1977: Temporal correlations of antecedent precipitation with Nimbus 5 ESMR brightness temperatures. Preprints 2nd Conf. Hydrometeor., Toronto, Ont., Canada, Amer. Meteor. Soc., pp 311-315.

McFarland, M.J., and P.H. Harder, 1982: Development of an early warning system of crop moisture conditions using passive microwave. Final rep. RSC-4659, NASA contr. NAS 9-16556, Remote Sensing Center, Texas A&M Univ., 111 pp.

McFarland, M.J., and P.H. Harder, 1983: Crop moisture condition assessment with passive microwave radiometry. 1983. Preprints International Geoscience and Remote Sensing Symposium Digest, IEEE, New York, Section PS-2, pp. 4.1-4.5

Meneely, J.M., 1977: Application of the electrically scanning microwave radiometer (EMSR) to classification of the moisture condition of the ground. Earth Satellite Corporation, Washington, DC, Final Rep. under NASA contr. NAS 5-22328, 39 pp.

NAS, 1977: Microwave remote sensing from space for earth resource surveys. NASA CR-157891, Committee on Remote Sensing Programs for Earth Resource Surveys, National Research Council, National Academy of Sciences, Washington, DC, 141 pp.

Newton, R.W., 1977: Microwave remote sensing and its application to soil moisture detection. Tech. Rep. RSC-81, Remote Sensing Center, Texas A&M Univ., 500 pp.

Newton, R.W., 1980: Microwave soil moisture measurements and analysis. Final Rep. RSC-3058 under NASA contr. NAS 9-13904, Remote Sensing Center, Texas A&M Univ., 370 pp.

Newton, R.W., B.V. Clark, J.F. Paris, and W.M. Pitchford, 1982: Orbiting passive microwave sensor simulation applied to soil mois-ture estimation. TEES-TR-43753-82, Remote Sensing Center, Texas A&M Univ., 208 pp.

Njoku, E.G., and J.A. Kong, 1977: Theory for passive microwave remote sensing of near-surface soil moisture. J. Geophy. Res., 82,3108-3118.

Pandey, P.C., and R.K. Kakar, 1983: A two step linear statistical technique using leaps and bounds procedure for retrieval of geophysical parameters from microwave radiometric data. IEEE Trans. Geosci. & Rem. Sens., GE-21,208-214.

Paris, J.F., 1971: Transfer of thermal microwaves in the atmosphere. Rep. under NASA contr. NGR-44-001-098, Dept of Meteorology, Texas A&M Univ., 2 vols., 468 pp.

Reeves, R.G., ed., 1975: Manual of Remote Sensing, Amer. Soc. Photogramm., Falls Church, VA, 2 vols, 2144 pp.

Reinschmiedt, L.L., 1973: Study of the relationship between rainfall and field work time available and its effect on optimal machinery selection. M.S. Thesis, Oklahoma State Univ., Stillwater, OK. Cited in McFarland and Beach (1981).

Saxton, K.E., and A.T. Lenz, 1967: Antecedent retention indexes predict soil moisture. J. Hydraulics Div, Proc. ASCE, HY4,223-241.

Schmugge, T.J., 1978: Remote sensing of surface soil moisture. J. Appl. Meteor., 17,1549-1557.

Schmugge, T.J., 1980a: Microwave approaches in hydrology. Photogramm. Eng. & Rem. Sens., 46,495-507.

Schmugge, T.J., 1980b: Soil moisture sensing with microwave radiometers, 1980 Machine Processing of Remotely Sensed Data Symposium, pp 346-354.

Schmugge, T.J., B.J. Blanchard, A. Anderson, and J.R. Wang, 1978: Soil moisture sensing with aircraft observations of the diurnal range of surface temperature. Water Resour. Bull., 14,798-807.

Schmugge, T.J., P. Gloersen, T. Wilheit, and F. Geiger, 1974: Remote sensing of soil moisture with microwave rediometers. J. Geophy. Res., 79,317-323.

Schmugge, T.J., T.J. Jackson, and H.L. McKim, 1979: Survey of methods for soil moisture determination. NASA TM 80587, Goddard Space Flight Center, Greenbelt, MD, 74 pp.

Schmugge, T.J., J.M. Meneely, A. Rango, and R. Neff, 1977: Satellite microwave observations of soil moisture variations. Water Resour. Bull., 13,265-281.

Schmugge, T.J., T. Wilheit, W. Webster, Jr., and P. Gloersen, 1976: Remote sensing of soil moisture with microwave radiometers-II. NASA TN D-8321, Goddard Space Flight Center, Greenbelt, MD, 34 pp.

Shortley, G. and D. Williams, 1965: Elements of Physics, 4th Ed., Prentice-Hall, Inc., Englewood Cliffs, NJ, 956 pp.

Smith, M.R., and R.W. Newton, 1983: The prediction of root zone soil moisture with a water balance - microwave emission model. Tech. Rep. RSC-136 under NASA contr. NAG 5-31, Remote Sensing Center, Texas A&M Univ., 148 pp.

Spencer, R.W., D.W. Martin, B.B. Hinton, and J.A. Weinman, 1983: Satellite microwave radiances correlated with radar rain rates over land. Nature, 304,(5922)141-143.

Stogryn, A., 1970: The brightness temperature of a vertically structured medium. Radio Sci., 5,1397-1406.

Stucky, B.E., 1975: Analysis of SKYLAB S193 apparent brightness temperatures in a thunderstorm environment. M.S. Thesis, Dept of Meteorology, Univ. of Okla., Norman, 59 pp.

Theis, S.W., 1979: Surface soil moisture estimation with the Electrically Scanning Microwave Radiometer (ESMR). M.S. Thesis, Dept. of Meteorology, Texas A&M Univ., 45 pp.

Theis, S.W., M.J. McFarland, W.D. Rosenthal, and C.L. Jones, 1982: Microwave Remote Sensing of Soil Moisture. NASA CR 166822, Goddard Space Flight Center, Greenbelt, MD, 131 pp.

Tsang, L., and J.A. Kong, 1975: The brightness temperature of a half-space random medium with nonuniform temperature profile. Radio Sci., 10,1025-1033.

Tsang, L., and J.A. Kong, 1976a: Emissivity of half-space random media. Radio Sci., 11,593-598.

Tsang, L., and J.A. Kong, 1976b: Thermal microwave emission from half-space random media. Radio Sci., 11,599-609.

Tsang, L., and J.A. Kong, 1976c: Microwave remote sensing of a two-layer random medium. IEEE Trans. Antennas and Propagation, AP-24, 283-288.

Tsang, L., and J.A. Kong, 1980: Thermal microwave emission from a three-layer random medium with three-dimensional variations. IEEE Trans. Geosci. & Rem. Sens., GE-18,212-216.

Tsang, L., and R.W. Newton, 1980: Microwave emission from soils with rough interfaces. Tech. Rep. RSC-107 under NASA contr. NAG 5-31, Remote Sensing Center, Texas A&M Univ., 30 pp.

Tsang, L., E. Njoku, and J.A. Kong, 1975: Microwave thermal emission from a stratified medium with nonuniform temperature distribution. J. Appl. Phys., 46,5127-5133.

Van Bavel, C.H.M., and R. Lascano, 1980: CONSERVB - a numerical method to compute soil water content and temperature profiles under a bare surface. Tech. rep. RSC-134 under NASA contr. 9-13904, Remote Sensing Center, Texas A&M Univ., 73 pp.

Walker, J.D., 1978: Techniques for remotely sensing watershed runoff potential. Tech. rep. RSC-98 under NASA contr. NSG-5156, Remote Sensing Center, Texas A&M Univ., 72 pp.

Wang, J.R., and B.J. Choudhury, 1981: Remote sensing of soil moisture content over bare field at 1.4 GHz frequency. J. Geophy. Res., 86,5277-5282.

Wang, J.R., and T.J. Schmugge, 1978: An empirical model for the complex dielectric permittivity of soils as a function of water content. NASA TM 79659, Goddard Space Flight Center, Greenbelt, MD, 35 pp.

Wang, J.R., and T.J. Schmugge, 1980: An empirical model for the complex dielectric permittivity of soils as a function of water content. IEEE Trans. Geosci. Elec., GE-18,288-295.

Wang, J.R., J.C. Shiue, S.L. Chuang, and M. Dombrowski, 1980: Thermal microwave emissions from vegetated fields: a comparison between theory and experiment. NASA TM-80739, Goddard Space Flight Center, Greenbelt, MD, 27 pp.

Wang, J.R., J.C. Shiue, and J.E. McMurtrey, III, 1980: Microwave remote sensing of soil moisture content over bare and vegetated fields. Geophy. Res. Letters, 7,801-804.

Weger, E., 1960: Apparent sky temperatures in the microwave region. J. Meteor., 17,159-165.

Wilheit, T., 1978: Radiative transfer in a plane stratified dielectric. IEEE Trans. Geosci. Elec., GE-16,138-143.

APPENDIX A

REGRESSION PLOTS FOR SEASONS 2-6

This appendix presents the individual seasonal regression results for a single grid cell in the south area, row 09, column 29, for each of ϕ_5, ϕ_7, and ϕ_{11}. In each graph, the abscissa is estimated API obtained from the regression model; the ordinate is API from the climatic database. The diagonal line is, thus, the one-to-one slope line, not the line of best fit. Analogous graphs for the entire year are presented in Chapter 4.

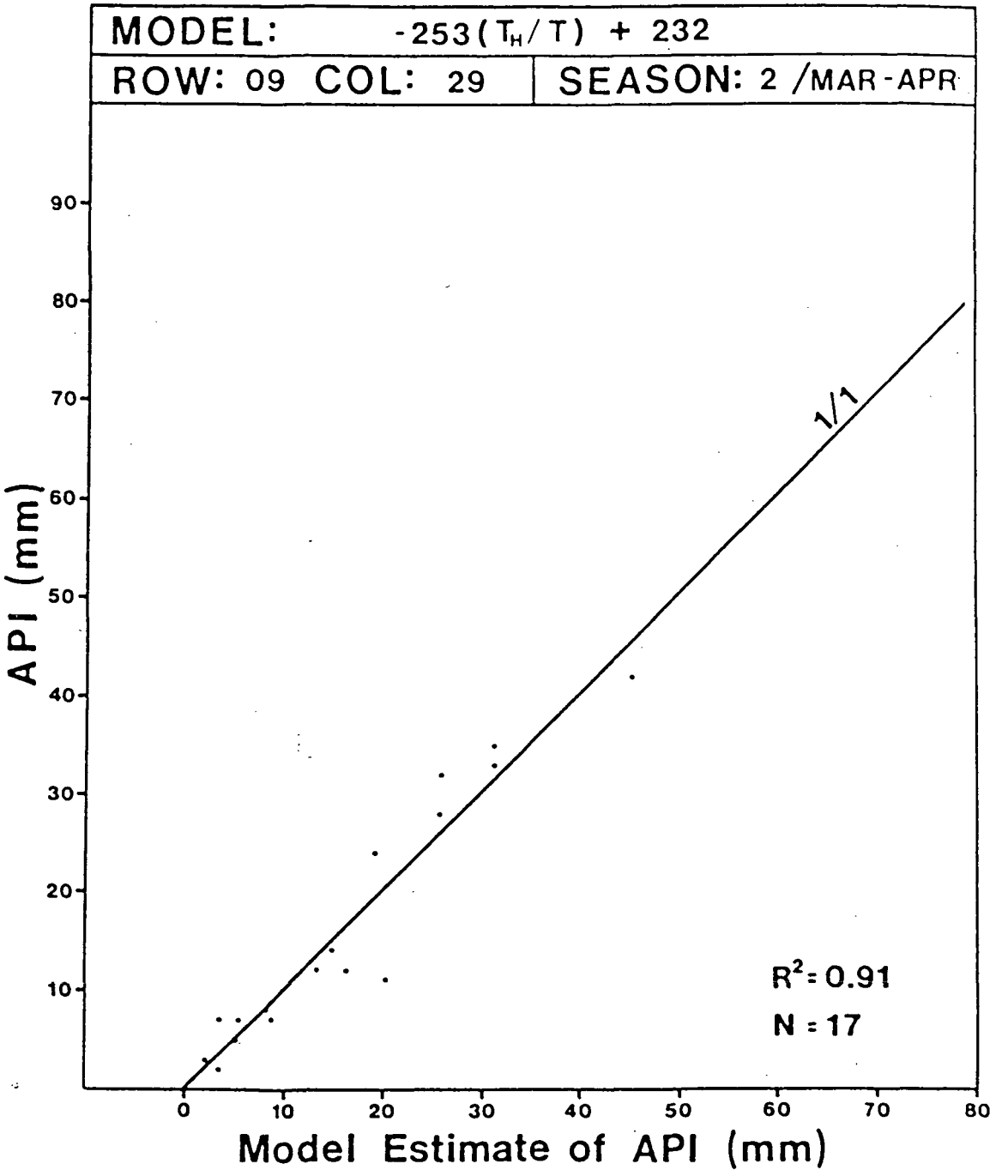

Figure A-1. Regression of API on ϕ_s, season 2, row 09, column 29, south area.

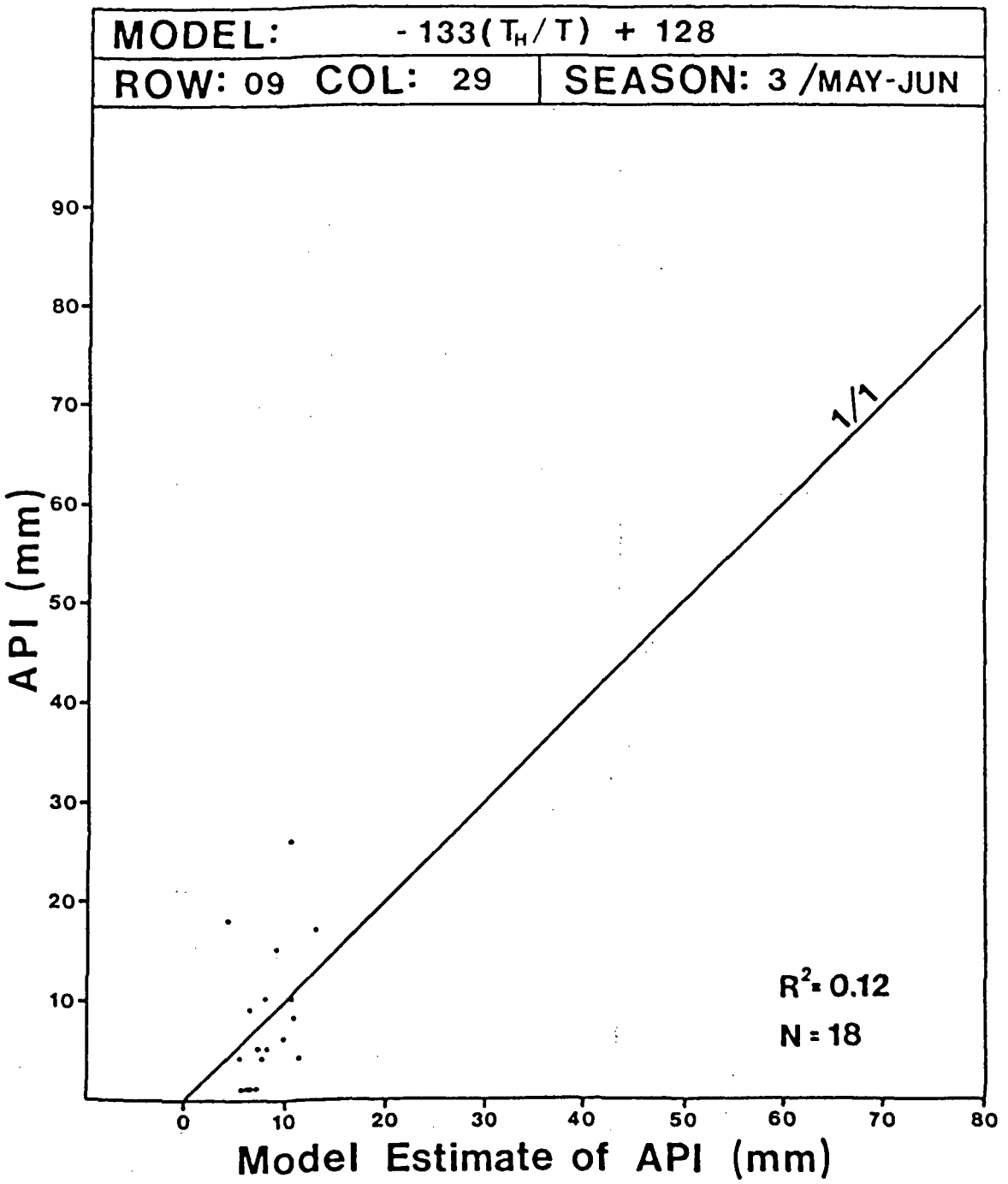

Figure A-2. Regression of API on ϕ_s, season 3, row 09, column 29, south area.

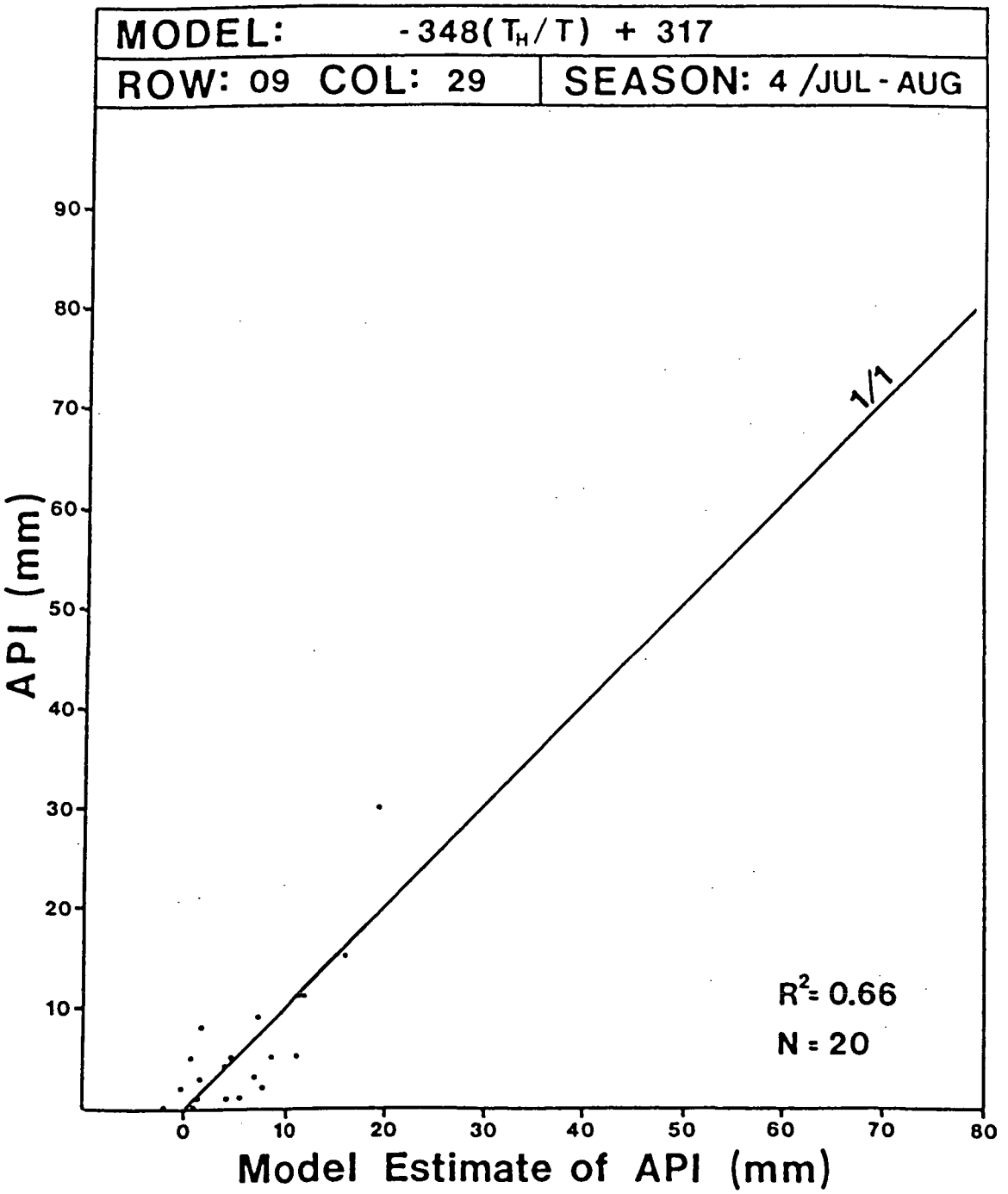

Figure A-3. Regression of API on ϕ_s, season 4, row 09, column 29, south area.

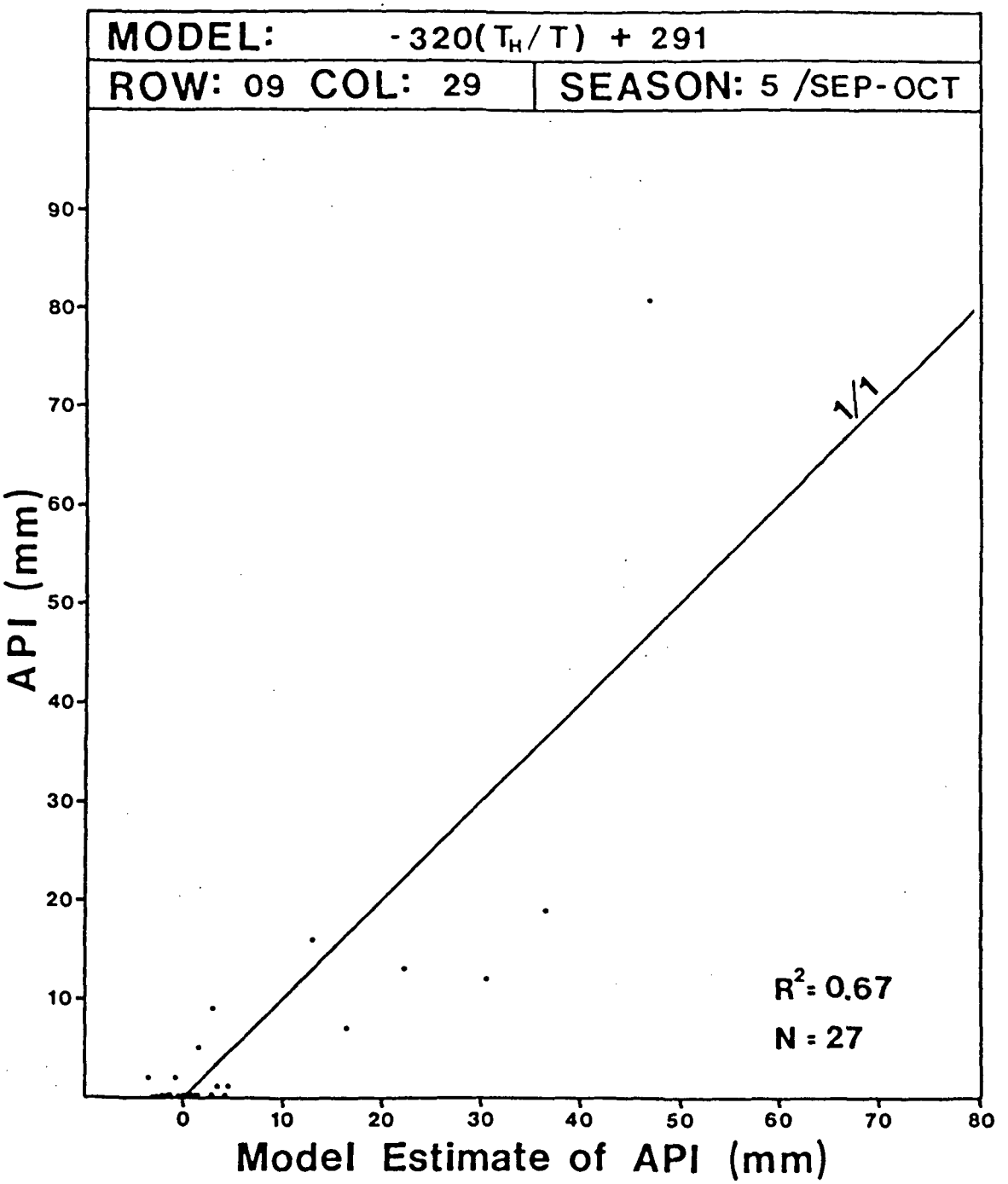

Figure A-4. Regression of API on ϕ_s, season 5, row 09, column 29, south area.

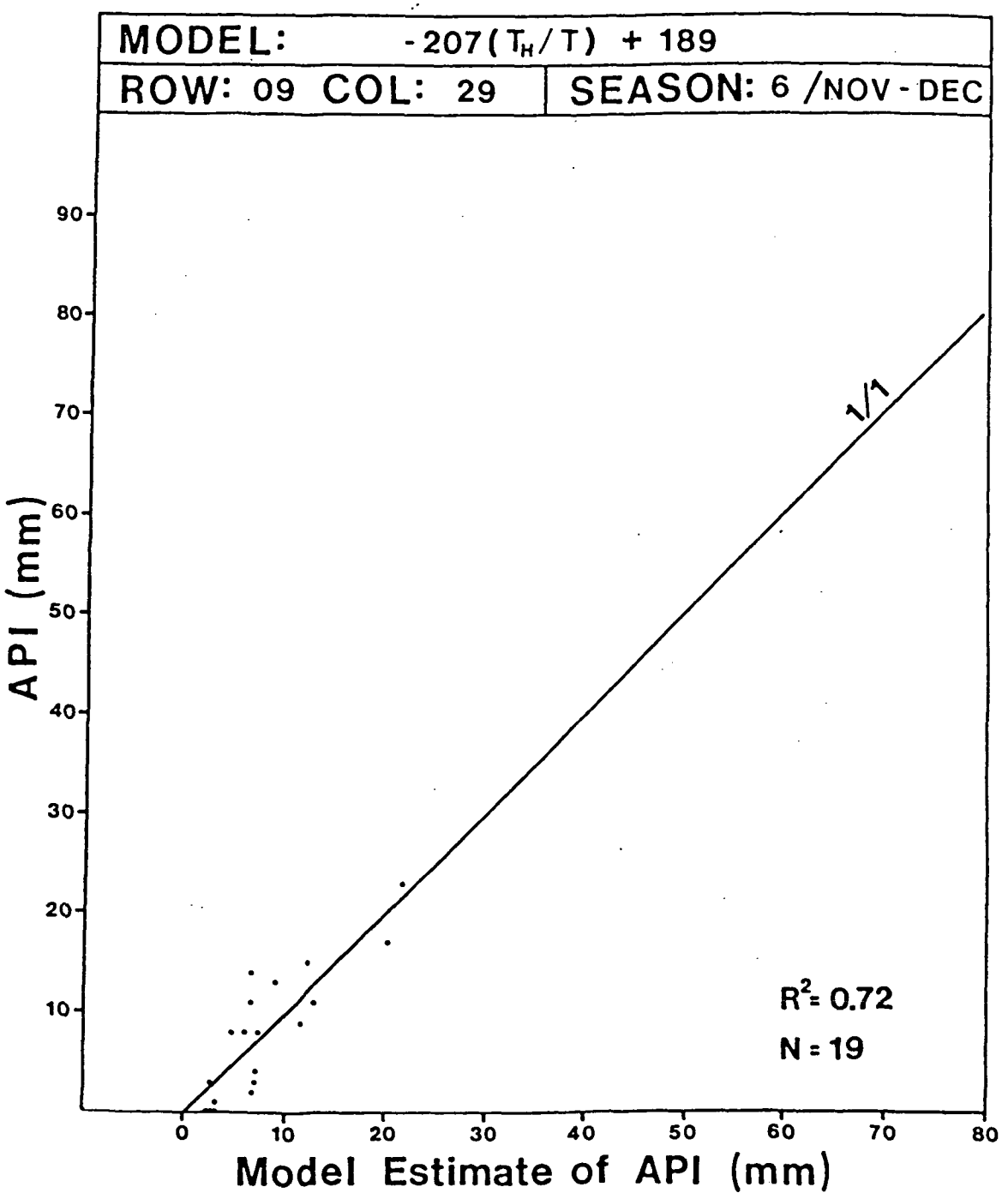

Figure A-5. Regression of API on ϕ_s, season 6, row 09, column 29, south area.

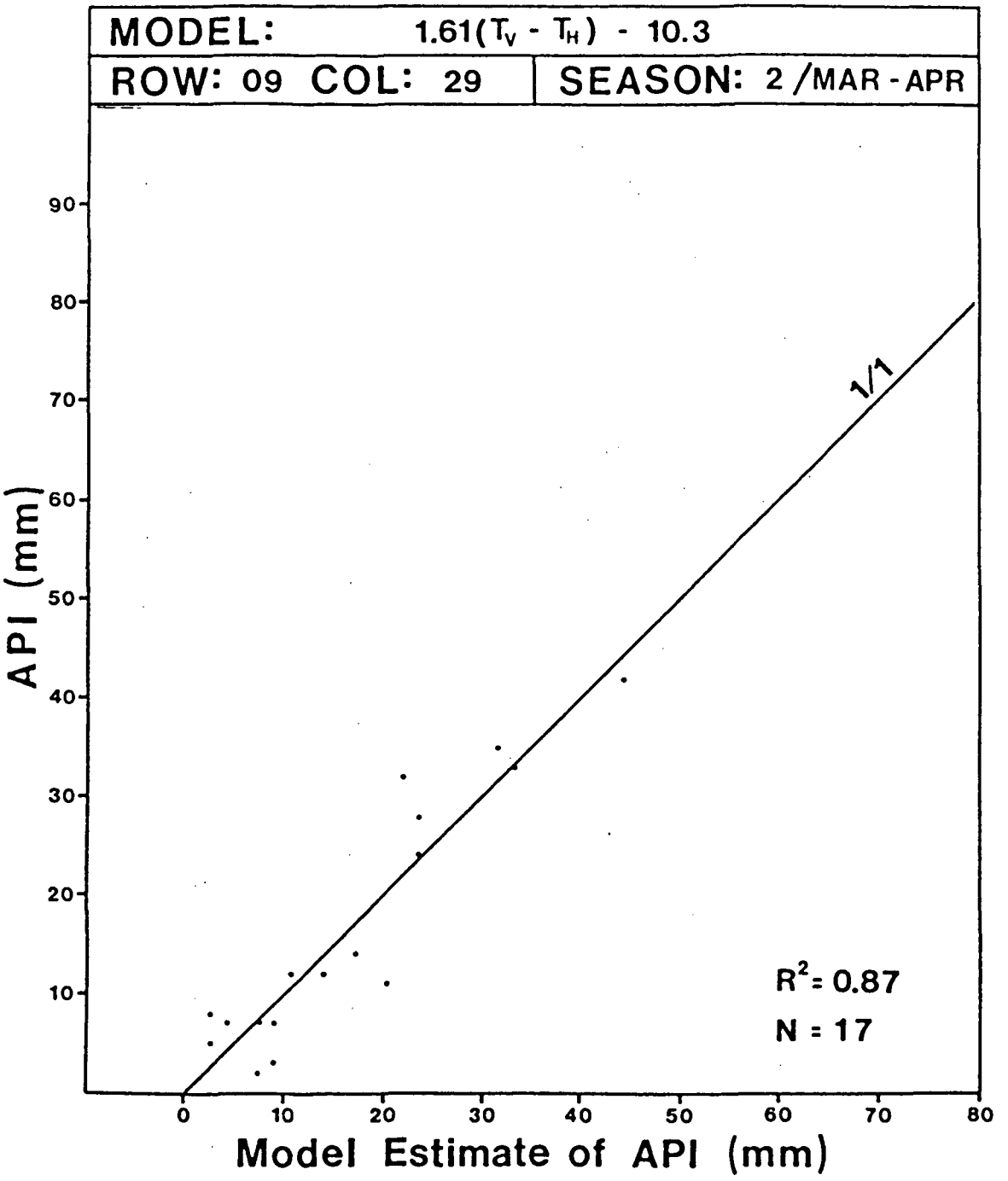

Figure A-6. Regression of API on ϕ, , season 2, row 09, column 29, south area.

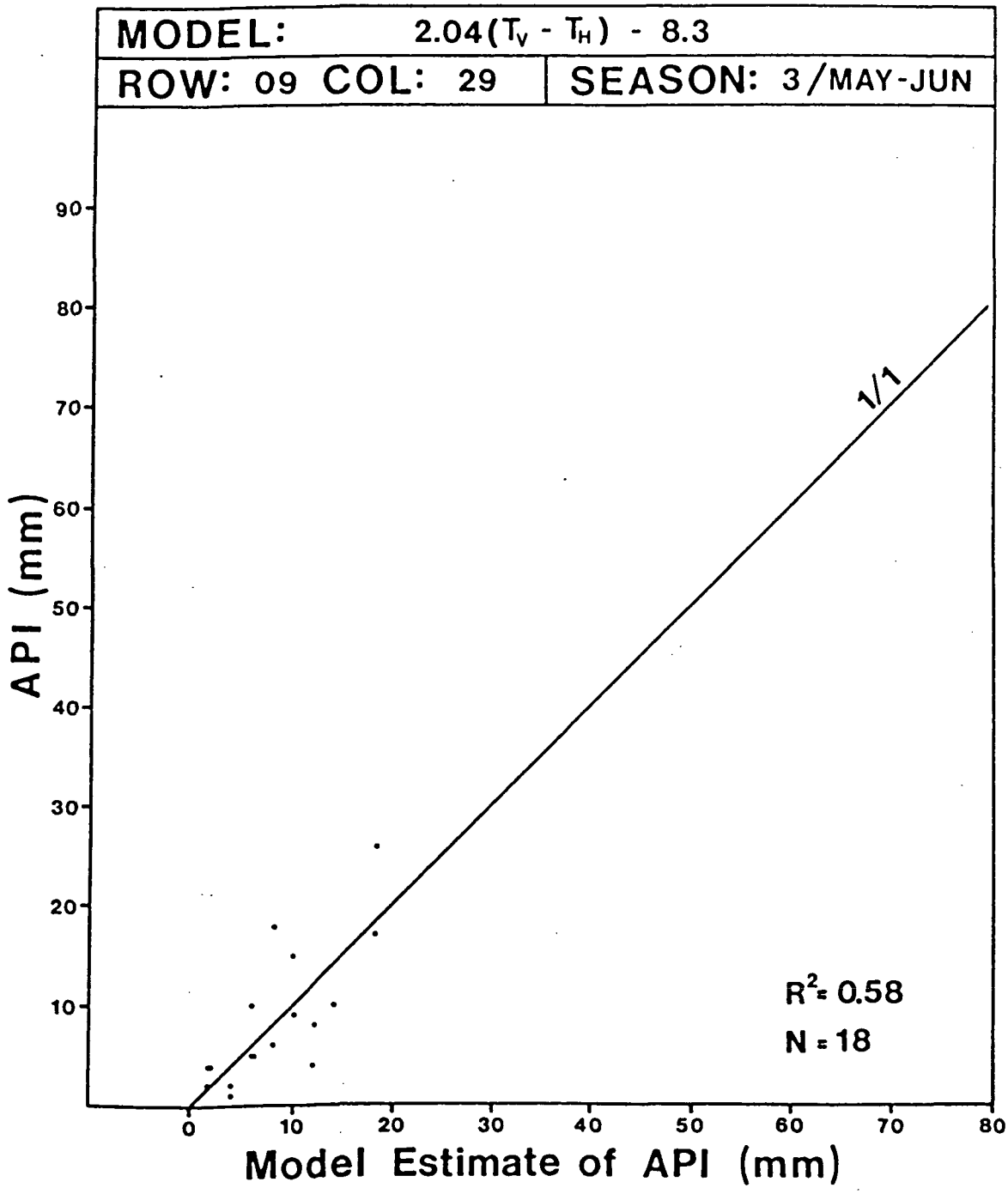

Figure A-7. Regression of API on ϕ_7, season 3, row 09, column 29, south area.

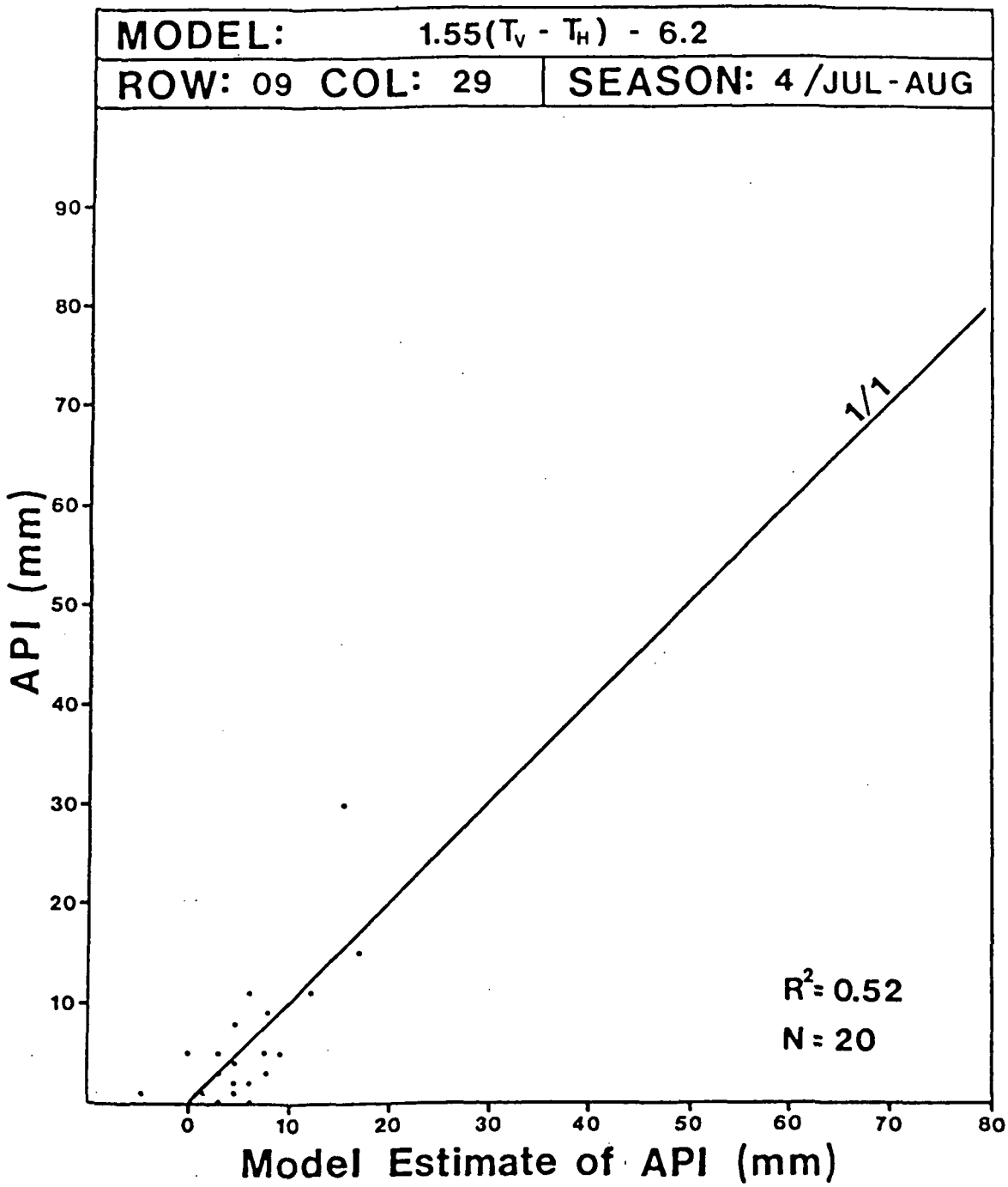

Figure A-8. Regression of API on ϕ,, season 4, row 09, column 29, south area.

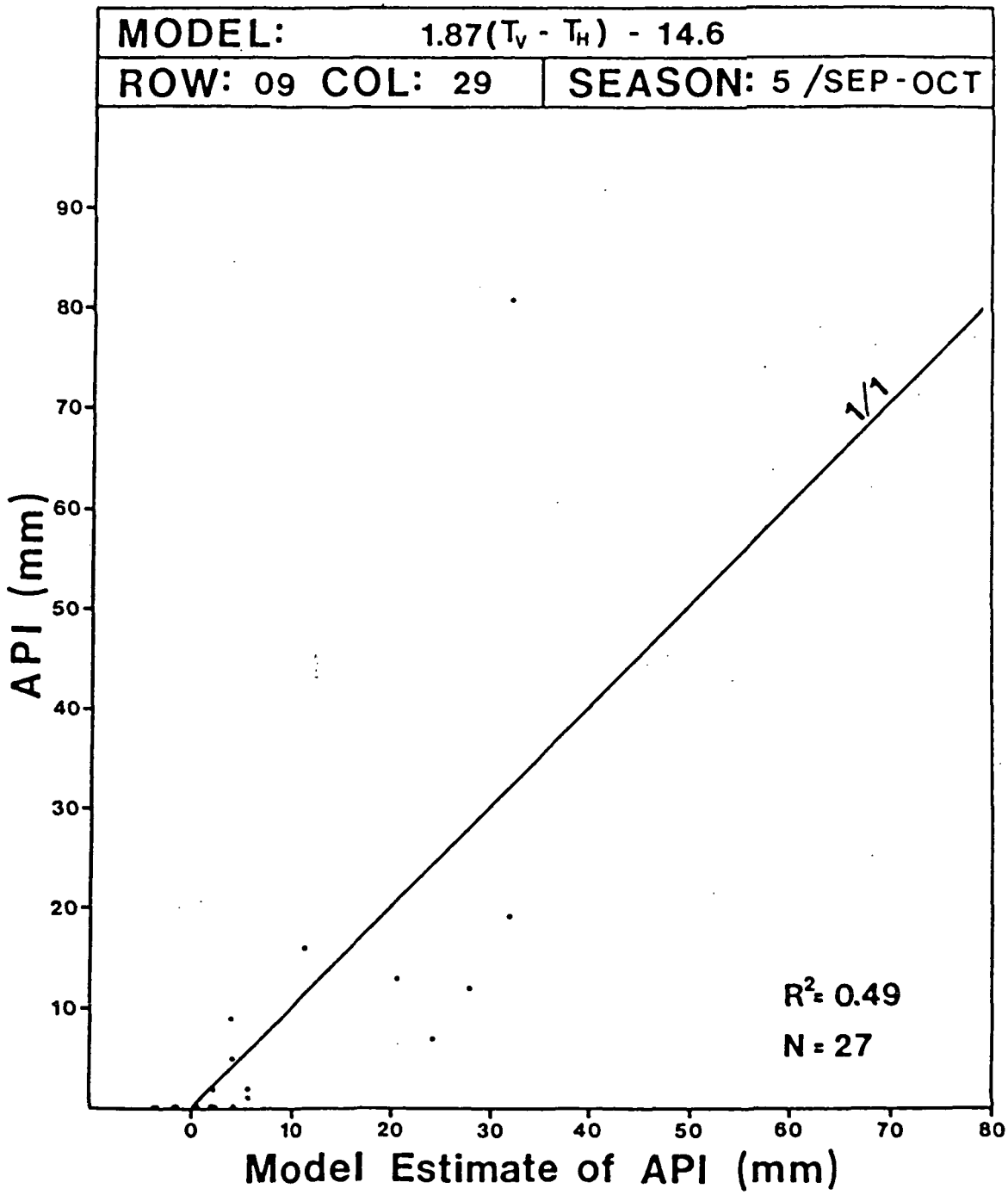

Figure A-9. Regression of API on ϕ, , season 5, row 09, column 29, south area.

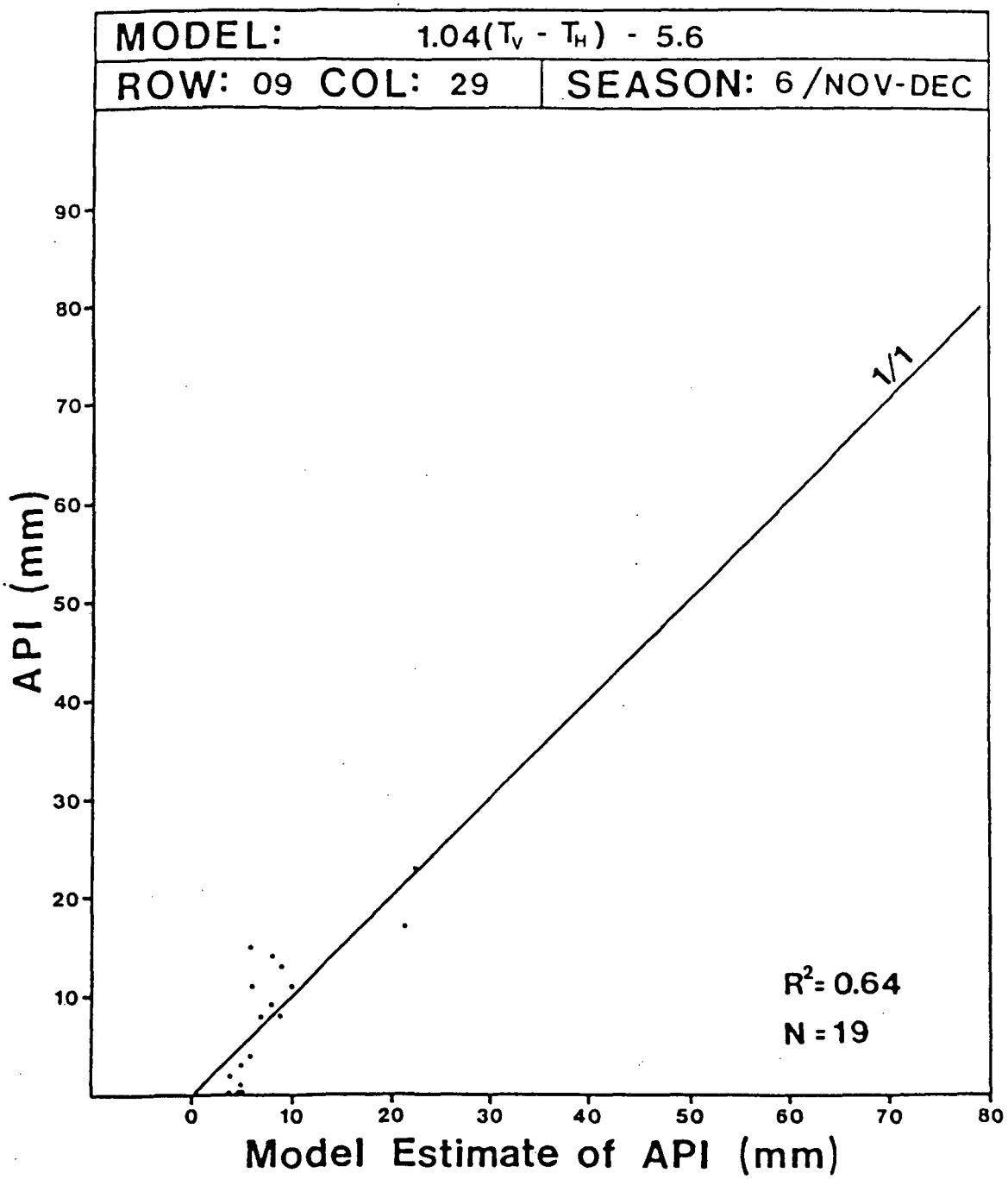

Figure A-10. Regression of API on ϕ_7, season 6, row 09, column 29, south area.

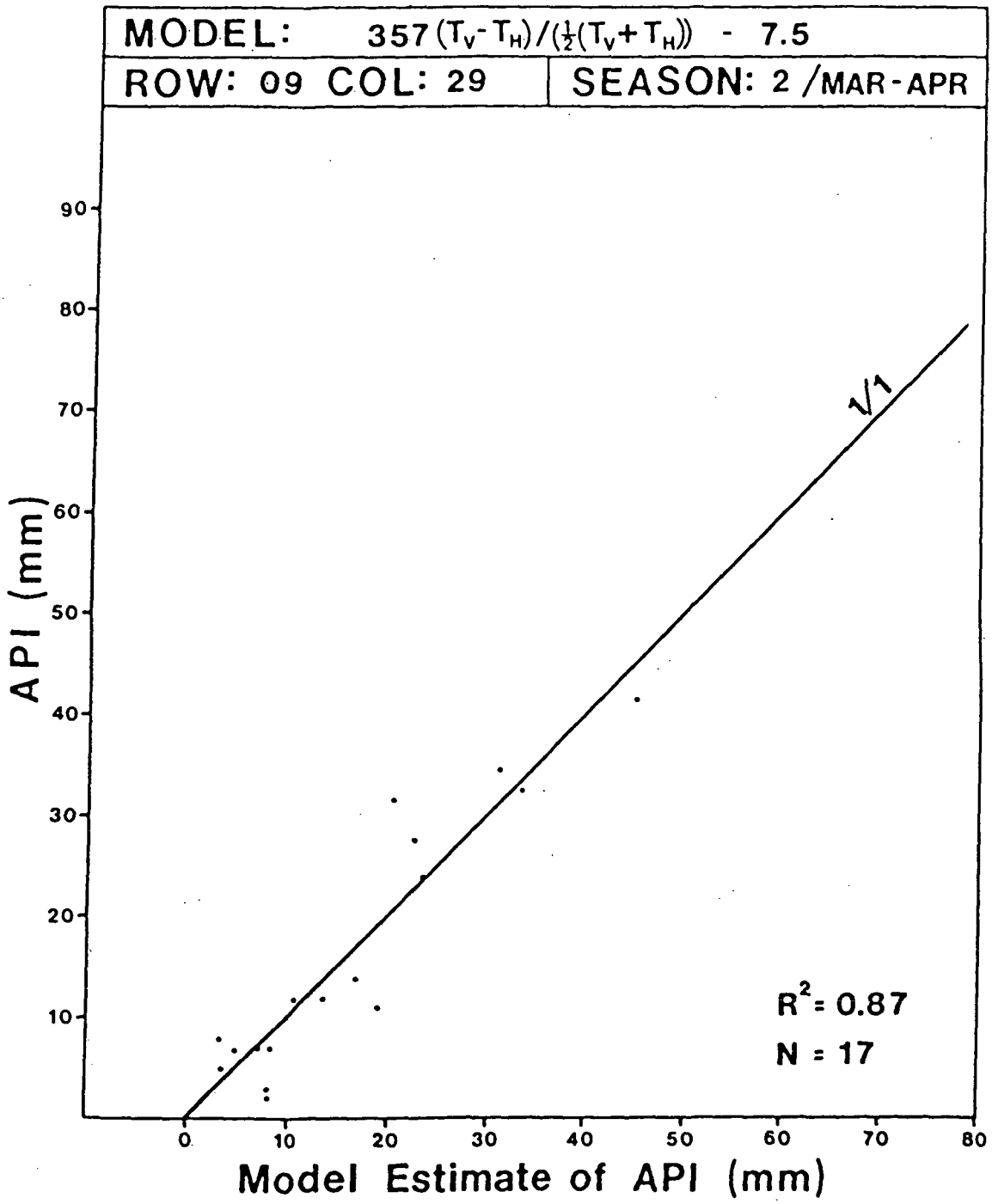

Figure A-11. Regression of API on ϕ_{11}, season 2, row 09, column 29, south area.

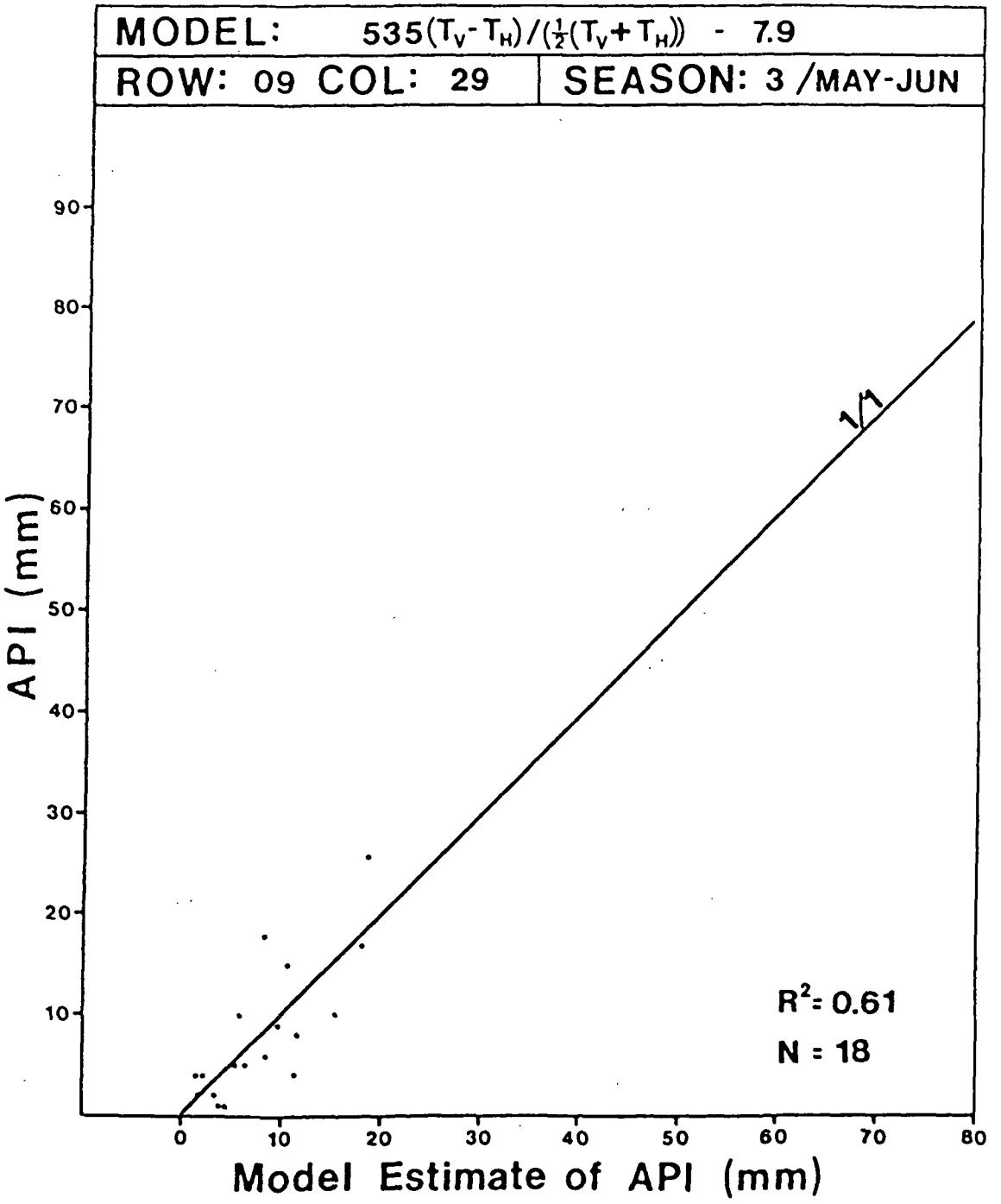

Figure A-12. Regression of API on ϕ_{11}, season 3, row 09, column 29, south area.

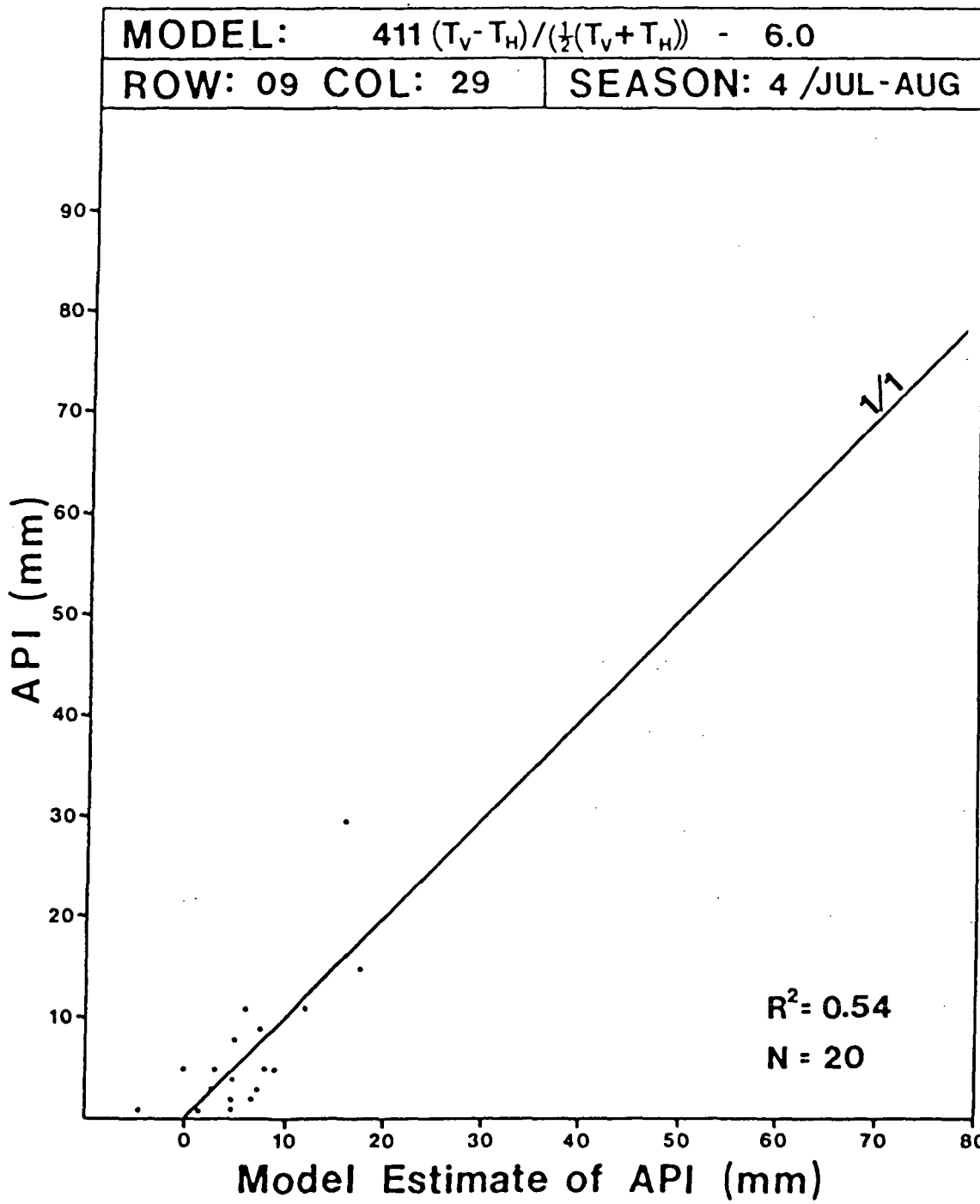

Figure A-13. Regression of API on ϕ_{11}, season 4, row 09, column 29, south area.

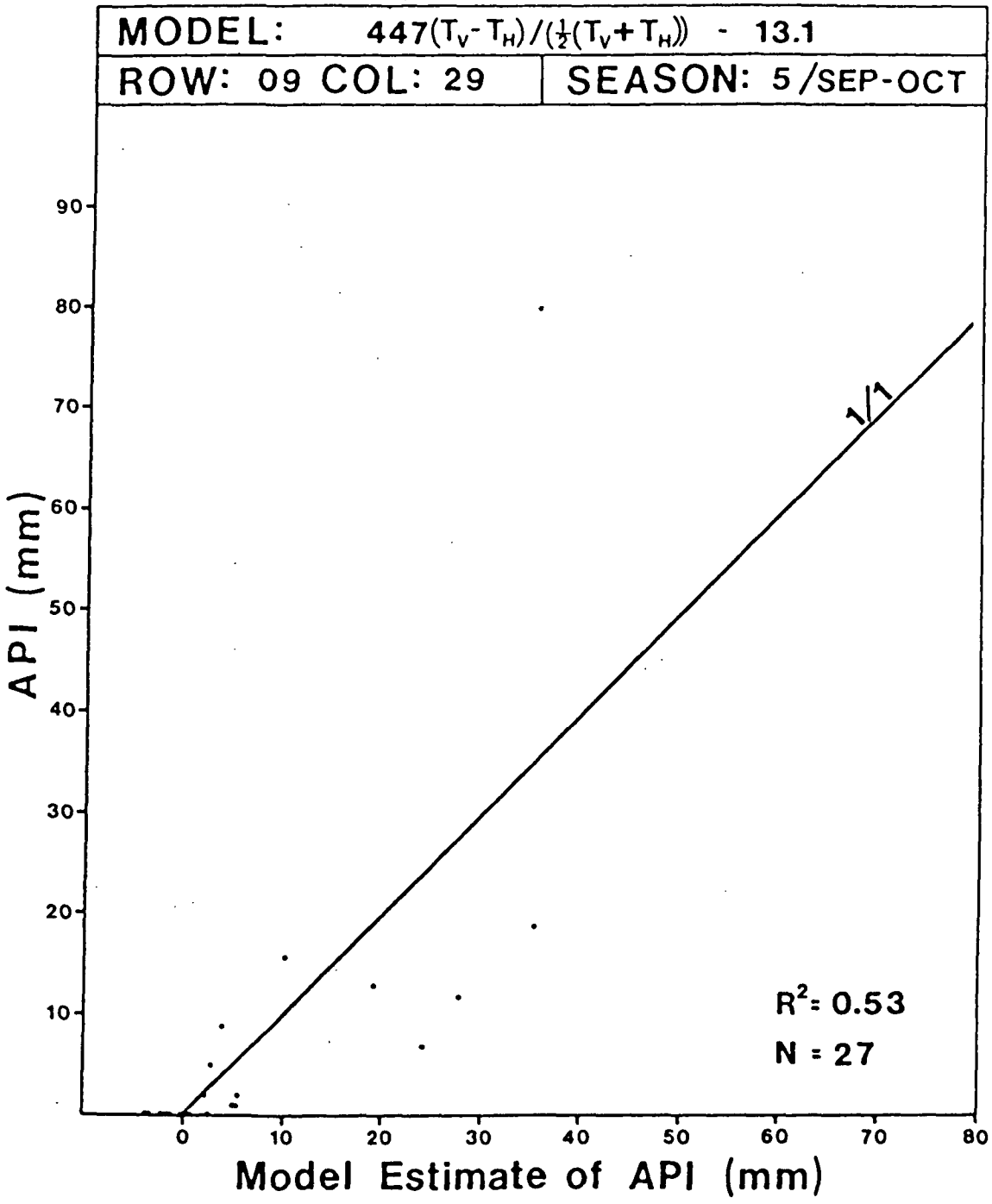

Figure A-14. Regression of API on ϕ_{11}, season 5, row 09, column 29, south area.

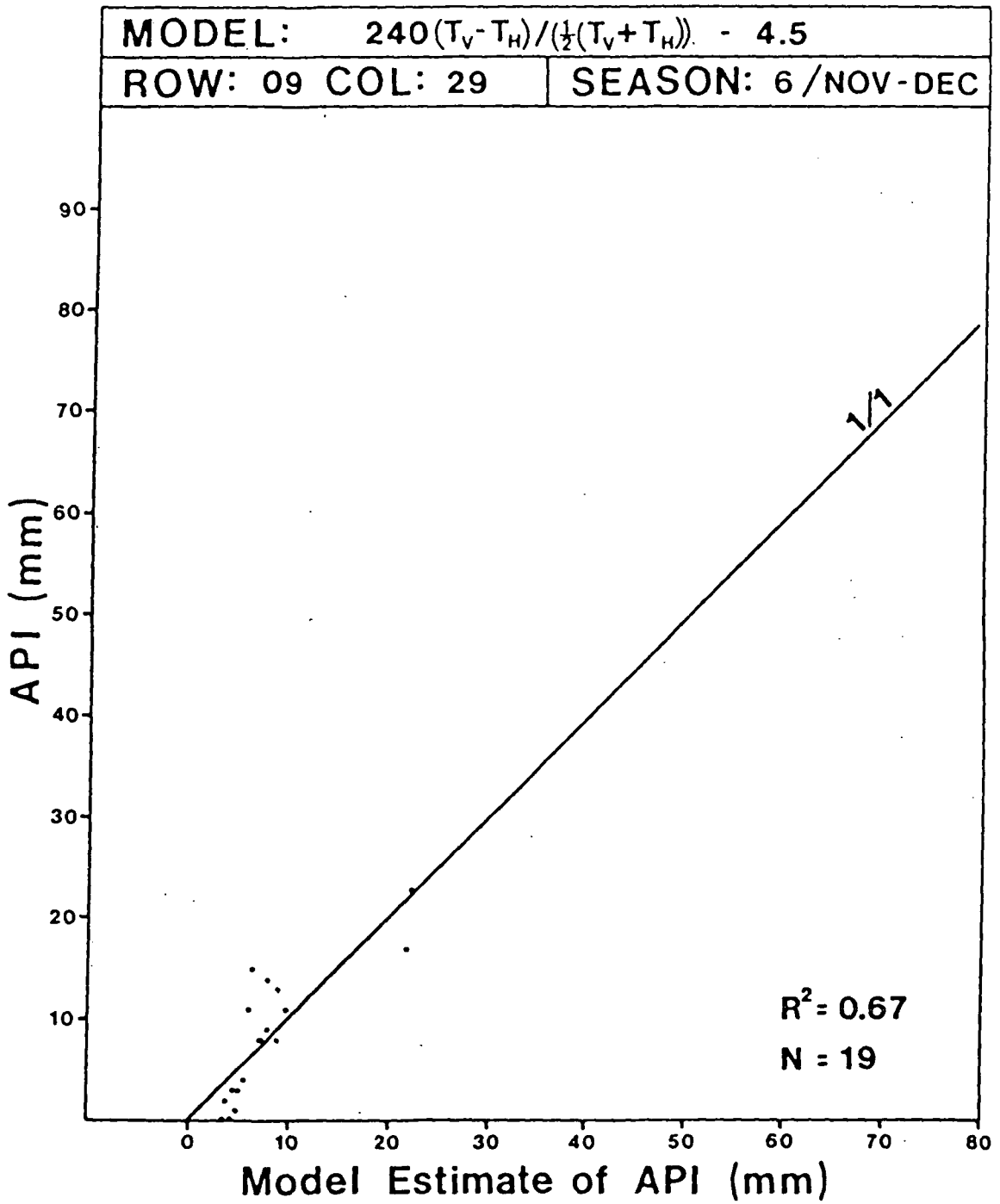

Figure A-15. Regression of API on ϕ_{11}, season 6, row 09, column 29, south area.

APPENDIX B

TIME SERIES PLOTS

This appendix presents plots, in the time domain, of API against regression model estimates of API. The solid curve is API from the climatic database. The large and small dots are, respectively, API estimates from the annual and seasonal regression models. For comparision, the seasons are demarcated along the top of the graphs and the days with snow cover are indicated at the bottom.

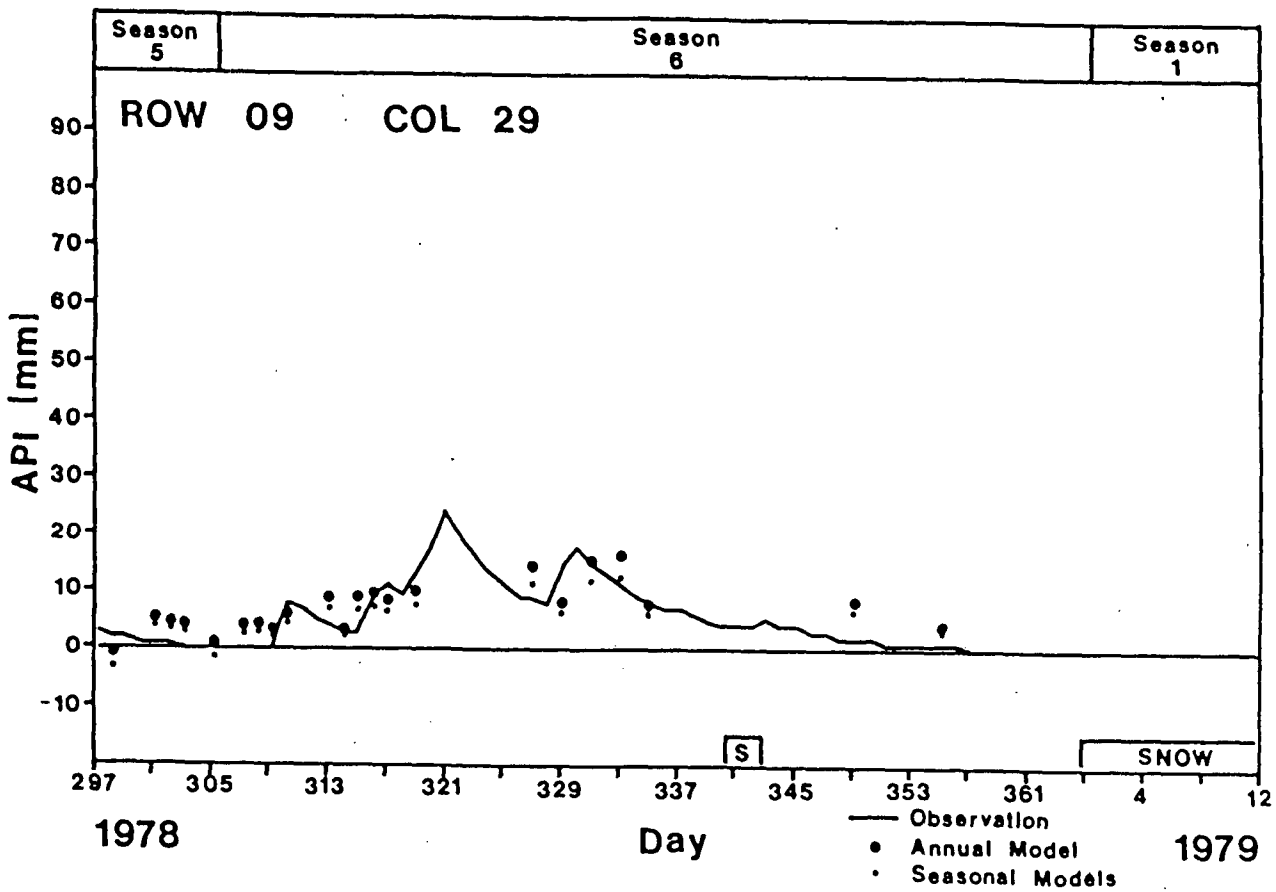

Figure B-1a. Time series plots of API and regression model estimates of API based on ϕ_s , row 09, column 29, south area.

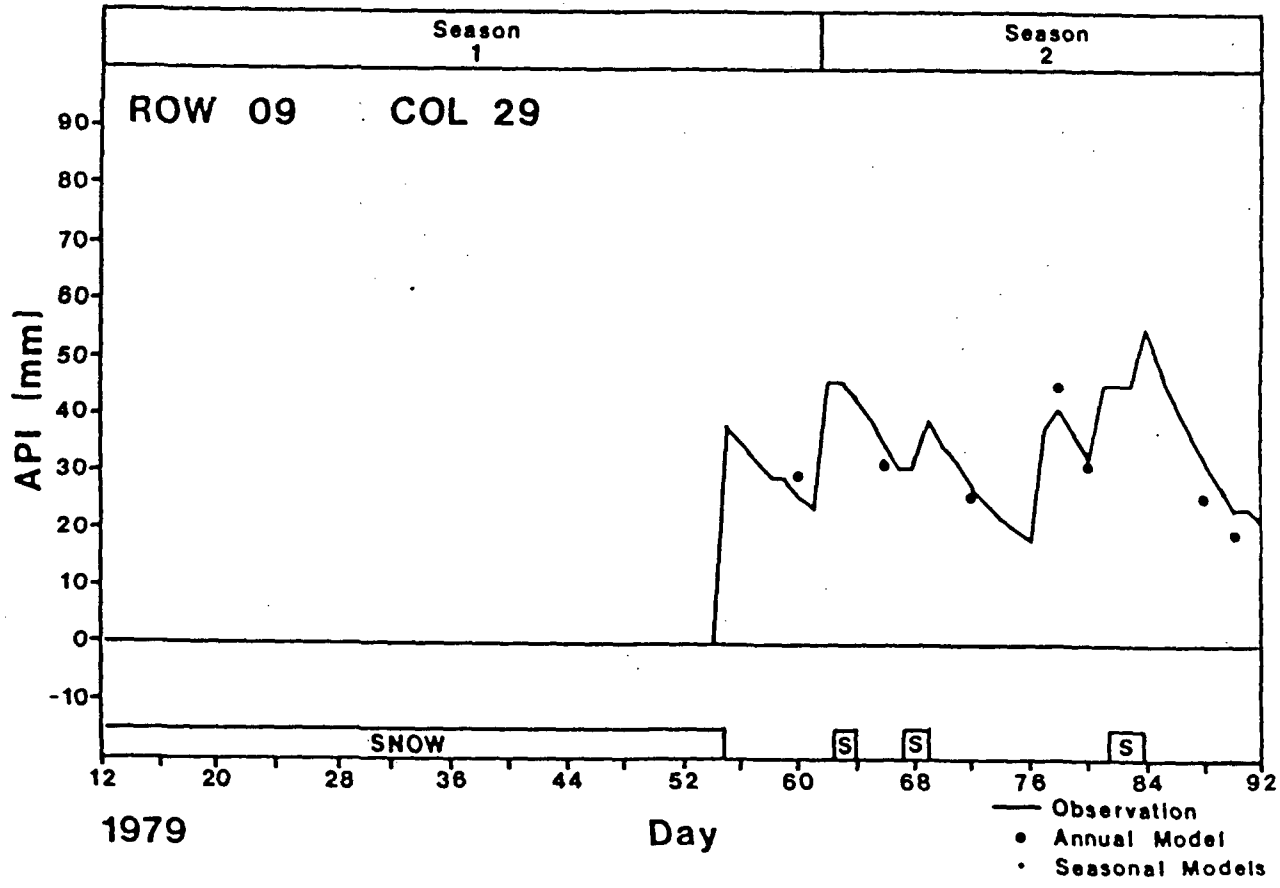

Figure B-1b. Time series plots of API and regression model estimates of API based on ϕ_s , row 09, column 29, south area.

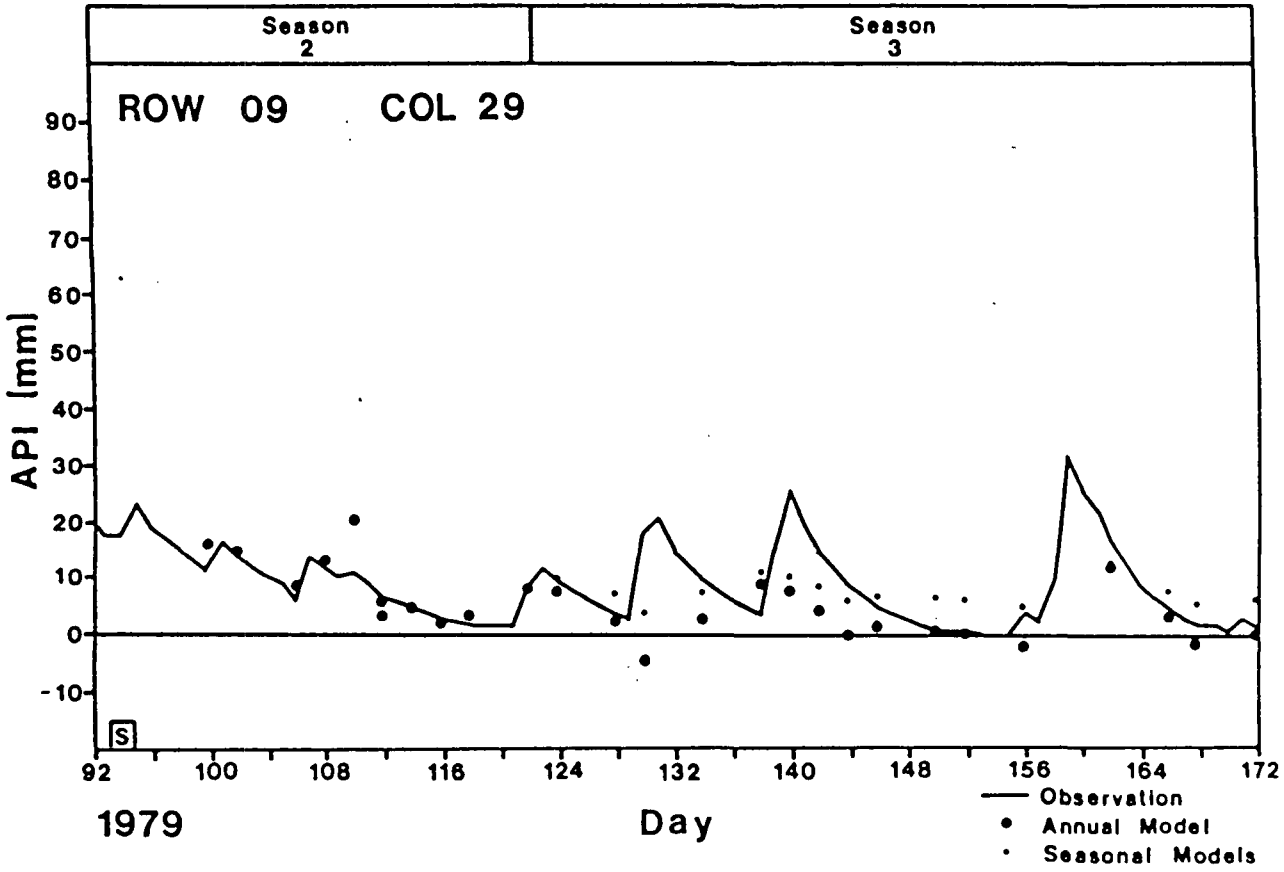

Figure B-1c. Time series plots of API and regression model estimates of API based on ϕ_s , row 09, column 29, south area.

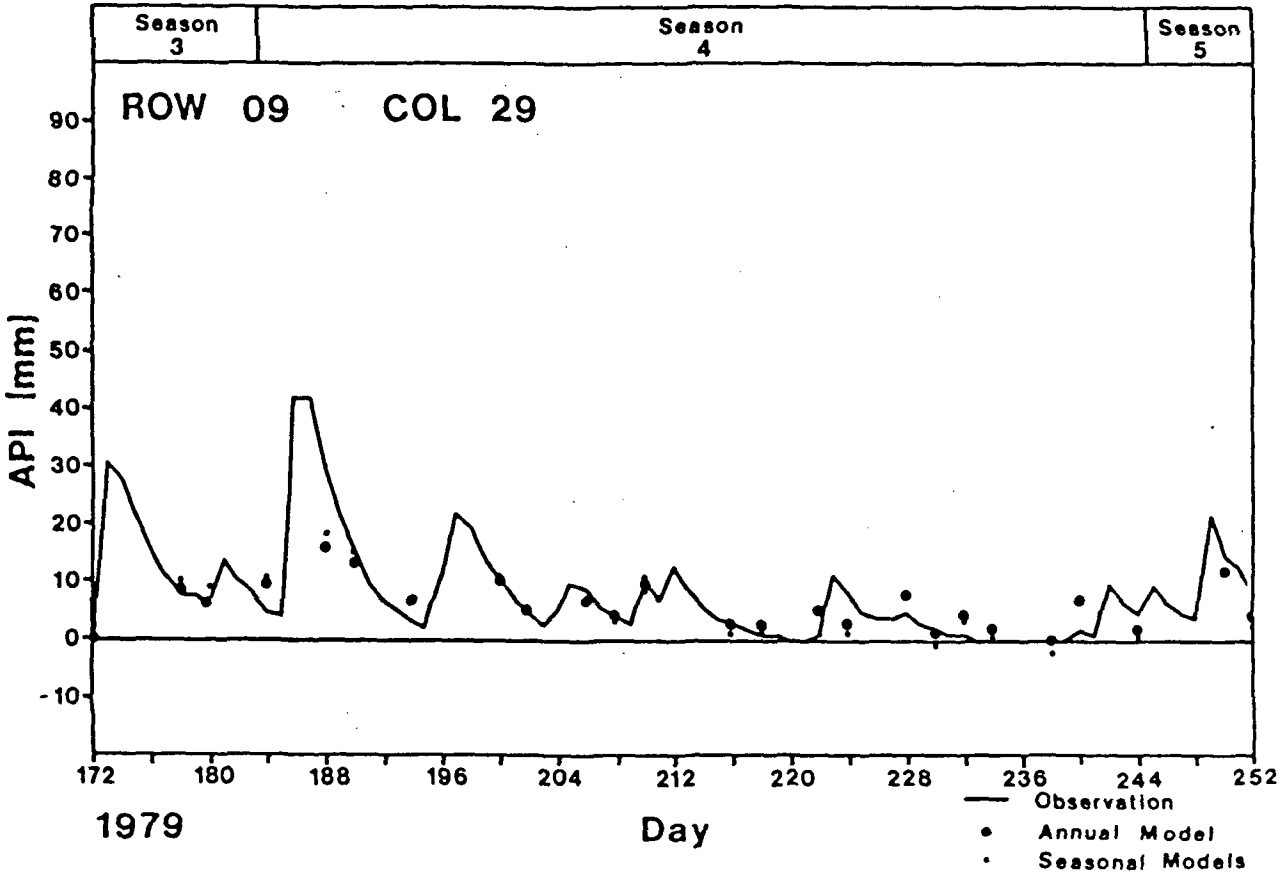

Figure B-1d. Time series plots of API and regression model estimates of API based on ϕ_s , , row 09, column 29, south area.

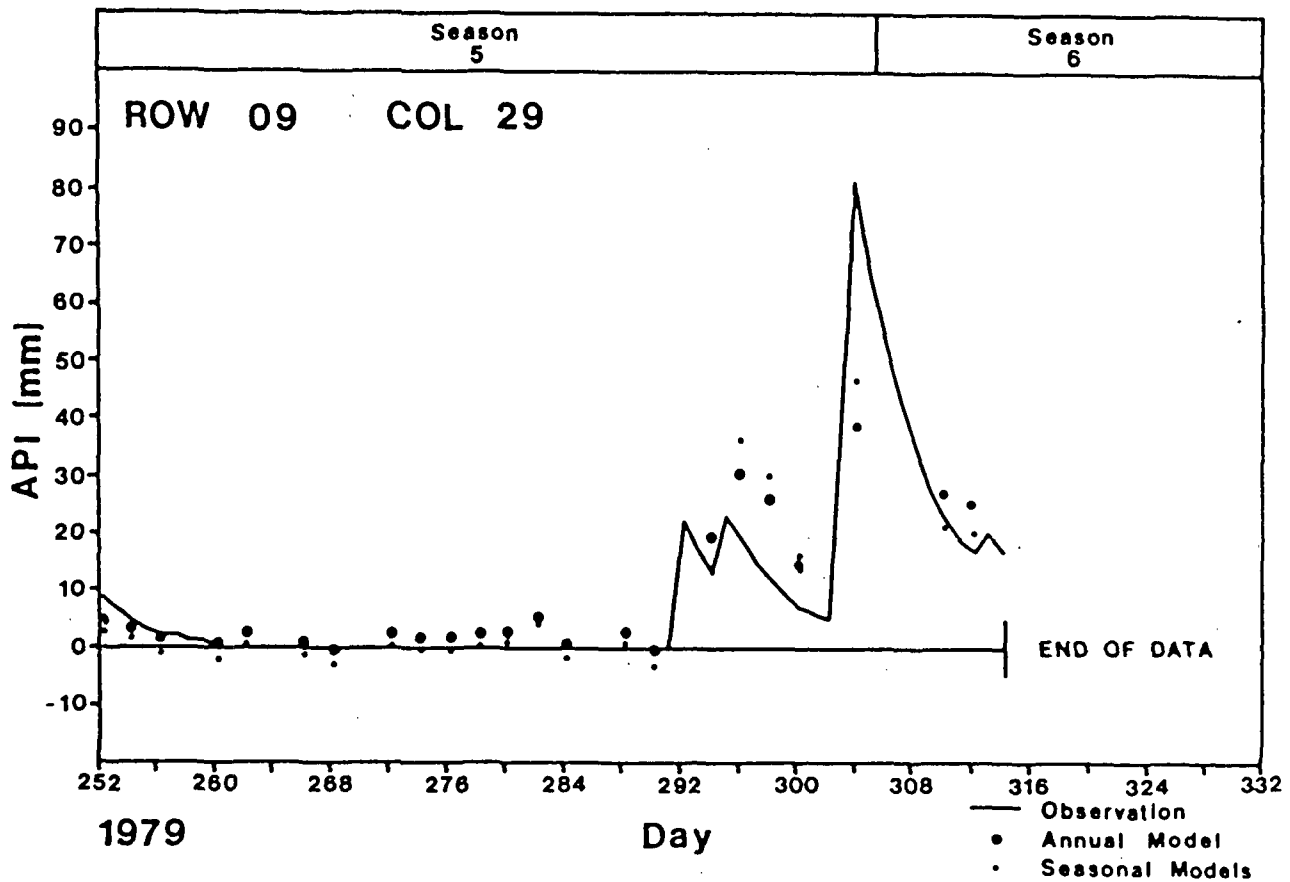

Figure B-1e. Time series plots of API and regression model estimates of API based on ϕ_s , row 09, column 29, south area.

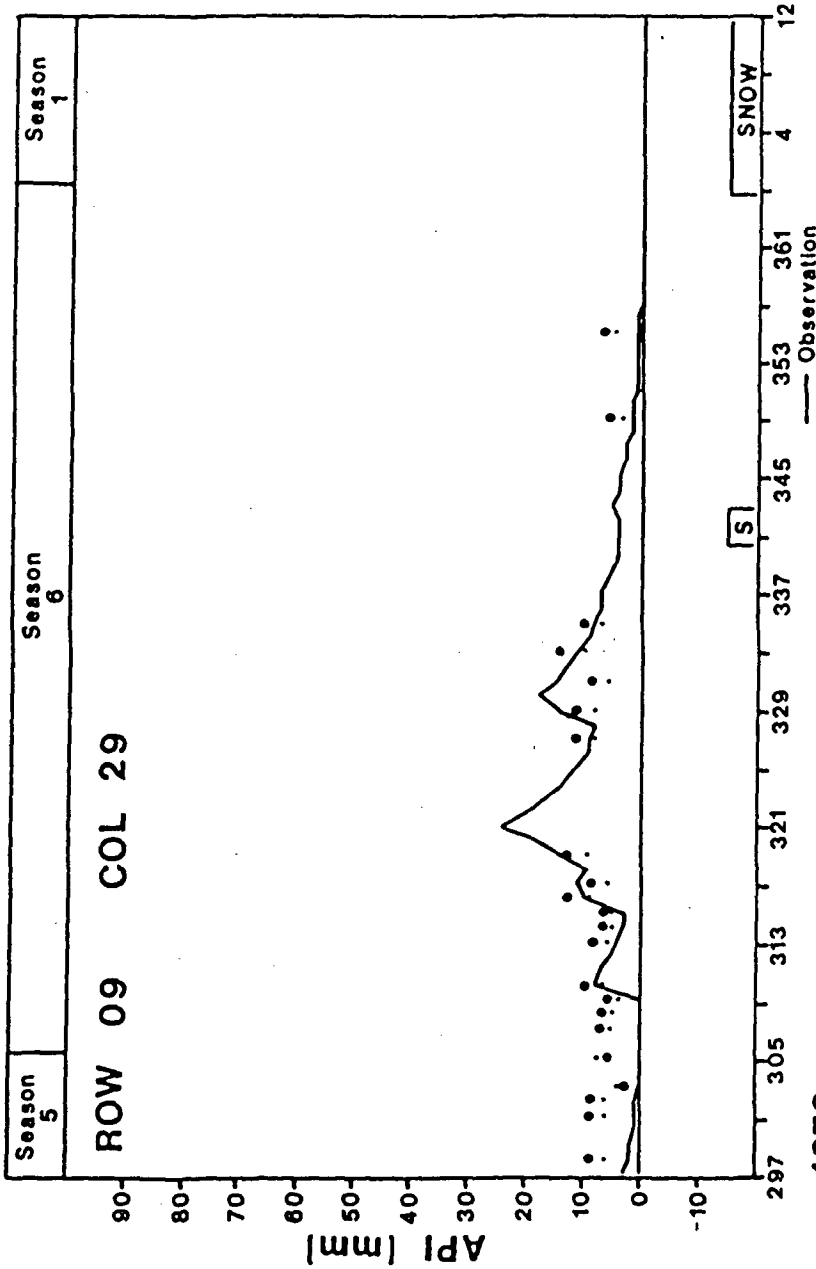

Figure B-2a. Time series plots of API and regression model estimates of API based on ϕ_7, row 09, column 29, south area.

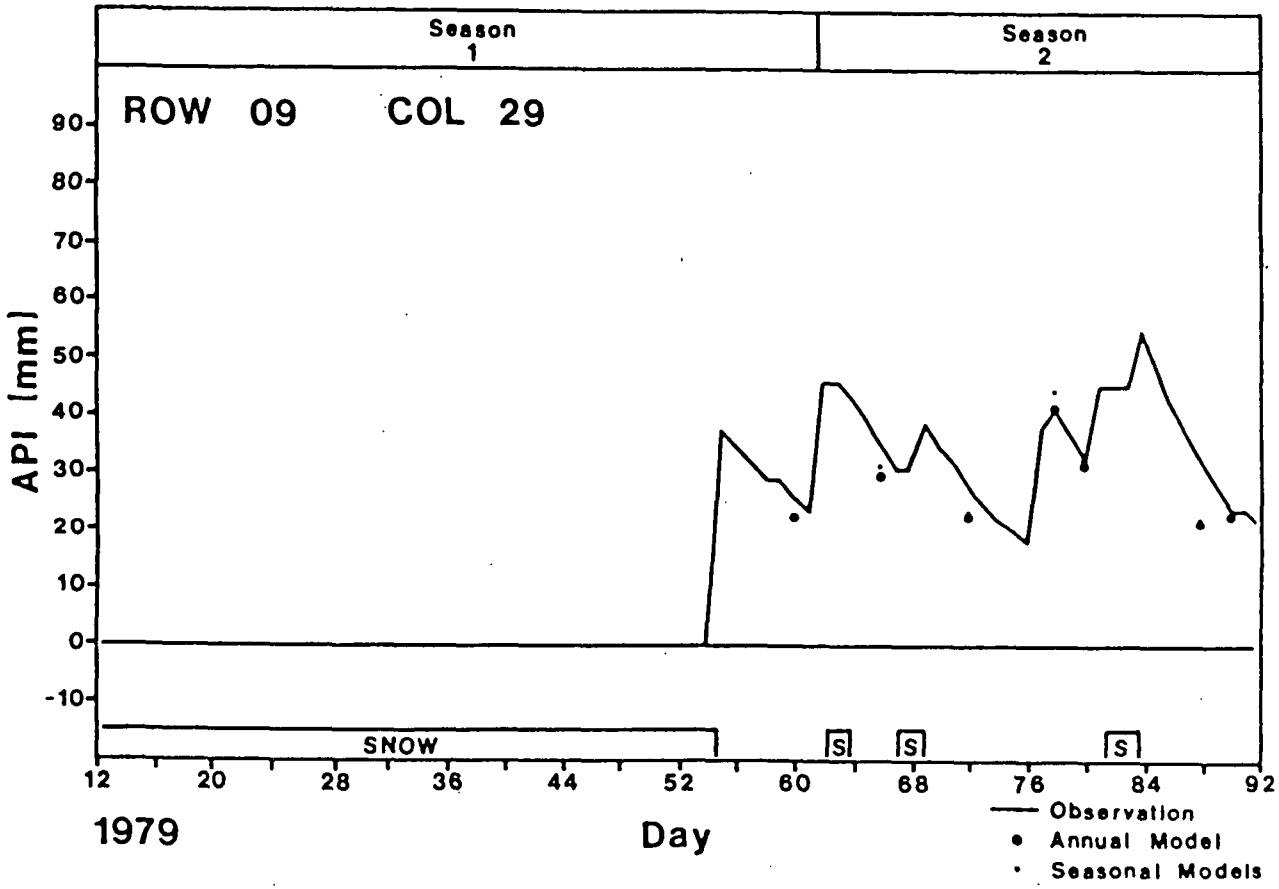

Figure B-2b. Time series plots of API and regression model estimates of API based on ϕ, , row 09, column 29, south area.

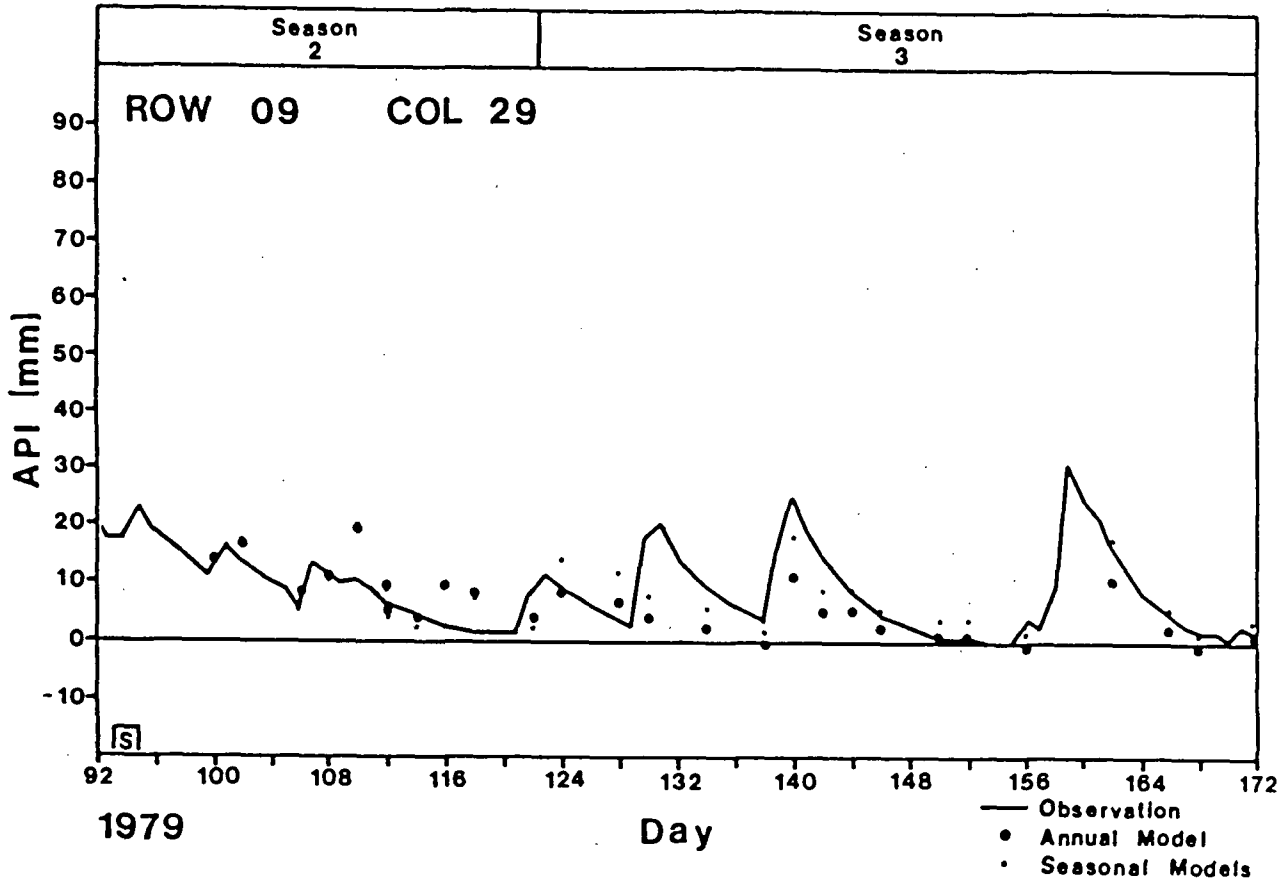

Figure B-2c. Time series plots of API and regression model estimates of API based on ϕ, , row 09, column, 29, south area.

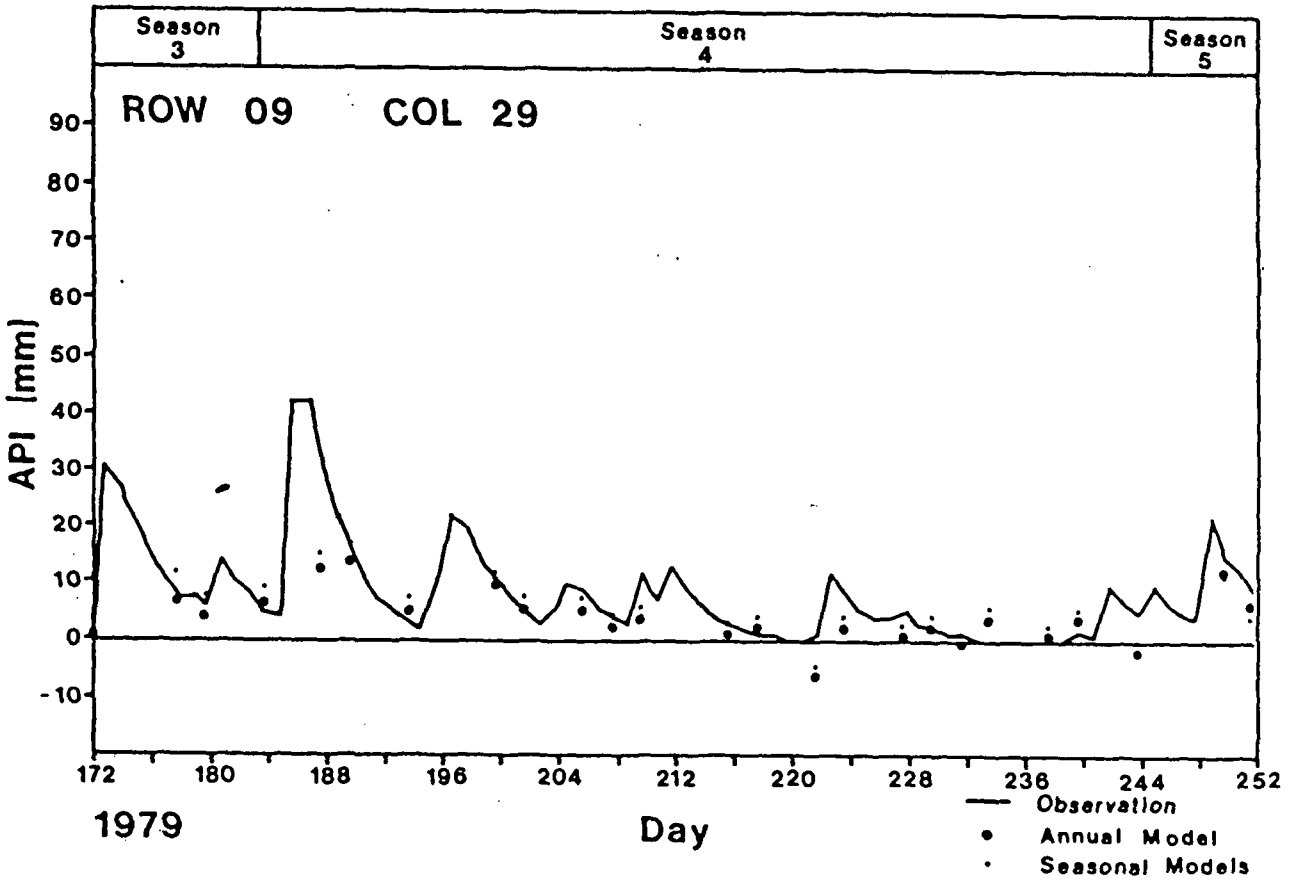

Figure B-2d. Time series plots of API and regression model estimates of API based on ϕ, , row 09, column 29, south area.

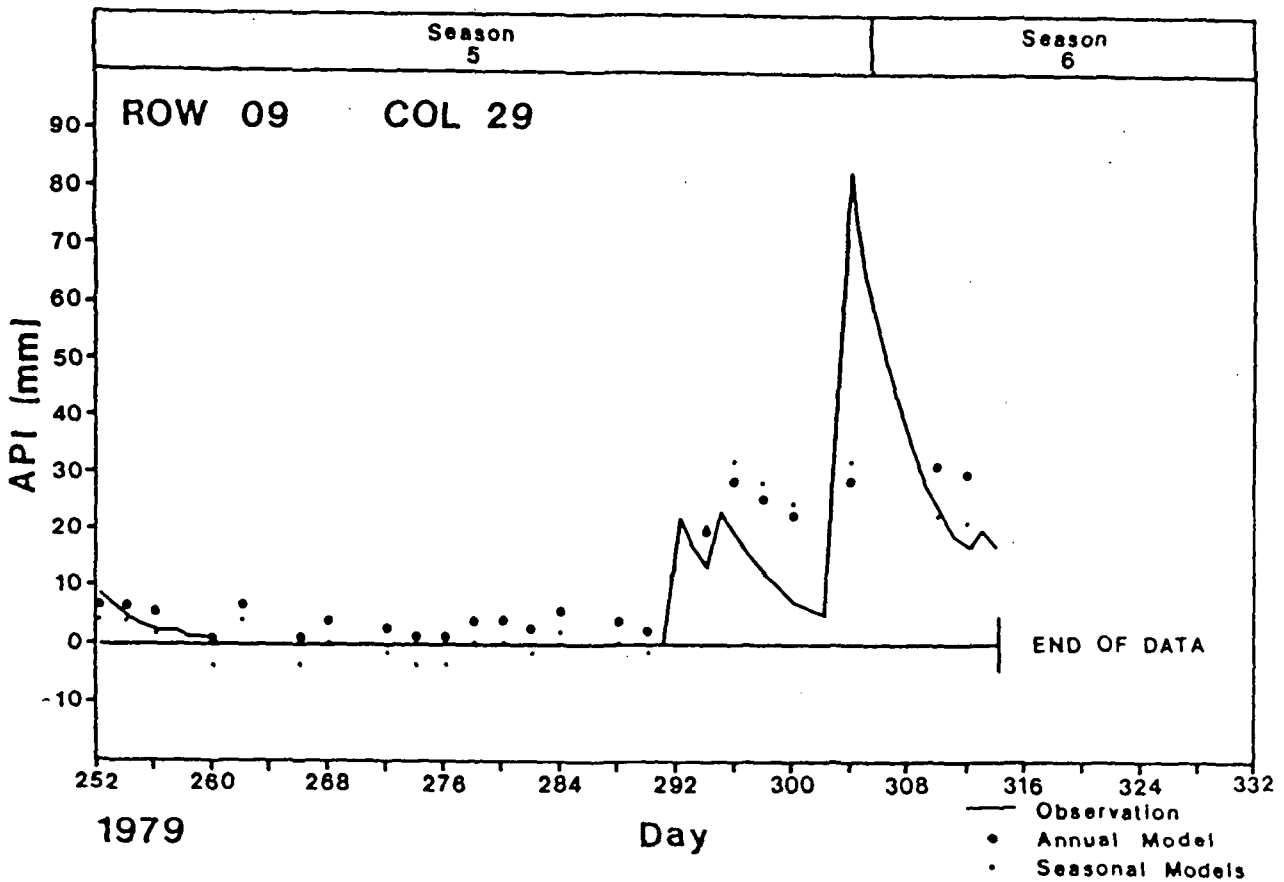

Figure B-2e. Time series plots of API and regression model estimates of API based on ϕ, , row 09, column, 29, south area.

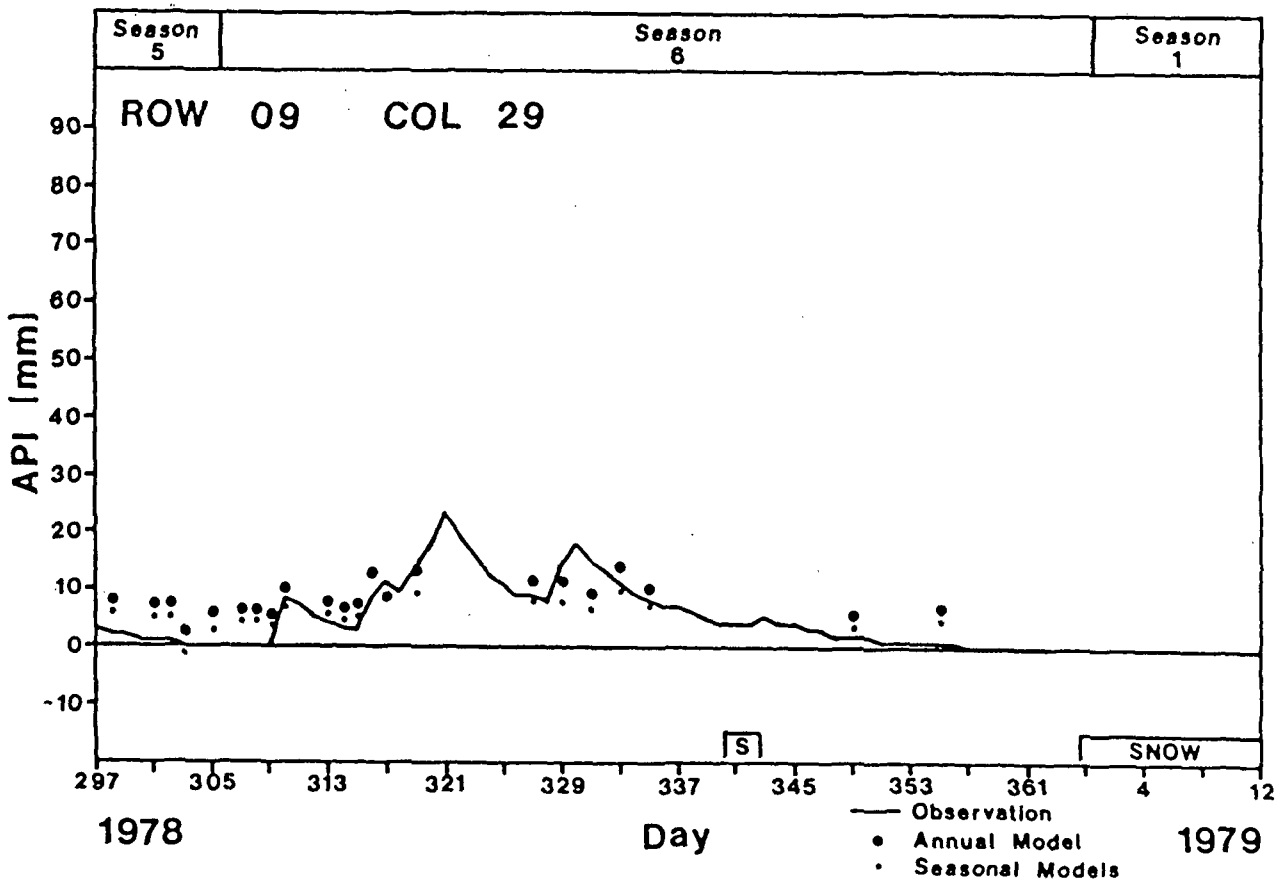

Figure B-3a. Time series plots of API and regression model estimates of API based on ϕ_{11}, row 09, column 29, south area.

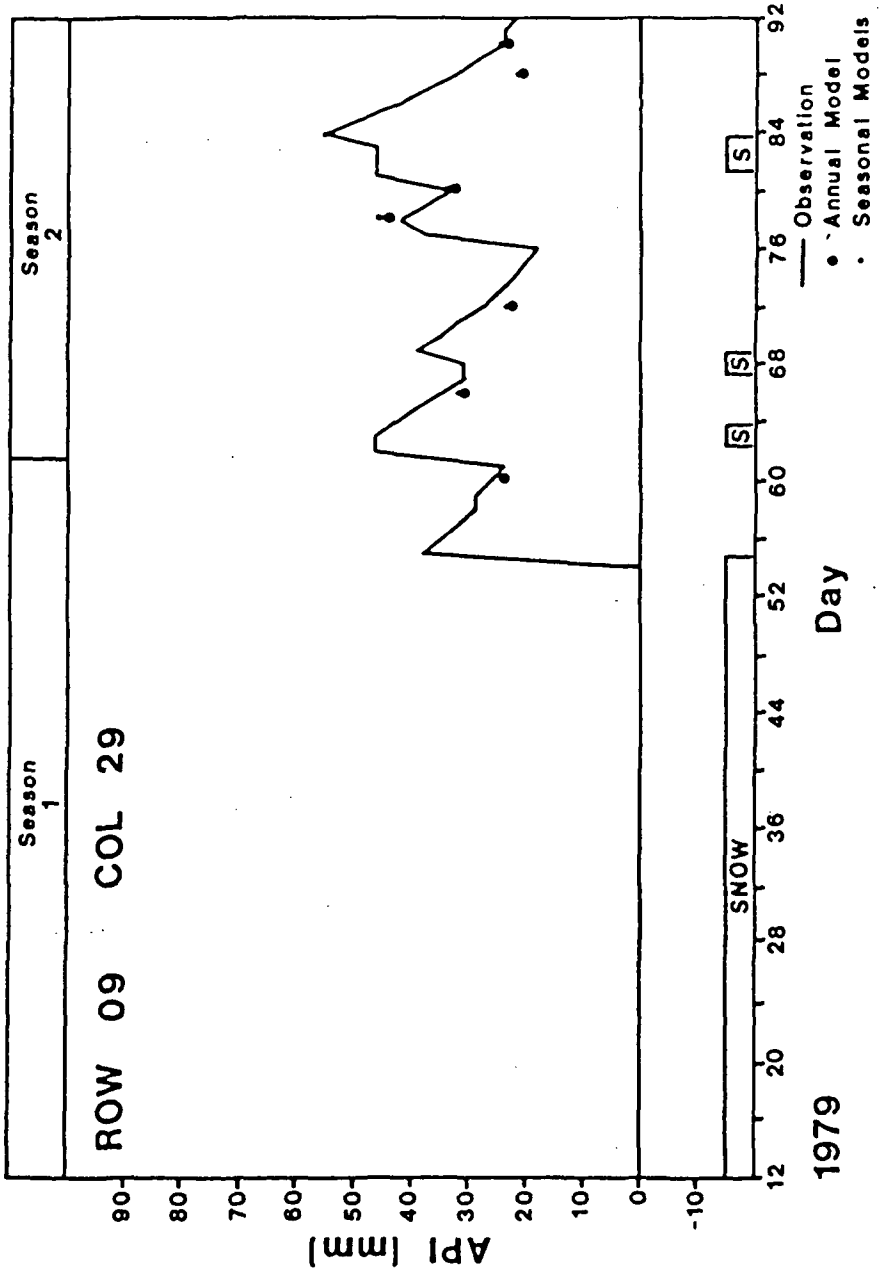

Figure B-3b. Time series plots of API and regression model estimates of API based on $\phi_{1,1}$, row 09, column 29, south area.

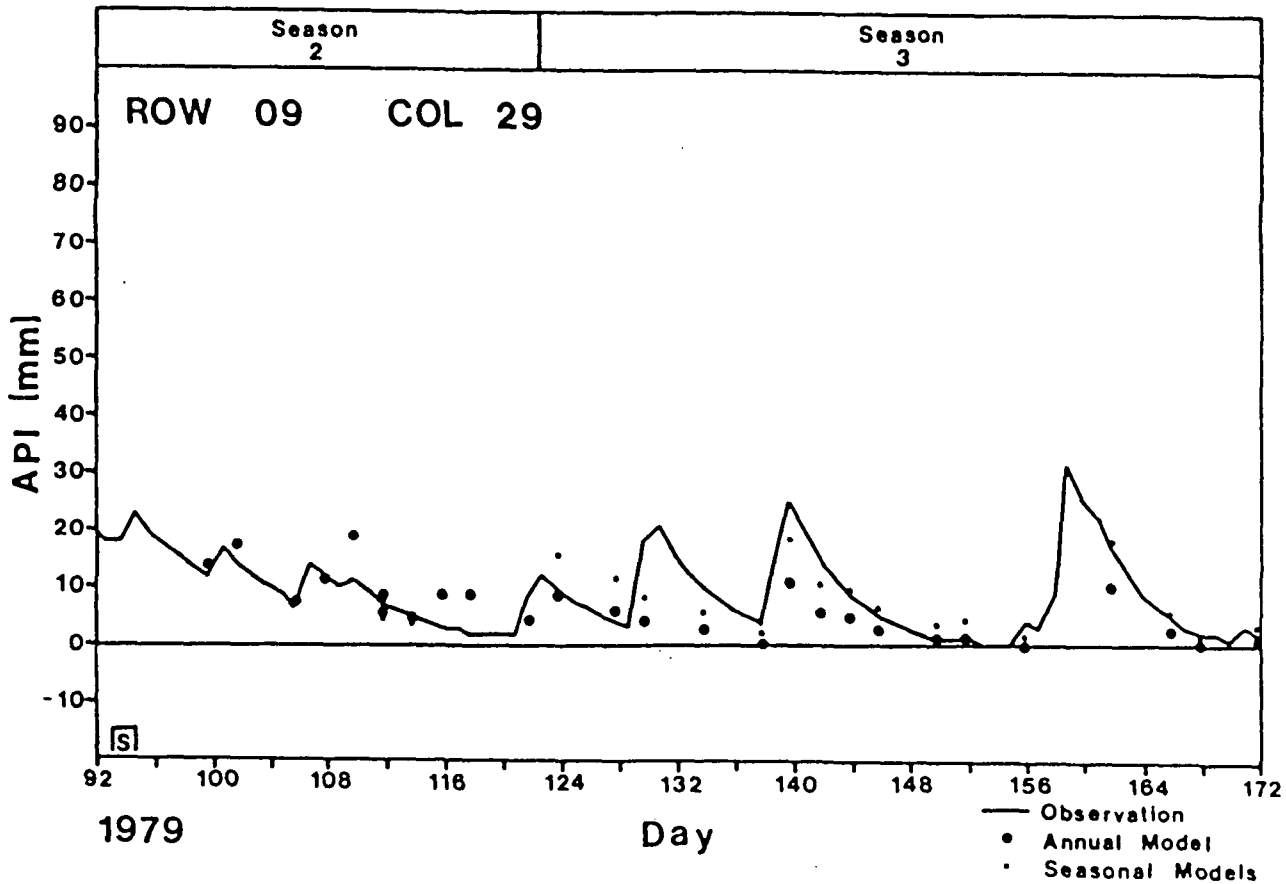

Figure B-3c. Time series plots of API and regression model estimates of API based on ϕ_{11}, row 09, column 29, south area.

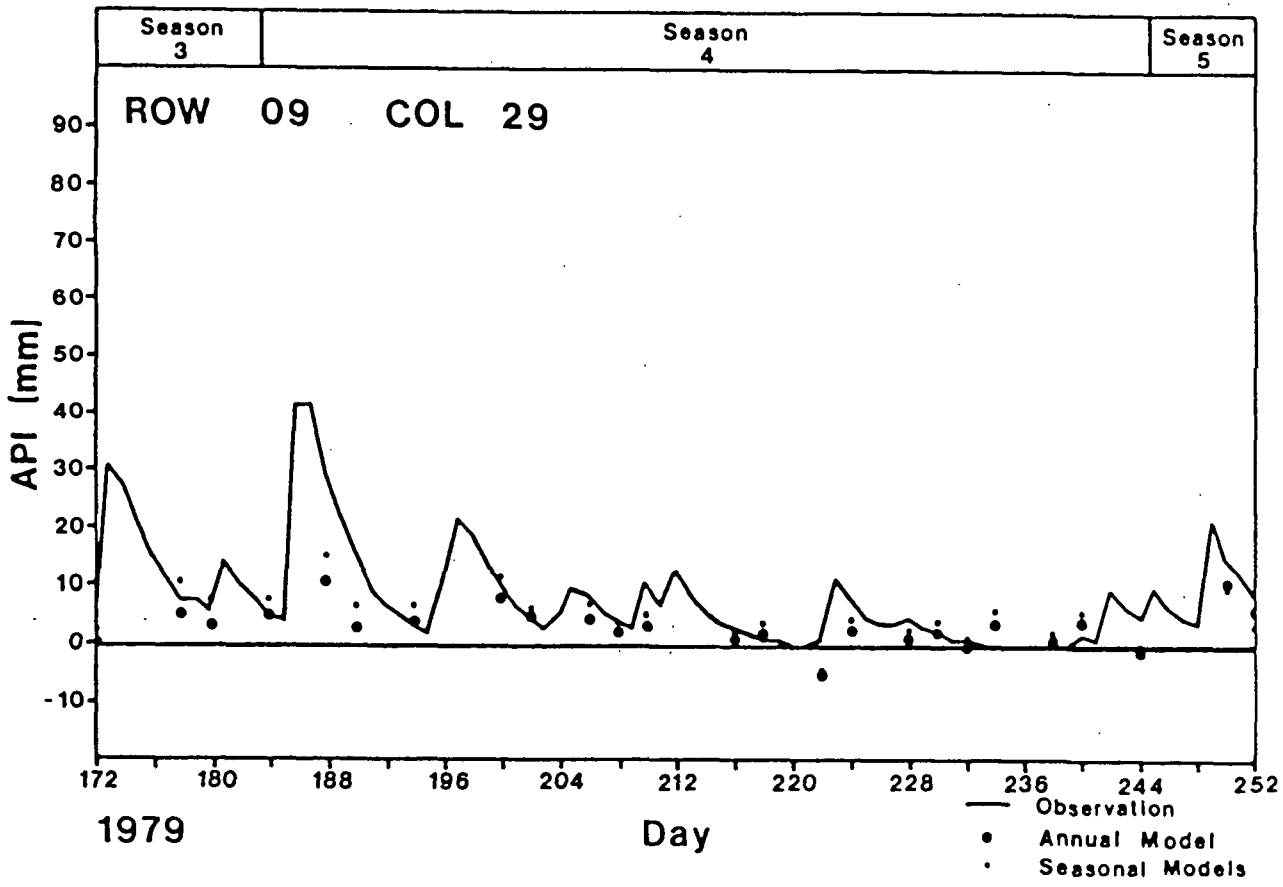

Figure B-3d. Time series plots of API and regression model estimates of API based on ϕ_{11} , row 09, column 29, south area.

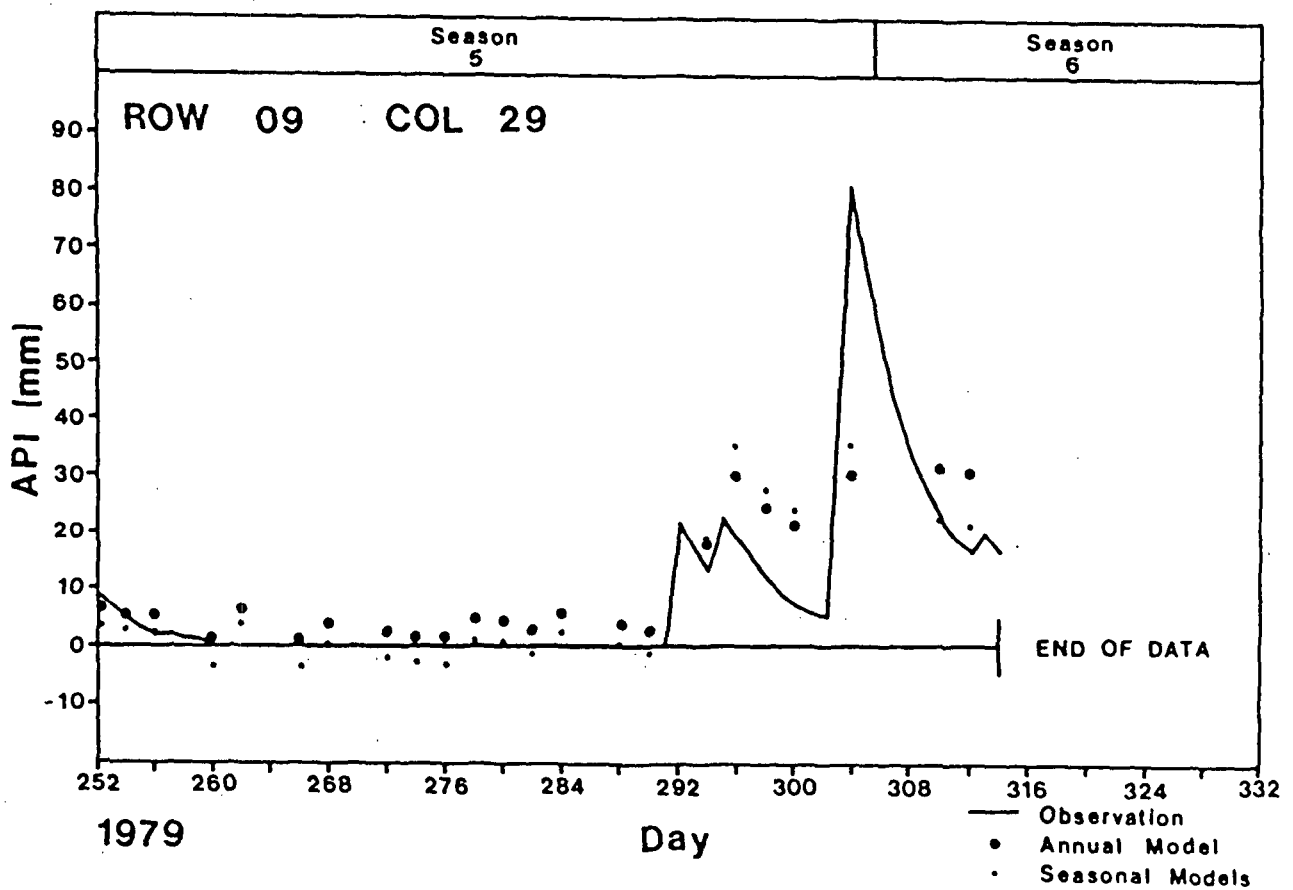

Figure B-3e. Time series plots of API and regression model estimates of API based on $\phi_{1,1}$, row 09, column 29, south area.

APPENDIX C

SCATTER PLOTS OF ϕ_5 and ϕ_7 FOR SEASONS 2-6

The following figures demonstrate the linear relationship between two of the microwave indices used in this report. In each graph, the abscissa is ϕ_5, the normalized horizontal brightness temperature or emissivity; the ordinate is ϕ_7, the difference between polarized channels. The summary graph with data with the entire year is presented in Chapter 4.

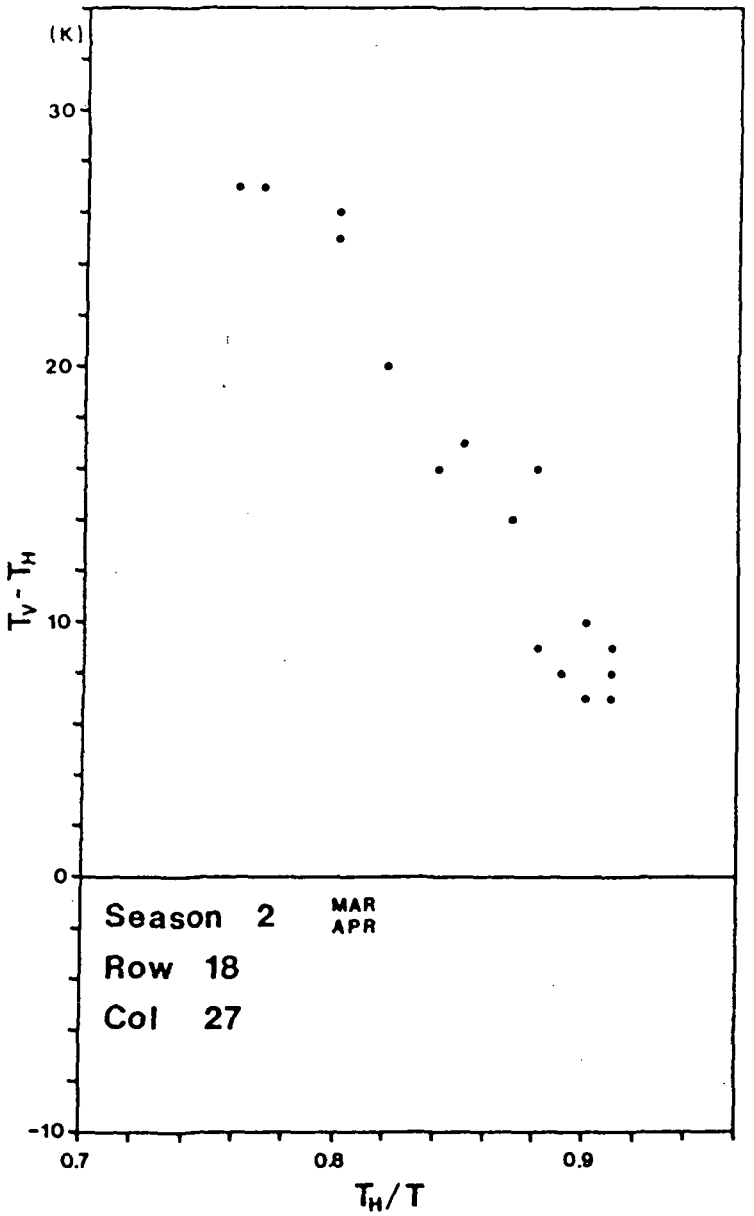

Figure C-1. Scatter plot of emissivity and polarization indices, season 2, row 18, column 27, south area.

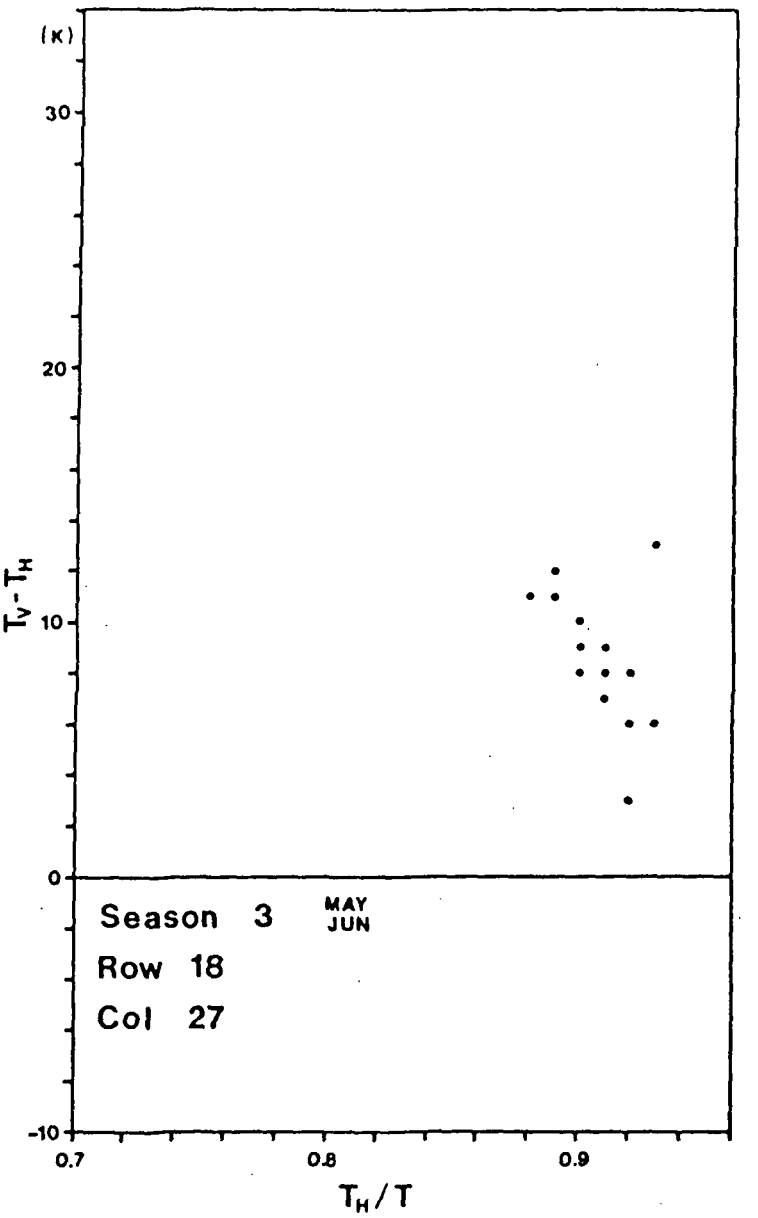

Figure C-2. Scatter plot of emissivity and polarization indices, season 3, row 18, column 27, south area.

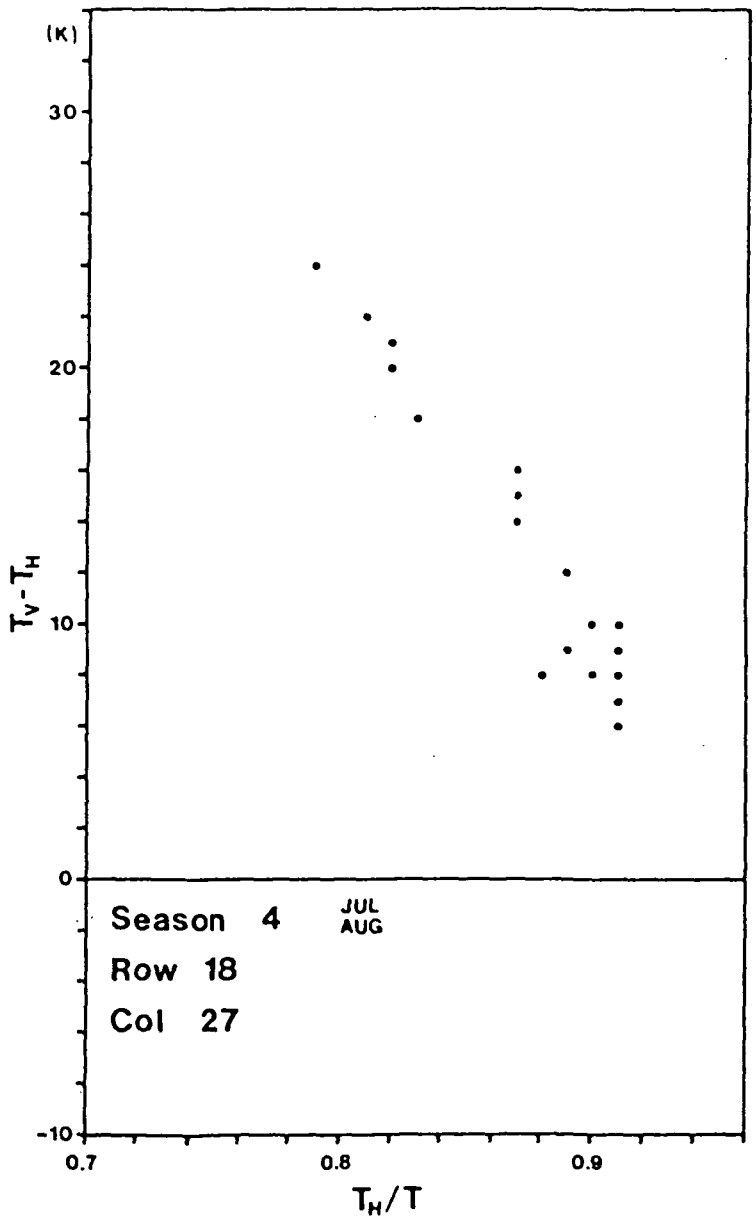

Figure C-3. Scatter plot of emissivity and polarization indices, season 4, row 18, column 27, south area.

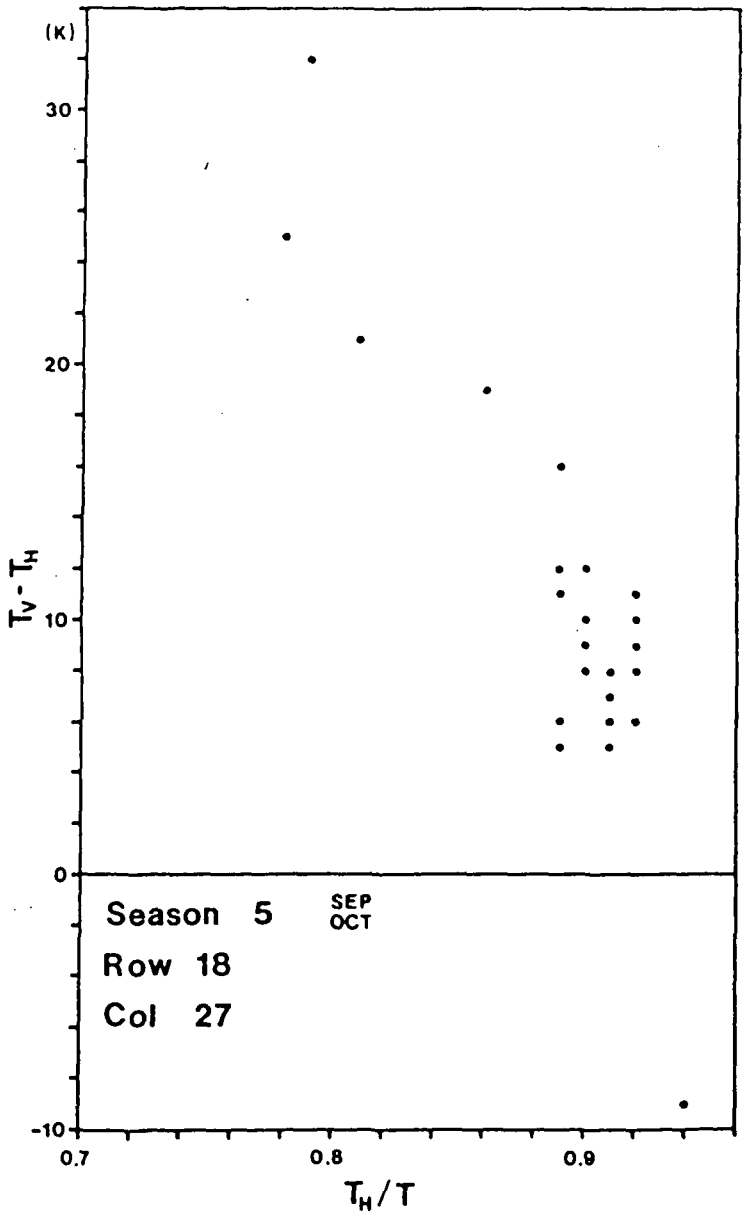

Figure C-4. Scatter plot of emissivity and polarization indices, season 5, row 18, column 27, south area.

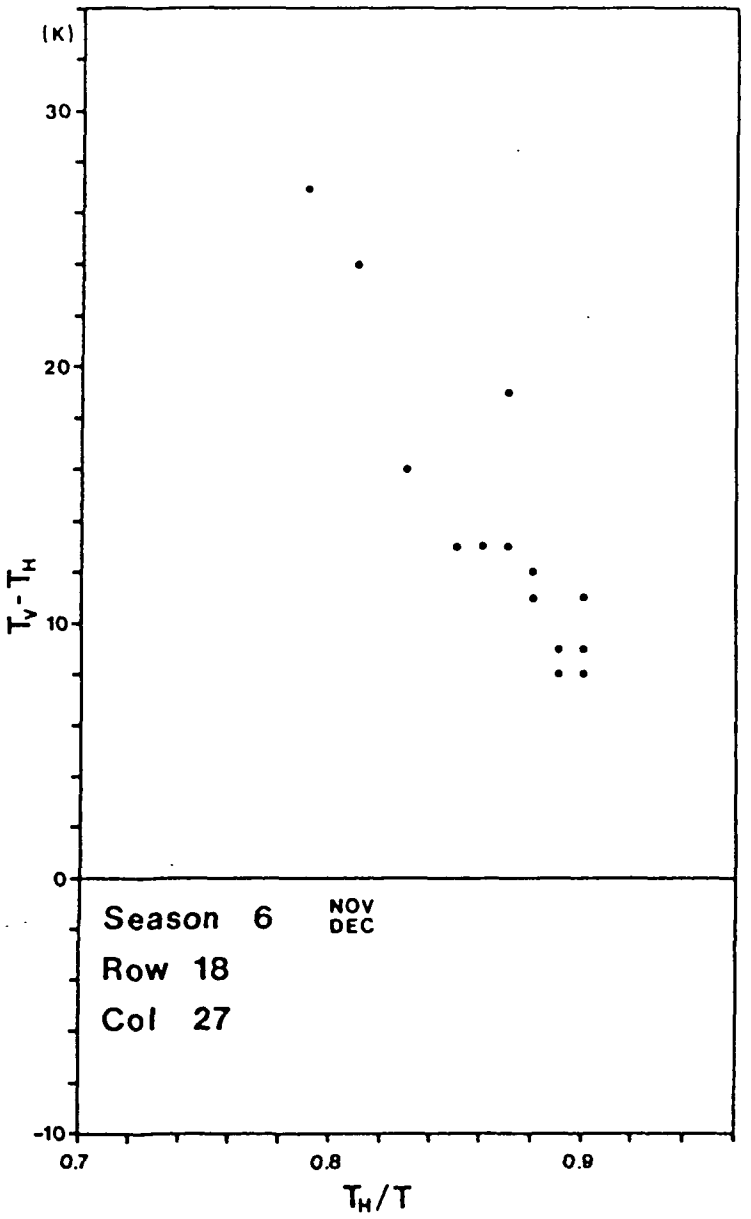

Figure C-5. Scatter plot of emissivity and polarization indices, season 6, row 18, column 27, south area.

APPENDIX D
TABULATION OF INITIAL SCREENING RESULTS

TABLE D-1

Correlation Coefficients Between API and Indices

South Row 09 COL 29 N=102 Season 0 (Full Year)

BASIC INDICES

INDEX	CORR	L	U	Significant abs(CORR) = 0.19
ϕ_{01}	-0.37	-0.53	-0.19	[sin(B * (DAY - D0)) + 1.0]
ϕ_{02}	-0.25	-0.43	-0.06	[T]
ϕ_{03}	-0.70	-0.79	-0.58	[T_h]
ϕ_{04}	-0.59	-0.70	-0.45	[T_v]
ϕ_{05}	-0.81	-0.87	-0.74	[T_h / T]
ϕ_{06}	-0.72	-0.80	-0.61	[T_v / T]
ϕ_{07}	0.75	0.65	0.82	[T_v - T_h]
ϕ_{08}	0.74	0.64	0.82	[(T_v - T_h) / T]
ϕ_{09}	0.76	0.67	0.83	[(T_v - T_h) / T_h]
ϕ_{10}	0.76	0.67	0.83	[(T_v - T_h) / T_v]
ϕ_{11}	0.76	0.67	0.83	[2.0 * (T_v - T_h) / (T_v + T_h)]
ϕ_{12}	-0.66	-0.76	-0.54	[(T_v + T_h) / 2.0]
ϕ_{13}	-0.80	-0.72	-0.86	[(T_v + T_h) / (2.0 * T)]
ϕ_{14}	0.76	0.67	0.84	[(T_v + T_h) / (2.0 * T_h)]
ϕ_{15}	-0.76	-0.83	-0.67	[(T_v + T_h) / (2.0 * T_v)]
ϕ_{16}	0.77	0.67	0.84	[(T_v - T_h) * 2.0 * T / (T_v + T_h)]
ϕ_{17}	0.75	0.65	0.82	[(T_v - T_h) * 2.0 * T_h / (T_v + T_h)]
ϕ_{18}	0.75	0.65	0.83	[(T_v - T_h) * 2.0 * T_v / (T_v + T_h)]

SQUARE-ROOT INDICES

INDEX	CORR	L	U
ϕ_{19}	-0.40	-0.56	-0.23
ϕ_{20}	-0.25	-0.43	-0.06
ϕ_{21}	-0.70	-0.79	-0.59
ϕ_{22}	-0.60	-0.71	-0.45
ϕ_{23}	-0.82	-0.87	-0.74
ϕ_{24}	-0.72	-0.80	-0.61
ϕ_{25}	0.72	0.61	0.80
ϕ_{26}	0.72	0.61	0.80
ϕ_{27}	0.74	0.64	0.82
ϕ_{28}	0.74	0.63	0.81
ϕ_{29}	0.74	0.63	0.82
ϕ_{30}	-0.67	-0.76	-0.54
ϕ_{31}	-0.81	-0.86	-0.72
ϕ_{32}	0.76	0.66	0.83
ϕ_{33}	-0.76	-0.67	-0.83
ϕ_{34}	0.74	0.64	0.82
ϕ_{35}	0.72	0.61	0.80
ϕ_{36}	0.73	0.62	0.81

SQUARED INDICES

INDEX	CORR	L	U
ϕ_{37}	-0.31	-0.48	-0.13
ϕ_{38}	-0.25	-0.43	-0.06
ϕ_{39}	-0.69	-0.78	-0.57
ϕ_{40}	-0.58	-0.70	-0.44
ϕ_{41}	-0.81	-0.87	-0.73
ϕ_{42}	-0.71	-0.79	-0.60
ϕ_{43}	0.75	0.65	0.82
ϕ_{44}	0.74	0.64	0.82
ϕ_{45}	0.75	0.64	0.82
ϕ_{46}	0.75	0.66	0.83
ϕ_{47}	0.75	0.65	0.82
ϕ_{48}	-0.65	-0.75	-0.52
ϕ_{49}	-0.79	-0.86	-0.71
ϕ_{50}	0.76	0.67	0.83
ϕ_{51}	-0.76	-0.83	-0.66
ϕ_{52}	0.76	0.66	0.83
ϕ_{53}	0.75	0.65	0.82
ϕ_{54}	0.74	0.64	0.82

All correlations were significant at the 0.05 level.

TABLE D-2

Correlation Coefficients Between API and Indices
South Row 09 Col 29 N=17 Season 2 (MAR - APR)

BASIC INDICES

INDEX	CORR	L	U	Significant abs(CORR) = 0.48
ϕ_{01}	-0.93	-0.98	-0.82	[sin(B * (DAY - DO)) + 1.0]
ϕ_{02}	-0.10	-0.56	+0.40	[T]
ϕ_{03}	-0.87	-0.95	-0.67	[T_h]
ϕ_{04}	-0.72	-0.89	-0.36	[T_v]
ϕ_{05}	-0.96	-0.98	-0.88	[T_h / T]
ϕ_{06}	-0.89	-0.96	-0.72	[T_v / T]
ϕ_{07}	0.93	0.81	0.98	[T_v - T_h]
ϕ_{08}	0.93	0.80	0.97	[(T_v - T_h) / T]
ϕ_{09}	0.93	0.81	0.97	[(T_v - T_h) / T_h]
ϕ_{10}	0.93	0.82	0.98	[(T_v - T_h) / T_v]
ϕ_{11}	0.93	0.81	0.98	[2.0 * (T_v - T_h) / (T_v + T_h)]
ϕ_{12}	-0.82	-0.93	-0.57	[(T_v + T_h) / 2.0]
ϕ_{13}	-0.95	-0.98	-0.85	[(T_v + T_h) / (2.0 * T)]
ϕ_{14}	0.93	0.81	0.97	[(T_v + T_h) / (2.0 * T_h)]
ϕ_{15}	-0.93	-0.98	-0.82	[(T_v + T_h) / (2.0 * T_v)]
ϕ_{16}	0.93	0.82	0.98	[(T_v - T_h) * 2.0 * T / (T_v+T_h)]
ϕ_{17}	0.93	0.81	0.97	[(T_v - T_h) * 2.0 * T_h / (T_v +T_h)]
ϕ_{18}	0.93	0.81	0.98	[(T_v - T_h) * 2.0 * T_v / (T_v +T_h)]

SQUARE-ROOT INDICES

INDEX	CORR	L	U
ϕ_{19}	-0.93	-0.97	-0.80
ϕ_{20}	-0.10	-0.55	+0.40
ϕ_{21}	-0.87	-0.95	-0.68
ϕ_{22}	-0.72	-0.89	-0.37
ϕ_{23}	-0.96	-0.98	-0.88
ϕ_{24}	-0.89	-0.96	-0.72
ϕ_{25}	0.92	0.79	0.97
ϕ_{26}	0.92	0.78	0.97
ϕ_{27}	0.93	0.81	0.97
ϕ_{28}	0.93	0.80	0.97
ϕ_{29}	0.93	0.80	0.97
ϕ_{30}	-0.83	-0.94	-0.57
ϕ_{31}	-0.95	-0.98	-0.85
ϕ_{32}	0.93	0.82	0.98
ϕ_{33}	-0.93	-0.98	-0.82
ϕ_{34}	0.93	0.81	0.97
ϕ_{35}	0.92	0.78	0.97
ϕ_{36}	0.92	0.79	0.97

SQUARED INDICES

INDEX	CORR	L	U
ϕ_{37}	-0.91	-0.97	-0.76
ϕ_{38}	-0.11	-0.56	+0.39
ϕ_{39}	-0.86	-0.95	-0.66
ϕ_{40}	-0.71	-0.89	-0.35
ϕ_{41}	-0.96	-0.98	-0.88
ϕ_{42}	-0.89	-0.96	-0.71
ϕ_{43}	0.91	0.77	0.97
ϕ_{44}	0.91	0.76	0.97
ϕ_{45}	0.89	0.72	0.96
ϕ_{46}	0.91	0.75	0.97
ϕ_{47}	0.90	0.74	0.96
ϕ_{48}	-0.82	-0.93	-0.55
ϕ_{49}	-0.94	-0.98	-0.85
ϕ_{50}	0.93	0.81	0.97
ϕ_{51}	-0.93	-0.98	-0.82
ϕ_{52}	0.90	0.74	0.96
ϕ_{53}	0.92	0.79	0.97
ϕ_{54}	0.91	0.76	0.97

Underlined correlations were not significant at the 0.05 level.

TABLE D-3

Correlation Coefficients Between API and Indices
South Row 09 Col 29 N=18 Season 3 (MAY - JUN)

BASIC INDICES

INDEX	CORR	L	U	Significant abs(CORR) = 0.47
ϕ_{01}	-0.33	-0.69	+0.16	[sin(B * (DAY - D0)) + 1.0]
ϕ_{02}	-0.40	-0.73	+0.09	[T]
ϕ_{03}	-0.55	-0.81	-0.11	[t_h]
ϕ_{04}	-0.39	-0.73	+0.09	[t_v]
ϕ_{05}	-0.35	-0.70	+0.14	[t_h / T]
ϕ_{06}	+0.05	-0.43	+0.51	[t_v / T]
ϕ_{07}	0.76	0.45	0.91	[$t_v - t_h$]
ϕ_{08}	0.79	0.50	0.92	[$(t_v - t_h)$ / T]
ϕ_{09}	0.78	0.49	0.91	[$(t_v - t_h)$ / t_h]
ϕ_{10}	0.78	0.49	0.91	[$(t_v - t_h)$ / t_v]
ϕ_{11}	0.78	0.49	0.91	[2.0 * $(t_v - t_h)$ / $(t_v + t_h)$]
ϕ_{12}	-0.48	-0.77	-0.02	[$(t_v + t_h)$ / 2.0]
ϕ_{13}	-0.17	-0.59	+0.32	[$(t_v + t_h)$ / (2.0 * T)]
ϕ_{14}	0.78	0.49	0.91	[$(t_v + t_h)$ / (2.0 * t_h)]
ϕ_{15}	-0.78	-0.91	-0.49	[$(t_v + t_h)$ / (2.0 * t_v)]
ϕ_{16}	0.75	0.44	0.90	[$(t_v - t_h)$ * 2.0 * T / $(t_v + t_h)$]
ϕ_{17}	0.76	0.45	0.91	[$(t_v - t_h)$ * 2.0 * t_h /(t_v+t_h)]
ϕ_{18}	0.76	0.46	0.91	[$(t_v - t_h)$ * 2.0 * t_v /(t_v+t_h)]

SQUARE-ROOT INDICES

INDEX	CORR	L	U
ϕ_{19}	-0.33	-0.69	+0.16
ϕ_{20}	-0.40	-0.73	+0.09
ϕ_{21}	-0.55	-0.81	-0.11
ϕ_{22}	-0.39	-0.73	+0.09
ϕ_{23}	-0.35	-0.70	+0.14
ϕ_{24}	0.05	-0.43	+0.51
ϕ_{25}	0.75	0.44	0.90
ϕ_{26}	0.77	0.48	0.91
ϕ_{27}	0.77	0.47	0.91
ϕ_{28}	0.77	0.47	0.91
ϕ_{29}	0.77	0.47	0.91
ϕ_{30}	-0.48	-0.77	-0.02
ϕ_{31}	-0.17	-0.59	+0.31
ϕ_{32}	0.77	0.48	0.91
ϕ_{33}	-0.77	-0.91	-0.47
ϕ_{34}	0.74	0.42	0.90
ϕ_{35}	0.75	0.44	0.90
ϕ_{36}	0.75	0.44	0.90

SQUARED INDICES

INDEX	CORR	L	U
ϕ_{37}	-0.33	-0.69	+0.16
ϕ_{38}	-0.40	-0.73	+0.09
ϕ_{39}	-0.55	-0.81	-0.11
ϕ_{40}	-0.40	-0.73	+0.09
ϕ_{41}	-0.34	-0.70	+0.15
ϕ_{42}	0.05	-0.42	+0.51
ϕ_{43}	0.77	0.47	0.91
ϕ_{44}	0.80	0.53	0.92
ϕ_{45}	0.79	0.51	0.92
ϕ_{46}	0.79	0.51	0.92
ϕ_{47}	0.79	0.51	0.92
ϕ_{48}	-0.48	-0.77	-0.02
ϕ_{49}	-0.17	-0.59	+0.32
ϕ_{50}	0.78	0.49	0.91
ϕ_{51}	-0.78	-0.91	-0.49
ϕ_{52}	0.76	0.45	0.90
ϕ_{53}	0.77	0.47	0.91
ϕ_{54}	0.77	0.47	0.91

Underlined correlations were not significant at the 0.05 level.

TABLE D-6
Correlation Coefficients Between API and Indices
South Row 09 Col 29 N=19 Season 6 (NOV - DEC)

BASIC INDICES

INDEX	CORR	L	U	Significant abs(CORR) = 0.45
ϕ 01	+0.04	-0.42	+0.49	[sin(B * (DAY - DO)) + 1.0]
ϕ 02	-0.69	-0.87	-0.34	[T]
ϕ 03	-0.90	-0.96	-0.76	[T_h]
ϕ 04	-0.80	-0.92	-0.55	[T_v]
ϕ 05	-0.85	-0.94	-0.64	[T_h / T]
ϕ 06	-0.57	-0.81	-0.16	[T_v / T]
ϕ 07	0.80	0.55	0.92	[T_v - T_h]
ϕ 08	0.82	0.58	0.93	[(T_v - T_h) / T]
ϕ 09	0.82	0.57	0.93	[(T_v - T_h) / T_h]
ϕ 10	0.82	0.59	0.93	[(T_v - T_h) / T_v]
ϕ 11	0.82	0.58	0.93	[2.0 * (T_v - T_h) / (T_v+T_h)]
ϕ 12	-0.87	-0.95	-0.70	[(T_v + T_h) / 2.0]
ϕ 13	-0.80	-0.92	-0.54	[(T_v + T_h) / (2.0 * T)]
ϕ 14	0.82	0.57	0.93	[(T_v + T_h) / (2.0 * T_h)]
ϕ 15	-0.82	-0.93	-0.59	[(T_v + T_h) / (2.0 * T_v)]
ϕ 16	0.81	0.55	0.92	[(T_v - T_h) * 2.0 * T/(T_v+T_h)]
ϕ 17	0.81	0.55	0.92	[(T_v-T_h) * 2.0 * T_h/(T_v+T_h)]
ϕ 18	0.80	0.54	0.92	[(T_v-T_h) * 2.0 * T_v/(T_v+T_h)]

SQUARE-ROOT INDICES

INDEX	CORR	L	U
ϕ 19	+0.09	-0.38	+0.52
ϕ 20	-0.69	-0.87	-0.34
ϕ 21	-0.91	-0.96	-0.77
ϕ 22	-0.81	-0.92	-0.56
ϕ 23	-0.85	-0.94	-0.64
ϕ 24	-0.57	-0.81	-0.16
ϕ 25	0.82	0.59	0.93
ϕ 26	0.84	0.63	0.94
ϕ 27	0.84	0.63	0.94
ϕ 28	0.85	0.64	0.94
ϕ 29	0.85	0.64	0.94
ϕ 30	-0.88	-0.95	-0.70
ϕ 31	-0.80	-0.92	-0.54
ϕ 32	0.82	0.57	0.93
ϕ 33	-0.82	-0.93	-0.58
ϕ 34	0.83	0.60	0.93
ϕ 35	0.83	0.59	0.93
ϕ 36	0.82	0.59	0.93

SQUARED INDICES

INDEX	CORR	L	U
ϕ 37	-0.04	-0.48	+0.42
ϕ 38	-0.69	-0.87	-0.34
ϕ 39	-0.90	-0.96	-0.75
ϕ 40	-0.80	-0.92	-0.54
ϕ 41	-0.85	-0.94	-0.65
ϕ 42	-0.57	-0.81	-0.16
ϕ 43	0.76	0.46	0.90
ϕ 44	0.77	0.48	0.91
ϕ 45	0.76	0.46	0.90
ϕ 46	0.77	0.48	0.91
ϕ 47	0.76	0.47	0.90
ϕ 48	-0.87	-0.95	-0.68
ϕ 49	-0.80	-0.92	-0.54
ϕ 50	0.81	0.57	0.93
ϕ 51	-0.82	-0.93	-0.59
ϕ 52	0.76	0.46	0.90
ϕ 53	0.76	0.47	0.90
ϕ 54	0.75	0.46	0.90

Underlined correlations were not significant at the 0.05 level.

TABLE D-5
Correlation Coefficients Between API and Indices
South Row 09 Col 29 N=27 Season 5 (SEP - OCT)

BASIC INDICES

INDEX	CORR	L	U	Significant abs(CORR) = 0.38
ϕ_{01}	-0.26	-0.58	+0.13	[sin(B * (DAY - DO)) + 1.0]
ϕ_{02}	-0.14	-0.50	+0.25	[T]
ϕ_{03}	-0.70	-0.85	-0.44	[T_h]
ϕ_{04}	-0.62	-0.81	-0.31	[T_v]
ϕ_{05}	-0.82	-0.91	-0.64	[T_h / T]
ϕ_{06}	-0.83	-0.92	-0.66	[T_v / T]
ϕ_{07}	0.70	0.43	0.85	[T_v - T_h]
ϕ_{08}	0.70	0.43	0.85	[(T_v - T_h) / T]
ϕ_{09}	0.73	0.49	0.87	[(T_v - T_h) / T_h]
ϕ_{10}	0.73	0.48	0.87	[(T_v - T_h) / T_v]
ϕ_{11}	0.73	0.48	0.87	[2.0 * (T_v - T_h) / (T_v + T_h)]
ϕ_{12}	-0.67	-0.84	-0.39	[(T_v + T_h) / 2.0]
ϕ_{13}	-0.84	-0.92	-0.67	[(T_v + T_h) / (2.0 * T)]
ϕ_{14}	0.73	0.49	0.87	[(T_v + T_h) / (2.0 * T_h)]
ϕ_{15}	-0.73	-0.87	-0.48	[(T_v + T_h) / (2.0 * T_v)]
ϕ_{16}	0.73	0.48	0.87	[(T_v - T_h) * 2.0 * T/(T_v+T_h)]
ϕ_{17}	0.69	0.42	0.85	[(T_v - T_h) * 2.0 * T_h/(T_v+T_h)]
ϕ_{18}	0.70	0.44	0.85	[(T_v - T_h) * 2.0 * T_v/(T_v+T_h)]

SQUARE-ROOT INDICES

INDEX	CORR	L	U
ϕ_{19}	-0.27	-0.59	+0.12
ϕ_{20}	-0.14	-0.50	-0.25
ϕ_{21}	-0.71	-0.86	-0.45
ϕ_{22}	-0.63	-0.81	-0.32
ϕ_{23}	-0.82	-0.92	-0.65
ϕ_{24}	-0.84	-0.92	-0.67
ϕ_{25}	0.68	0.40	0.84
ϕ_{26}	0.67	0.39	0.84
ϕ_{27}	0.70	0.44	0.86
ϕ_{28}	0.70	0.43	0.85
ϕ_{29}	0.70	0.44	0.85
ϕ_{30}	-0.68	-0.84	-0.41
ϕ_{31}	-0.84	-0.92	-0.68
ϕ_{32}	0.73	0.49	0.87
ϕ_{33}	-0.73	-0.87	-0.48
ϕ_{34}	0.70	0.44	0.85
ϕ_{35}	0.67	0.39	0.84
ϕ_{36}	0.68	0.40	0.84

SQUARED INDICES

INDEX	CORR	L	U
ϕ_{37}	-0.23	-0.56	+0.16
ϕ_{38}	-0.14	-0.50	+0.25
ϕ_{39}	-0.68	-0.84	-0.41
ϕ_{40}	-0.60	-0.80	-0.29
ϕ_{41}	-0.81	-0.91	-0.62
ϕ_{42}	-0.82	-0.92	-0.64
ϕ_{43}	0.73	0.48	0.87
ϕ_{44}	0.72	0.47	0.86
ϕ_{45}	0.77	0.55	0.89
ϕ_{46}	0.76	0.54	0.89
ϕ_{47}	0.76	0.54	0.89
ϕ_{48}	-0.66	-0.83	-0.37
ϕ_{49}	-0.83	-0.92	-0.65
ϕ_{50}	0.73	0.49	0.87
ϕ_{51}	-0.72	-0.87	-0.47
ϕ_{52}	0.77	0.55	0.89
ϕ_{53}	0.72	0.47	0.86
ϕ_{54}	0.73	0.49	0.87

Underlined correlations were not significant at The 0.05 level.

TABLE D-6
Correlation Coefficients Between API and Indices
South Row 09 Col 29 N=19 Season 6 (NOV - DEC)

BASIC INDICES

INDEX	CORR	L	U	Significant abs(CORR) = 0.45
ϕ 01	+0.04	-0.42	+0.49	[sin(B * (DAY - D0)) + 1.0]
ϕ 02	-0.69	-0.87	-0.34	[T]
ϕ 03	-0.90	-0.96	-0.76	[T_h]
ϕ 04	-0.80	-0.92	-0.55	[T_v]
ϕ 05	-0.85	-0.94	-0.64	[T_h / T]
ϕ 06	-0.57	-0.81	-0.16	[T_v / T]
ϕ 07	0.80	0.55	0.92	[T_v - T_h]
ϕ 08	0.82	0.58	0.93	[(T_v - T_h) / T]
ϕ 09	0.82	0.57	0.93	[(T_v - T_h) / T_h]
ϕ 10	0.82	0.59	0.93	[(T_v - T_h) / T_v]
ϕ 11	0.82	0.58	0.93	[2.0 * (T_v - T_h) / (T_v+T_h)]
ϕ 12	-0.87	-0.95	-0.70	[(T_v + T_h) / 2.0]
ϕ 13	-0.80	-0.92	-0.54	[(T_v + T_h) / (2.0 * T)]
ϕ 14	0.82	0.57	0.93	[(T_v + T_h) / (2.0 * T_h)]
ϕ 15	-0.82	-0.93	-0.59	[(T_v + T_h) / (2.0 * T_v)]
ϕ 16	0.81	0.55	0.92	[(T_v - T_h) * 2.0 * T/(T_v+T_h)]
ϕ 17	0.81	0.55	0.92	[(T_v-T_h) * 2.0 * T_h/(T_v+T_h)]
ϕ 18	0.80	0.54	0.92	[(T_v-T_h) * 2.0 * T_v/(T_v+T_h)]

SQUARE-ROOT INDICES

INDEX	CORR	L	U
ϕ 19	+0.09	-0.38	+0.52
ϕ 20	-0.69	-0.87	-0.34
ϕ 21	-0.91	-0.96	-0.77
ϕ 22	-0.81	-0.92	-0.56
ϕ 23	-0.85	-0.94	-0.64
ϕ 24	-0.57	-0.81	-0.16
ϕ 25	0.82	0.59	0.93
ϕ 26	0.84	0.63	0.94
ϕ 27	0.84	0.63	0.94
ϕ 28	0.85	0.64	0.94
ϕ 29	0.85	0.64	0.94
ϕ 30	-0.88	-0.95	-0.70
ϕ 31	-0.80	-0.92	-0.54
ϕ 32	0.82	0.57	0.93
ϕ 33	-0.82	-0.93	-0.58
ϕ 34	0.83	0.60	0.93
ϕ 35	0.83	0.59	0.93
ϕ 36	0.82	0.59	0.93

SQUARED INDICES

INDEX	CORR	L	U
ϕ 37	-0.04	-0.48	+0.42
ϕ 38	-0.69	-0.87	-0.34
ϕ 39	-0.90	-0.96	-0.75
ϕ 40	-0.80	-0.92	-0.54
ϕ 41	-0.85	-0.94	-0.65
ϕ 42	-0.57	-0.81	-0.16
ϕ 43	0.76	0.46	0.90
ϕ 44	0.77	0.48	0.91
ϕ 45	0.76	0.46	0.90
ϕ 46	0.77	0.48	0.91
ϕ 47	0.76	0.47	0.90
ϕ 48	-0.87	-0.95	-0.68
ϕ 49	-0.80	-0.92	-0.54
ϕ 50	0.81	0.57	0.93
ϕ 51	-0.82	-0.93	-0.59
ϕ 52	0.76	0.46	0.90
ϕ 53	0.76	0.47	0.90
ϕ 54	0.75	0.46	0.90

Underlined correlations were not significant at the 0.05 level.

APPENDIX E

SIMPLE LINEAR REGRESSION RESULTS

The following tables present the results of simple linear regression of API on each of three indices, by season and annually, for all of the individual grid cells used in temporal analysis, Phases I, II, and III.

TABLE E-1

Simple Linear Regressions of API on Three Indices, By Season

South Area Grid Cell: Row 09 Column 29

		PHI 05			PHI 07			PHI 11		
Sn	N	CORR	SLOPE	INTCP	CORR	SLOPE	INTCP	CORR	SLOPE	INTCP
0	102	-0.81	-253	232	0.75	1.44	-7.6	0.76	335	-6.0
2	17	-0.96	-253	232	0.93	1.61	-10.3	0.93	357	-7.5
3	18	-0.35	-133	128	0.76	2.04	-8.3	0.78	535	-7.9
4	20	-0.81	-348	317	0.72	1.55	-6.2	0.73	411	-6.0
5	27	-0.82	-320	291	0.70	1.87	-14.6	0.73	447	-13.1
6	19	-0.85	-207	189	0.80	1.04	-5.6	0.82	240	-4.5

Underlined statistics differ insignificantly from zero (alpha=0.05).
Minimum significant abs(CORR) = 0.19 for Season 0
Minimum significant abs(CORR) = 0.48 for Season 2
Minimum significant abs(CORR) = 0.47 for Season 3
Minimum significant abs(CORR) = 0.44 for Season 4
Minimum significant abs(CORR) = 0.38 for Season 5
Minimum significant abs(CORR) = 0.45 for Season 6

TABLE E-2

Simple Linear Regressions of API on Three Indices, By Season

South Area Grid Cell: Row 03 Column 29

		PHI 05			PHI 07			PHI 11		
Sn	N	CORR	SLOPE	INTCP	CORR	SLOPE	INTCP	CORR	SLOPE	INTCP
0	104	-0.81	-309	283	[0.71]	1.90	-10.8	[0.74]	454	-9.3
2	16	-0.87	-327	296	0.86	2.43	-20.3	0.88	555	-17.2
3	19	-0.80	-240	224	0.85	1.55	-5.8	0.86	390	-5.0
4	22	-0.60	-353	321	0.37	1.51	-4.7	0.38	403	-4.6
5	29	-0.84	-455	413	[0.56]	2.19	-15.6	[0.62]	577	-15.6
6	17	-0.61	-266	243	0.65	1.54	-8.8	0.69	379	-8.3

Bracketted CORR values differ significantly from largest abs(CORR).
Underlined statistics differ insignificantly from zero (alpha=0.05).
Minimum significant abs(CORR) = 0.19 for Season 0
Minimum significant abs(CORR) = 0.50 for Season 2
Minimum significant abs(CORR) = 0.45 for Season 3
Minimum significant abs(CORR) = 0.42 for Season 4
Minimum significant abs(CORR) = 0.37 for Season 5
Minimum significant abs(CORR) = 0.48 for Season 6

TABLE E-3

Simple Linear Regressions of API on Three Indices, By Season

South Area Grid Cell: Row 10 Column 33

		PHI 05			PHI 07			PHI 11		
Sn	N	CORR	SLOPE	INTCP	CORR	SLOPE	INTCP	CORR	SLOPE	INTCP
0	100	-0.52	-239	223	[0.34]	0.94	0.7	[0.36]	241	0.8
2	15	-0.77	-310	284	0.83	2.45	-17.8	0.85	576	-15.5
3	18	-0.46	-411	384	0.20	1.34	3.6	0.21	351	3.9
4	20	-0.43	-370	344	0.33	1.80	-1.1	0.35	507	-1.3
5	26	-0.76	-220	203	0.53	1.06	-5.0	0.53	271	-4.7
6	20	-0.22	-81	80	0.13	0.30	4.4	0.22	131	2.0

Bracketted CORR values differ significantly from largest abs(CORR).
Underlined statistics differ insignificantly from zero (alpha=0.05).
Minimum significant abs(CORR) = 0.20 for Season 0
Minimum significant abs(CORR) = 0.51 for Season 2
Minimum significant abs(CORR) = 0.47 for Season 3
Minimum significant abs(CORR) = 0.44 for Season 4
Minimum significant abs(CORR) = 0.39 for Season 5
Minimum significant abs(CORR) = 0.44 for Season 6

TABLE E-4

Simple Linear Regressions of API on Three Indices, By Season

South Area Grid Cell: Row 12 Column 27

		PHI 05			PHI 07			PHI 11		
Sn	N	CORR	SLOPE	INTCP	CORR	SLOPE	INTCP	CORR	SLOPE	INTCP
0	109	-0.81	-257	235	0.78	1.54	-10.0	0.80	349	-7.7
2	16	-0.96	-213	197	0.93	1.46	-10.3	0.94	321	-7.5
3	19	-0.41	-215	204	0.47	2.38	-12.1	0.54	655	-12.7
4	23	-0.82	-270	246	0.72	1.25	-5.7	0.72	323	-5.1
5	31	-0.94	-410	371	0.91	2.46	-20.7	0.92	554	-17.1
6	18	-0.90	-313	278	0.84	1.56	-15.4	0.87	355	-13.6

Underlined statistics differ insignificantly from zero (alpha=0.05).
Minimum significant abs(CORR) = 0.19 for Season 0
Minimum significant abs(CORR) = 0.50 for Season 2
Minimum significant abs(CORR) = 0.45 for Season 3
Minimum significant abs(CORR) = 0.41 for Season 4
Minimum significant abs(CORR) = 0.35 for Season 5
Minimum significant abs(CORR) = 0.47 for Season 6

TABLE E-5

Simple Linear Regressions of API on Three Indices, By Season

South Area Grid Cell: Row 13 Column 20

		PHI 05			PHI 07			PHI 11		
Sn	N	CORR	SLOPE	INTCP	CORR	SLOPE	INTCP	CORR	SLOPE	INTCP
0	99	-0.81	-246	227	0.78	1.61	-9.9	0.78	377	-8.1
2	18	-0.90	-240	221	0.89	1.60	-10.2	0.89	373	-8.3
3	17	-0.73	-277	260	0.73	1.83	-6.5	0.75	453	-5.4
4	20	-0.90	-363	332	0.89	2.23	-14.9	0.89	554	-13.1
5	25	-0.93	-364	335	0.88	2.40	-18.2	0.90	558	-15.6
6	15	-0.57	-155	142	0.74	0.97	-7.0	0.76	237	-6.5

Underlined statistics differ insignificantly from zero (alpha=0.05).
Minimum significant abs(CORR) = 0.20 for Season 0
Minimum significant abs(CORR) = 0.47 for Season 2
Minimum significant abs(CORR) = 0.48 for Season 3
Minimum significant abs(CORR) = 0.44 for Season 4
Minimum significant abs(CORR) = 0.40 for Season 5
Minimum significant abs(CORR) = 0.51 for Season 6

TABLE E-6

Simple Linear Regressions of API on Three Indices, By Season

South Area Grid Cell: Row 14 Column 33

		PHI 05			PHI 07			PHI 11		
Sn	N	CORR	SLOPE	INTCP	CORR	SLOPE	INTCP	CORR	SLOPE	INTCP
0	106	-0.56	-201	190	[0.22]	0.34	5.8	[0.24]	95	5.6
2	16	-0.51	-117	116	0.39	0.63	6.1	0.42	158	6.1
3	17	-0.62	-479	446	0.37	2.62	-5.3	0.39	707	-5.3
4	20	-0.65	-701	648	0.07	0.47	4.4	0.10	184	3.5
5	27	-0.45	-117	109	-0.30	-0.15	3.8	-0.29	-38	3.7
6	24	-0.27	-114	111	0.27	0.64	2.2	0.34	205	0.5

Bracketted CORR values differ significantly from largest abs(CORR).
Underlined statistics differ insignificantly from zero (alpha=0.05).
Minimum significant abs(CORR) = 0.19 for Season 0
Minimum significant abs(CORR) = 0.50 for Season 2
Minimum significant abs(CORR) = 0.48 for Season 3
Minimum significant abs(CORR) = 0.44 for Season 4
Minimum significant abs(CORR) = 0.38 for Season 5
Minimum significant abs(CORR) = 0.40 for Season 6

TABLE E-7

Simple Linear Regressions of API on Three Indices, By Season

South Area Grid Cell: Row 15 Column 29

		PHI 05			PHI 07			PHI 11		
Sn	N	CORR	SLOPE	INTCP	CORR	SLOPE	INTCP	CORR	SLOPE	INTCP
0	104	-0.76	-162	152	0.68	0.98	-3.4	0.70	231	-2.4
2	19	-0.91	-181	171	0.85	1.10	-2.6	0.87	248	-1.0
3	18	-0.50	-189	182	0.17	0.43	7.2	0.22	142	6.4
4	20	-0.53	-100	94	0.38	0.40	0.0	0.38	104	0.1
5	27	-0.93	-148	135	0.87	1.05	-8.7	0.90	253	-7.7
6	18	-0.66	-127	120	0.58	0.70	-0.5	0.61	166	0.1

Underlined statistics differ insignificantly from zero (alpha=0.05).

Minimum significant abs(CORR) = 0.19 for Season 0
Minimum significant abs(CORR) = 0.45 for Season 2
Minimum significant abs(CORR) = 0.47 for Season 3
Minimum significant abs(CORR) = 0.44 for Season 4
Minimum significant abs(CORR) = 0.38 for Season 5
Minimum significant abs(CORR) = 0.47 for Season 6

TABLE E-8
Simple Linear Regressions of API on Three Indices, By Season

South Area Grid Cell: Row 18 Column 27

		PHI 05			PHI 07			PHI 11		
Sn	N	CORR	SLOPE	INTCP	CORR	SLOPE	INTCP	CORR	SLOPE	INTCP
0	105	-0.73	-169	157	0.67	0.98	-2.8	0.69	238	-2.2
2	19	-0.92	-211	199	0.85	1.30	-2.4	0.86	298	-0.8
3	18	-0.46	-296	279	0.31	1.11	0.3	0.39	360	-1.6
4	21	-0.75	-173	160	0.73	1.14	-6.3	0.73	280	-5.1
5	27	-0.95	-168	153	[0.79]	0.73	-4.6	[0.83]	192	-4.6
6	17	-0.69	-106	100	0.68	0.59	-0.4	0.69	137	0.2

Bracketted CORR values differ significantly from largest abs(CORR).
Underlined statistics differ insignificantly from zero (alpha=0.05).
Minimum significant abs(CORR) = 0.19 for Season 0
Minimum significant abs(CORR) = 0.45 for Season 2
Minimum significant abs(CORR) = 0.47 for Season 3
Minimum significant abs(CORR) = 0.43 for Season 4
Minimum significant abs(CORR) = 0.38 for Season 5
Minimum significant abs(CORR) = 0.48 for Season 6

TABLE E-9
Simple Linear Regressions of API on Three Indices, By Season

South Area Grid Cell: Row 29 Column 22

		PHI 05			PHI 07			PHI 11		
Sn	N	CORR	SLOPE	INTCP	CORR	SLOPE	INTCP	CORR	SLOPE	INTCP
0	110	-0.70	-202	186	0.62	1.11	-6.4	0.64	268	-5.3
2	22	-0.63	-130	126	0.61	0.85	0.3	0.61	193	1.7
3	17	-0.70	-266	246	0.57	1.47	-7.5	0.63	400	-7.8
4	21	-0.79	-216	198	[0.47]	0.84	-2.3	[0.50]	223	-2.2
5	27	-0.70	-157	142	0.65	0.78	-6.4	0.66	201	-6.1
6	18	-0.67	-102	94	0.71	0.79	-6.5	0.74	184	-5.6

Bracketted CORR values differ significantly from largest abs(CORR).
Underlined statistics differ insignificantly from zero (alpha=0.05).
Minimum significant abs(CORR) = 0.19 for Season 0
Minimum significant abs(CORR) = 0.42 for Season 2
Minimum significant abs(CORR) = 0.48 for Season 3
Minimum significant abs(CORR) = 0.43 for Season 4
Minimum significant abs(CORR) = 0.38 for Season 5
Minimum significant abs(CORR) = 0.47 for Season 6

TABLE E-10

Simple Linear Regressions of API on Three Indices, By Season

South Area Grid Cell: Row 21 Column 14

		PHI 05			PHI 07			PHI 11		
Sn	N	CORR	SLOPE	INTCP	CORR	SLOPE	INTCP	CORR	SLOPE	INTCP
0	116	-0.63	-171	158	0.58	1.15	-7.5	0.59	269	-6.2
2	19	-0.71	-85	80	0.63	0.56	-2.2	0.66	138	-1.8
3	19	-0.81	-297	274	0.65	1.64	-7.2	0.68	408	-6.2
4	20	-0.65	-207	194	0.68	1.65	-9.2	0.67	419	-8.1
5	29	-0.60	-109	100	0.50	0.55	-4.1	0.50	132	-3.6
6	21	-0.83	-360	322	0.88	2.32	-25.1	0.89	546	-22.8

Underlined statistics differ insignificantly from zero (alpha=0.05).
Minimum significant abs(CORR) = 0.18 for Season 0
Minimum significant abs(CORR) = 0.45 for Season 2
Minimum significant abs(CORR) = 0.45 for Season 3
Minimum significant abs(CORR) = 0.44 for Season 4
Minimum significant abs(CORR) = 0.37 for Season 5
Minimum significant abs(CORR) = 0.43 for Season 6

The REMOTE SENSING CENTER was established by authority of the Board of Directors of the Texas A&M University System on February 27, 1968. The CENTER is a consortium of four colleges of the University; Agriculture, Engineering, Geosciences, and Science. This unique organization concentrates on the development and utilization of remote sensing techniques and technology for a broad range of applications to the betterment of mankind.